PRINCIPLES OF NEUROMUSCULOSKELETAL COORDINATION IN HUMAN CYCLING

A L Robinson

PhD 2020

PRINCIPLES OF NEUROMUSCULOSKELETAL COORDINATION IN HUMAN CYCLING

AMY LOUISE ROBINSON

A thesis submitted in partial fulfilment of the requirements of Manchester Metropolitan University for the degree of

Doctor of Philosophy

School of Healthcare Sciences

Musculoskeletal Sciences & Sports Medicine Research Centre

In collaboration with Simon Fraser University

School of Biomedical Physiology and Kinesiology

2020

Table of Contents

List of Figures

List of Tables

Dissemination of Study Findings

Conference Presentations

Amy L. Robinson, James Wakeling & Emma Hodson-Tole (2019) Chainring Eccentricity Affects Muscle-Tendon Unit Mechanics During Cycling. **Published in: International Society of Biomechanics Congress XXVII** pp. 741 [Oral Presentation]

Amy L. Robinson, James Wakeling & Emma Hodson-Tole (2019) Effects of Chainring Eccentricity on Muscle-Tendon Unit Mechanics during Human Cycling. **BASES Biomechanics Interest Group Meeting.** [Oral Presentation]

Amy L. Robinson, James Wakeling & Emma Hodson-Tole (2018) Does the use of elliptical chainrings alter muscle-tendon unit velocities during human cycling? **Simon Fraser University Research Day** [Poster Presentation]

Acknowledgements

I wish to express my sincere appreciation to my supervisors, Dr Emma Hodson-Tole and Professor James Wakeling, for all your guidance and expertise. I cannot fathom how fortunate I am to have had two wonderful supervisors, who not only have imparted so much of their knowledge, but done so with endless encouragement, support and patience. I am eternally grateful that you took a chance on me and set me on a path from which I cannot look back. I hope I can continue to work with the enthusiasm you have both imparted. The past four years have taken me beyond anything I could expect from a PhD, immersing me into a topic I knew so little about and have gained so much passion for along the way. Thank you for welcoming me into your lab in Vancouver James; I am still coming to terms with how undeniably fortunate I have been for such an unbelievable experience, not only in the education and skills gained, but also the opportunity to develop lifelong friendships in one of the most beautiful places in the world.

I would also like to thank Dr Gregory May for his insight and knowledge of all things cycling related which helped lift this project off the ground and Dr Adrian Lai for all his help with OpenSim. I would especially like to thank the people that participated in this study for giving up their time and lots of their energy. And the team at Hope Tech, for your cooperation and expertise when developing the chainrings used in this study.

Thank you to all my former lab mates and colleagues, and current friends. Amanda, Sabrina, Steph and Vera; you became my family when I was far away from my own and the best group of people I could hope to meet. Thank you for being a continued support system even through the distance. I look forward to the many adventures that await us and the margaritas that will accompany them.

I wish to acknowledge the support of all my family, but in particular, I would like to thank my father for supporting me every day, picking me up when it got tough, offering endless encouragement and being a wonderful friend. And to my mother - the highs and lows associated with this body of work have not quite been the same without you here to share them with and I wish you were here to celebrate its culmination together, but I hope you would be proud. It is because of the two of you I have been able to chase my dreams, thank

you for your unwavering support of them and instilling my curiosity of the world, I dedicate this to you both.

To Vinny, whose lockdown experience was all the more boring whilst he shared the long hours with this thesis. Thank you for being the most considerate, kindest and supportive human being and best partner I could hope for. You have been here to applaud all of the successes and soften the falls and I could not have done it without you. And to our dogs, who made the vital contribution of reminding me of the aspects of life I deem most important.

And lastly, I would like to acknowledge the utter privilege that has been bestowed upon me, which has allowed me to study a subject simply because I am interested in it. The opportunities I have been so fortunate in receiving based on personal circumstance is something I never wish to take lightly, and I hope I can live up to.

Definition of Terms

Activation-deactivation dynamics	A mechanical muscle property describing the relationship between muscle excitation and creating force, and the activation ceasing and falling to zero. Encompasses the delay between neural activation arriving at the muscle and developing force and the delay between neural excitation and relaxation.
Aponeurosis	The fibrous connective tissue responsible for connecting muscles to bone, enveloping muscles, binding muscles together and binding muscles to other tissues.
Cadence	The number of revolutions of the crank arm performed per minute (rpm).
Chainring	A large cog which carries the chain on the bicycle and is attached to the crank.
Crank angle	The angle of the crank within the 0 - 360-degree pedal cycle.
Crank length	The length of the crank arm.
Crank orientation	The placement of the crank in relation to the major and minor axes of the non-circular chainring.
Dead centres	The area of the pedal cycle when one of the pedals is at the top dead centre (0°) and the other is at the bottom dead centre (180°) where little propulsive force can be exerted.
Degrees of freedom	The number of independent movements a rigid body has.
Drivetrain	A system comprising the components on the bicycle used to transmit power from the cyclist to the rear wheel.
Eccentricity	Value depicting the deviation of a curve from circularity.
Efficiency	The ratio of mechanical work accomplished to the metabolic energy expended to complete the work
Elliptical chainring	Refers specifically to a chainring whereby the features are oval in shape and have bi-axis symmetry.
EMG Intensity	EMG signal resolved in time and frequency permitting an approximation of the signal power within a given frequency band at each time point.
Excursion	Angle of the corresponding joint.
Fascicle	Bundles of muscle fibres bound together by the perimysium.

Load	Continuous application of an opposing force (Watts). In the SRM High Performance Ergometer, resistance is created through adding an electromagnetic field through a metal disk.
Moment arm	Length between a joint axis and the line of force acting on the joint. Larger moment arms create greater load about the joint axis via leverage.
Motor neuron	A nerve cell forming part of the pathway along which impulses pass from the brain or spinal cord to a muscle.
Motor unit	A motor neuron and the muscle fibres innervated by its axon.
Muscle-tendon unit	A muscle together with the attached tendons.
Muscle-tendon unit shortening velocity	The velocity at which the muscle-tendon unit complex shortens.
Muscle activation	The neural signal sent from the central nervous system to the muscle.
Muscle belly	A muscle without the attached tendons.
Muscle architecture	Arrangement of muscle fibres within a muscle relative to the axis of force generation.
Musculoskeletal system	The system of the muscles, bones and connective tissue responsible for converting activation signals from the central nervous system into mechanical output.
Muscle-tendon unit length	The distance from the muscle origin to insertion. Strongly influences the force producing capacities of the complex.
Neuromusculoskeletal system	The combination of the central nervous system and the musculoskeletal system. Functional movement is reliant on the synergy of these systems.
Non-circular chainring	Encompasses any chainring shape where the features deviate from a traditional circle.
Pedal cycle	A complete revolution of the pedal/crank arm.
Pedal speed	Linear velocity of the pedal.
Pedalling rate	The cycle frequency of the pedal.
Segment	Division of body parts into a series of segments linked together by joints.

Thesis Abstract

Optimisation of movement strategies during cycling is an area which has gathered a lot of attention over the past decade. Resolutions to augment performance have involved manipulations of bicycle mechanics, including chainring geometries. Elliptical chainrings are proposed to provide a greater effective diameter during the downstroke, manipulating mechanical leverage and resulting in greater power production during this period.

A review of the literature indicates that there is a pervasive gap in our understanding of how the theoretical underpinnings of elliptical chainrings might be translated to practical use. Despite reasonable theory of how these chainrings might enforce a variation in crank angular velocity and consequently alter force production, performance-based analyses have struggled to present evidence of this.

The purpose of this thesis was to provide a novel approach to this problem by combining experimental data with musculoskeletal modelling and evaluating how elliptical chainrings might influence crank reactive forces, joint kinematics, muscle-tendon unit behaviour and muscle activation. One main study was proposed to execute this analysis, and an anatomically constrained model was subsequently used to determine the joint kinematics and muscle-tendon unit behaviour. Bespoke elliptical chainrings were designed for this study and as such, different levels of chainring eccentricity (i.e. ratio of major to minor axis) and positioning against the crank were presented whilst controlling the influence of other variables known to affect the neuromuscular system such as cadence and load.

Findings presented in this thesis makes a new and major contribution in our understanding of the neuromusculoskeletal adaptations which occur when using elliptical chainrings, showing alterations in crank reaction force, muscle-tendon unit velocities, joint kinematics and muscle excitation over a range of cadences and loads, and provides direction for where the future of this research might be best applied.

Keywords: Elliptical chainrings; Cycling; Musculoskeletal modelling; Principal Component Analysis; Electromyography

Chapter 1 General Introduction

The advent of the modern bicycle is a mark of centuries of engineering success. Originating as the célérifère in 1790, the design of the bicycle has undergone countless innovations and manipulations in a bid to make it a safe and accessible transportation option for all (Figure 1.1). At first, major adjustments were needed, and consequently components such as a braking system, pedals, steerable front wheels, equal sized wheels with rubber tires and a lightweight frame were introduced over time. Accordingly, it has become an extremely efficient form of locomotion, making it no surprise that cycling has become such a popular mode of transport, with recreational and competitive sporting activity contributing to multiple levels of the global economy.

Figure 1.1 Origin of the modern bicycle. The célérifère bicycle of the late 18th Century and a modern-day road bicycle, a design which has largely plateaued aside from minor mechanical modifications aimed at reducing the impact of environmental factors. Figures adapted from Lallement's (1866) patent for the original French velocipede and Bikecad (2018).

Over the course of the 21st Century, bicycle technology has evolved past its initial design flaws and now minor modifications are responsible for its optimisation with the objective of reducing the energy cost of travelling a given distance. Cycle racing is one of the few sports where performance is ascertained by physical output in direct contact with a mechanical device, and as a result, much work has gone into understanding the factors that affect the bicycle and the cyclist in a bid to create the most mechanically efficient model across disciplines. One area which has received lots of attention is the crank-pedal interface and how factors such as crank length (Martin and Spirduso, 2001; Barratt et al., 2016) and anterior-posterior foot position on the pedal (Van Sickle and Hull, 2007) can affect cycling performance. Another consideration has been the design of non-circular

chainrings as a replacement of traditional circular chainrings in a bid to optimise cycling performance and/or efficiency (Hull et al., 1991; Hue et al., 2001; O'Hara et al., 2012).

Non-circular chainrings were first described in 1896 (Sharp, 1896), but drew little attention and quickly faded out of popularity. However, they underwent a resurgence in the late 1970s, with designs such as the Shimano Biopace (Okajima, 1983), the Harmonic that was later relaunched as the O'symetric (Malfait et al., 2006) and the Q-Ring (Cordova et al., 2014) perhaps being the most well-known. The use of non-circular chainrings is prolific across all cycling levels and disciplines. Q-Rings have been used by professional riders in victory in major events such as Tour de France, Giro d'Italia, Vueltra a España, Ironman and UCI MTB World Cup (RotorBike, 2020). The more unusually shaped O'Symetric chainrings have also led to victories across major events and is favoured by Team INEOS athlete Chris Froome, winning three Tour de France titles whilst using these systems (O'Symetric, 2020). Despite their prevalence within amateur and professional cycling communities, there are still a lot of uncertainties surrounding their use. It remains a contentious issue within the topic of non-circular chainrings of how performance-related variables are affected. Since their resurgence 50 years ago, little headway has been made in establishing how they might be used to optimise performance under experimental conditions with physiological and biomechanical parameters being affected in different ways within the literature (Bini and Dagnese, 2012). As such better insight needs to be provided to coaches and cyclists.

In addition to recreational and competitive arenas, cycling offers an excellent paradigm in laboratory experiments given its quasi-constrained nature in which the foot remains in contact with the pedal which rotates in a fixed motion and the pelvis can be kept in contact with the saddle. This level of kinematic control allows the researcher to independently alter cadence and load variables and explore the associated muscle-tendon unit behaviour. As such, cycling is an extremely valuable tool to investigate the *in vivo* response of the neuromuscular system to locomotion in a non-invasive manner. With this in mind, given the outcome of the pedalling motion is heavily reliant on the configuration of the bicycle, further manipulation of the mechanical components can serve as an additional element to study the effects of altered task mechanics on the response of the muscle-tendon unit and muscle activation dynamics. One way this could be achieved is through the use of non-circular chainrings, similar to those used in competition.

The purpose of this thesis was therefore to examine the acute neuromusculoskeletal responses to custom-made elliptical chainrings (Hope Tech, Barnoldswick, UK) in comparison to a circular chainring. There are different designs of non-circular chainrings available, but this thesis will investigate the effects of an elliptical shape. Several biomechanical parameters were collated in order to achieve this such as joint kinematics, reaction forces, muscle-tendon unit behaviour and muscle activation. Chapter Two will critically review the key concepts behind this topic and introduce the neuromusculoskeletal parameters that might contribute to acute adaptations to the elliptical chainrings.

Chapter 2. Literature Review

The overarching aim of this thesis is to quantify the acute adaptations of the neuromusculoskeletal system in response to cycling with elliptical chainrings of differing eccentricity and crank orientation. A secondary aim is to contribute to understandings of *in vivo* behaviour of the neuromusculoskeletal system during human locomotion, which has previously been difficult due to methodological challenges. The existing relevant literature will subsequently be introduced, reviewed and discussed. The focus of this review will be on those findings with specific relevance to the experimental chapters in this thesis, specifically the reaction forces at the pedal expressed during cycling, joint kinematics, muscle tendon unit behaviour and muscle activation dynamics.

2.1 Optimisation of the bicycle

Minimising metabolic cost is thought of as being a key factor of locomotion in humans and animals. Whilst a walking human might consume about 0.75 cal/g/km, energy consumption is reduced to about 0.15 cal/g/km over a given distance when using a bicycle, leading to a five-fold decrease in metabolic cost. This is in conjunction with a 3- to 4- fold increase in travelling velocity, giving cycling a marked advantage over walking. The improvement in metabolic cost is not just limited to human locomotion, but also surpasses machinery and other animals too, seemingly outdoing the course of natural evolution and making them number one in terms of moving creatures and machines (Fig 2.1; Wilson, 1973). The bicycle's evolution to the feat of engineering available today has therefore culminated in it being one of the most metabolically efficient forms of locomotion. Despite this there are still avenues for improvement through tailoring the bicycle equipment and large efforts have gone into exploring how to optimise metabolic (Hull et al., 1992; Hue et al., 2008) and mechanical work (Zamparo et al., 2002; Samozino et al., 2006). One area of interest is the product of the forces acting upon the bicycle and rider.

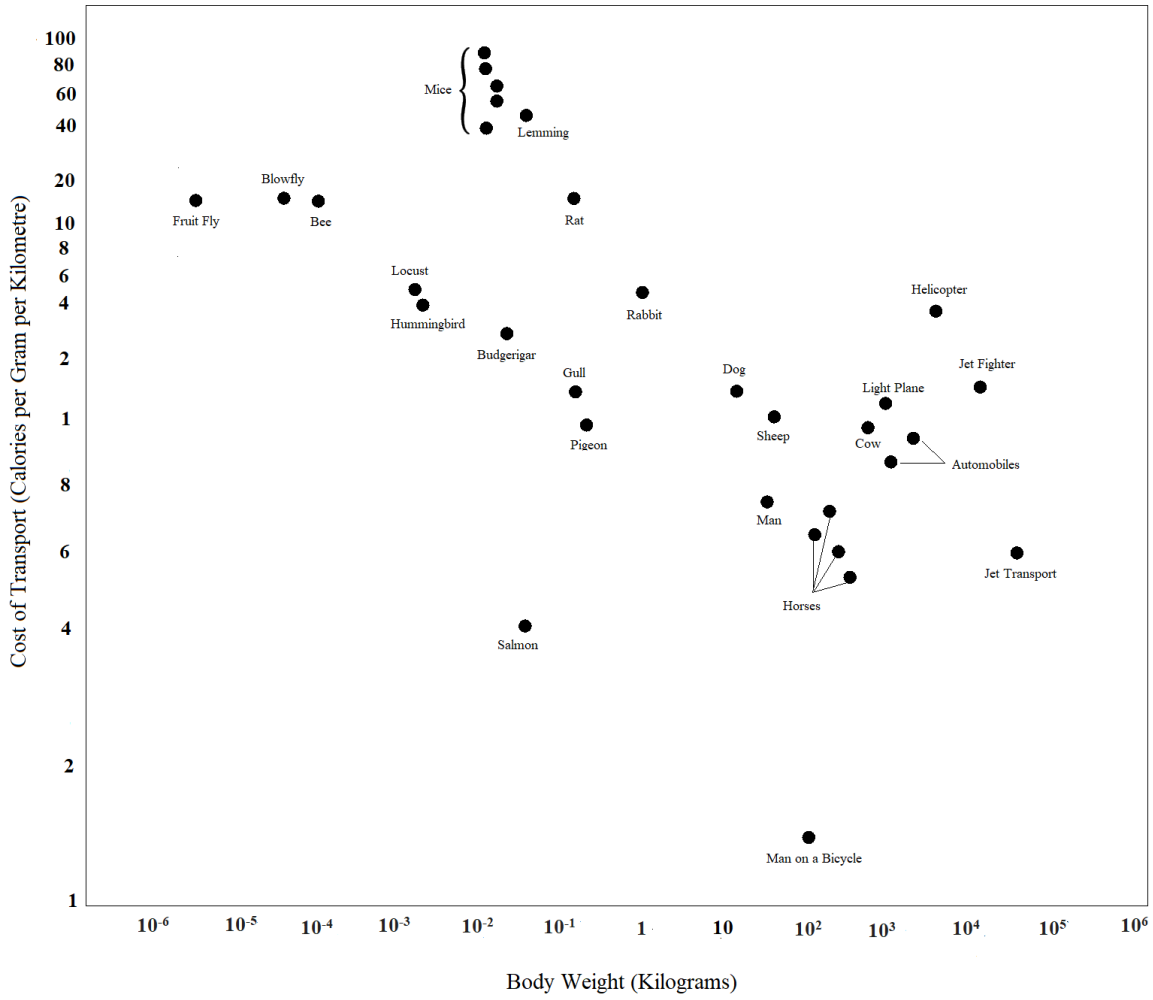

Figure 2.1 Rankings of travelling animals and machinery in terms of energy consumed whilst moving a certain distance as a function of body weight. Adapted from Wilson (1973).

2.2 Components of force

Cycling performance can be determined by the amount of propulsive forces produced versus the amount of resistive force that must be overcome. Augmentation of propulsive forces with simultaneous decrements in resistive forces will result in greater performance. The propulsive forces are often affected by internal biomechanical factors, external mechanical factors and their subsequent interactions. Alternately, resistive forces are a function of environmental forces and internal mechanical forces such as operations of the muscle fibre force-length-velocity profiles (Figure 2.2; Too, 1990).

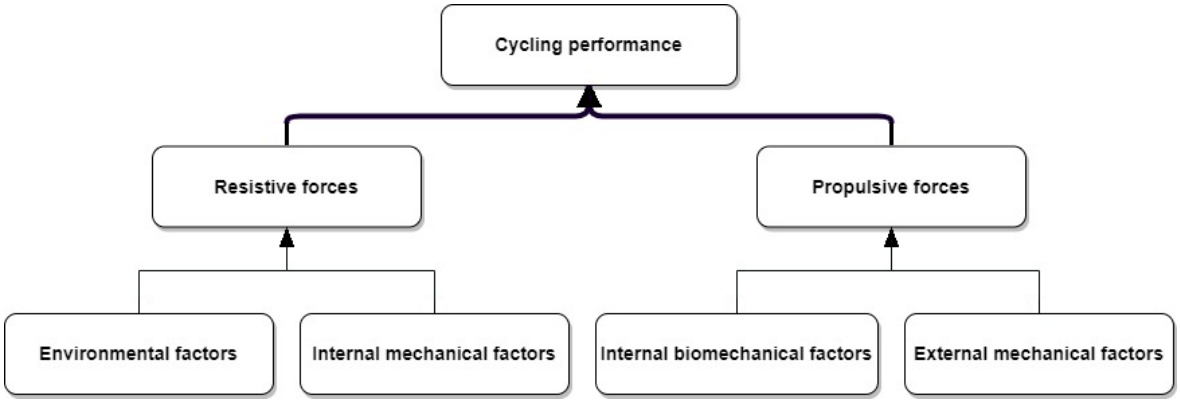

Figure 2.2 Factors affecting cycling performance. Adapted from Too (1990).

Internal mechanical factors include joint friction during movement, synovial fluid viscosity, and stiffness within the muscle fibres, connective tissue and collagen. Insufficient hydration can result in a decrease in levels of compliance within the collagen and increase in stiffness within connective tissues and muscle fibres which result in increments in internal resistive forces within the muscle fibres during contraction and movement (Haut and Haut, 1997; Maganaris et al., 2004; McDaniel et al., 2007). Heat applied externally to the muscle, joint and surrounding tissues acts to increase the temperature of the muscle fibres and consequently decrease the viscosity of the synovial fluid within the joint capsule, thus decreasing internal frictional forces and total resistive forces inhibiting muscle contraction and movement (Faulkner et al., 2013). Heat generated internally by the active contraction of muscle through a 'warm up' is generally more effective in enhancing potentiation of contractile complex and muscle activation (Škof et al., 2007) than external heat application. Warming up will also ensure that there is adequate lubrication of synovial fluid and the boundary lubricant lubricin (PRG4) in articulating cartilage surfaces placed under load, producing a coefficient of friction (μ) on the order of ~0.01 or less and thus helping to reduce damage of these surfaces during motion (Jay and Waller, 2014). These parameters are universally understood. Elite cycling competitors are ensured to be of adequate hydration levels prior to training and competition. Warm ups are commonplace, and more recently, specially designed heat pads have been implemented prior to elite competition to ensure that muscles remain at an optimum temperature between warm up and race onset (Faulkner et al., 2013).

There also exists a wealth of widely recognised information describing how environmental factors such as gravity, friction and air resistance influence cycling performance (Barry et al., 2015; Davies, 1980; Fintelman et al., 2015; Welbergen and Clijsen, 1990). The extent to which they impede the rider is governed by a plethora of considerations as identified in Figure 2.3. The axiomatic nature of environmental influences has made these factors far more predictable than those determining propulsion, thus allowing them to be uncoupled from the maintenance/maximisation of propelling the bicycle, and creates a paradigm which is well suited to modelling approaches (Defraeye et al., 2010; Blocken et al., 2013). As such, much has been done to minimise the impact of the resistive forces on the cyclist, whilst optimisation strategies concerning propulsion forces still presents challenges.

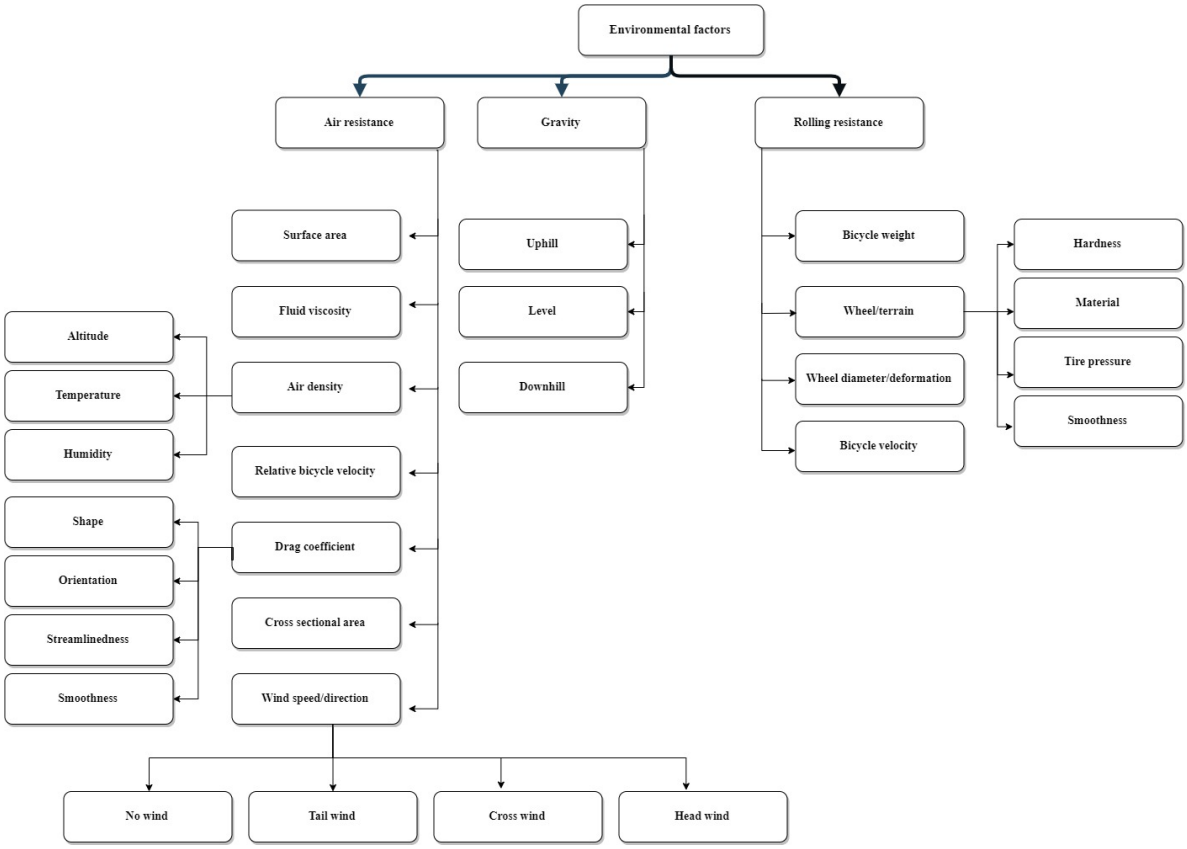

Figure 2.3 Environmental factors affecting cycling performance. Adapted from Too (1990).

Consequentially, the large emphasis placed upon reducing resistive forces dominates much of the performance strategies in place, and potentially limits consideration of how propulsive force could be maximised. This is in part due to the complexity of the interactions between the internal biomechanical variables related to force/torque development and power production (Figure 2.4). The intricacy of such relationships means

that they are seldom considered in the engineering of equipment and they remain largely misunderstood. Proficient manipulation of such variables can result in the modification of effective muscle force/torque/power production and the way this is transferred to the bicycle.

External mechanical factors presenting constraints are those imposed on the cyclist through the structural configuration of the bicycle and how it is engineered to interact with power transmission. There is an array of possibilities which include: seat tube angle; seat height; seat to pedal distance; crank arm length; handlebar positioning; chainring shape and diameter; foot-pedal position; gear ratios; wheel size, mass, diameter and inertial properties; body position, orientation, and joint configuration; and power transmission losses resulting from friction. Careful manipulation of these parameters has the ability to alter joint angle kinematics, muscle fibre length, resistance load, muscle mechanical advantage, and the ability to produce force/torque/power (Burke, 1986).

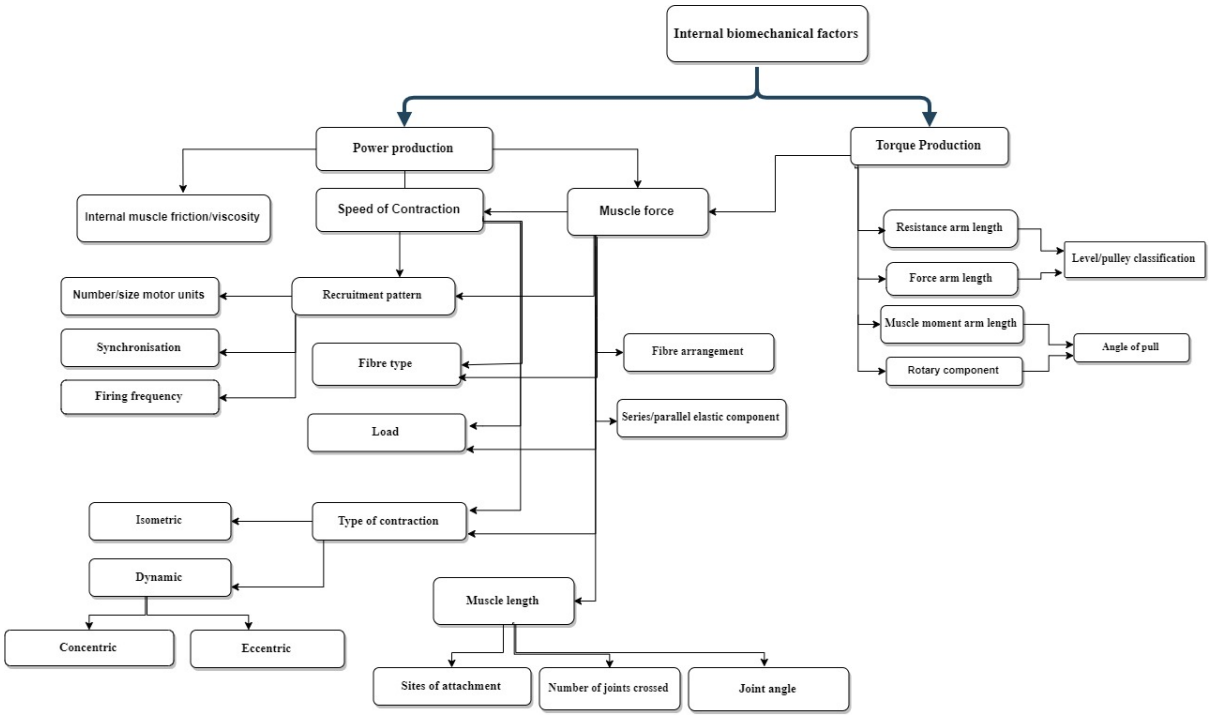

Figure 2.4 Internal biomechanical factors affecting cycling performance. Adapted from Too (1990).

Propulsive force is, therefore, a function of the interplay between internal biomechanical factors in developing force, torque and power. However, this notion is convoluted further when considering that alterations in bicycle geometry not only affect propulsive forces, but

also influence the type of resistive forces met in terms of environmental factors and the resulting interaction between these variables. Such changes have the ability to alter joint angles, muscle lengths and muscle moment arm lengths, therefore, affecting the effectiveness of force production via alterations in the tension-length, force-velocity-power relationships of multi-joint muscles, ultimately manifesting itself as a change in the energetics of cycling. Due to the complexity of musculoskeletal dynamics much of what is understood about skeletal muscle function during human locomotion has been indirectly inferred from correlations between anatomical classification, inverse dynamics analysis and electromyographic activity (EMG) analyses; however, there is a difficulty in developing causal relationships between muscle excitation and task performance during locomotion from these correlations alone (Kautz and Neptune, 2002). However, the implementation of mathematical arguments used to drive models have enabled researchers to gain valuable insight in those parameters and phenomena (Zajac, 1989; Winters, 1990) previously difficult to elucidate when solely relying on experimental data (Biewener et al., 1998; Shadwick et al., 1999). Using cycling as a paradigm to weave experimental data into model-driven simulations has provided insight into how forces interact between the leg segments and the external environment (Kautz et al., 1994; Raasch et al., 1997; Rankin and Neptune, 2008). Through the development of open-source simulation software (e.g. OpenSim; Delp et al., 2007), researchers can now investigate questions about muscle behaviour during locomotion and locomotion performance resulting from alterations in muscle behaviour. Within the context of this thesis, integrating musculoskeletal simulation and experimental data will be used to explore how the neuromusculoskeletal system responds to changes in drivetrain kinematics.

2.3 Decomposition of pedal forces

Developments in strain-gauge technology have led to an improved understanding of the interaction between pedal force and resultant crank torque. Pedal forces are commonly described in component terms, with those responsible for developing torque around the crank spindle being described as being propulsive forces. These loads are described as the normal (acts in the direction of the pedal arm) and tangential (acts tangentially to the circle being described by the pedal), or as labelled in Figure 2.5, F_N and F_T (Newmiller et al., 1988). It is only the F_T which contribute to the turning of the crank. With prior knowledge of the

pedal angle in relation to the crank angle, these components can be mathematically resolved into effective (F_E) and ineffective (F_{IN}) components. The F_E acts perpendicularly to the crank, generating a torque that is transmitted through the bicycle chain and to the wheel. It is seen to vary substantially throughout the pedal cycle, with peak torque typically occurring at approximately 100° past top dead centre. Most studies report negative F_E in the recovery phase, indicating that the effective component of pedal force is acting against the direction to crank propulsion, and resulting in resistive force for the contralateral leg. The F_{IN} component acts parallel to the crank arm and thus only acts to lengthen or compress the crank, and thus produces no useful external work in propelling the crank (Figure 2.5). The two schemes of force components at the crank and the pedal are related, however their relationship is dependent upon the positioning of the crank. The vector sum of the F_E and F_{IN} is the total force applied to the pedal and is referred to as the resultant force (F_R).

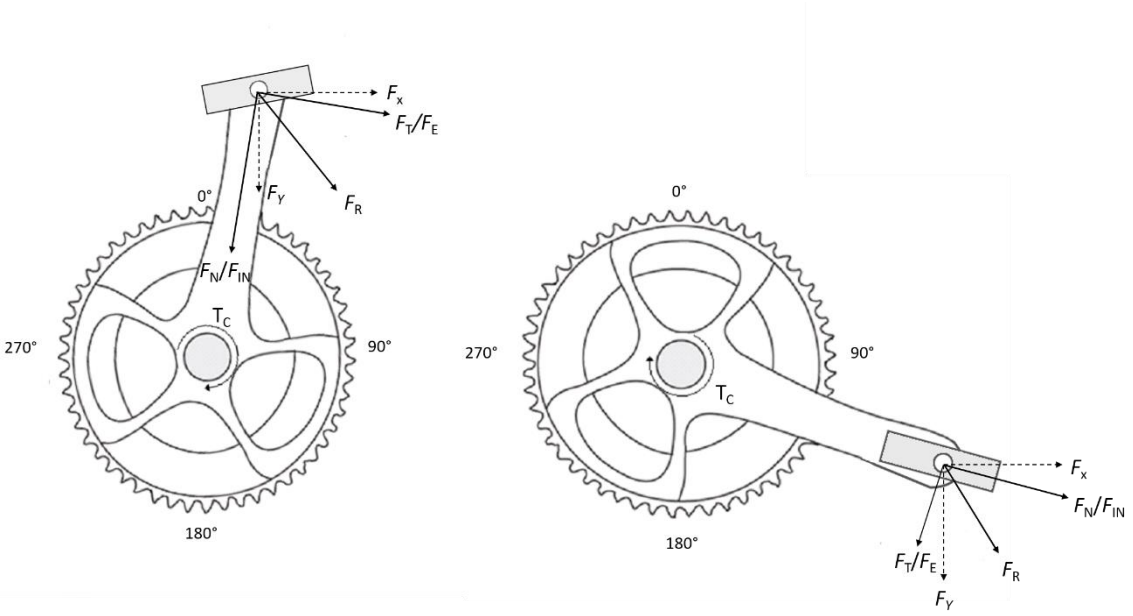

Figure 2.5 Schematic of forces acting on the pedal and relationship of crank angle on these schemes: resultant force (F_R), horizontal force (F_X), vertical force (F_Y), tangential force (F_T), normal force (F_N), effective force (F_E) and ineffective force (F_{IN}) applied to the pedal. T_C represents the torque created about the crank centre generated by F_E. Adapted from Coyle et al. (1991).

When considering the impact of the force components on cycling performance, pedal force effectiveness is a commonly used measure. It is defined as the ratio between the force magnitude perpendicular to the crank arm (i.e. producing a moment of force and consequently, work on the crank) and the F_R generated on the pedals, or the sine of the angle between pedal force and crank (Bini et al., 2013). It has been used as a gold standard

measure of pedalling technique, as applying optimally orientated forces on the pedal during cycling is a major component of skilled performance (Dorel et al., 2009). From an energetics perspective, energy usage could be considered wasteful given the lack of the ineffective static component of force overall contribution to external power. An increase in exercise intensity seems to be associated with an optimisation of the force applied to the pedals, and a decrease in effectiveness leads to an increase in oxygen uptake (Patterson and Moreno, 1990).

As already identified, F_{IN} produced at the bottom or top dead centres of the crank cycle does not contribute toward angular motion of the crank and, ultimately, crank propulsion; however, this does not mean this component is free of energy cost, given a requirement to convert the potential energy stored in the muscle-tendon units at the top dead centre to kinetic energy towards the bottom of the pedal cycle (Kautz and Hull, 1993). Similarly, if there is no resistance on the bicycle wheel, an energy requirement persists in order to keep pedalling, resulting in augmented internal work production. Changing the direction of the limb's motion over the course of bottom dead centre does not require energy from the ipsilateral leg, however, there is an energy cost associated with the contralateral leg lifting the other leg and the inertial effect of converting potential to kinetic energy which contributes to the angular momentum through the bottom dead-centre. Improving the effectiveness of the pedalling technique, whereby the contribution of F_{IN} is reduced whilst simultaneously increasing the ratio of F_E to F_R applied to the pedal, would increase the metabolic energy through increasing the magnitude of biceps femoris and its action as a hip and knee flexor (Mornieux et al., 2010). Despite the intention of this technique being to efficiently orient the total force on the pedal, due to the constrained position of body segments on the bicycle and of the muscle in respect to the bones, a certain amount of F_{IN} is needed to work efficiently.

Maximising F_E relative to total force implies minimising the F_{IN}, however, due to the constrained position of body segments on the bicycle and of the muscle in respect to the bones, a certain amount of F_{IN} is needed to work efficiently. This is represented in Figure 2.6, which depicts the manner in which pedal forces vary throughout the pedal cycle. Here, it can be seen that peak crank torque occurs at around 100° past top dead centre, and forces are most vertically orientated at top and bottom dead centre, which is where F_E are

close to zero, whilst, considerable F_{IN} are dominant in this sector. Abolishing these F_{IN} altogether would lead to significant muscle work given their role in supporting movement direction, despite no muscular work contributing to their production, signifying that they are not altogether wasted (Broker, 2003).

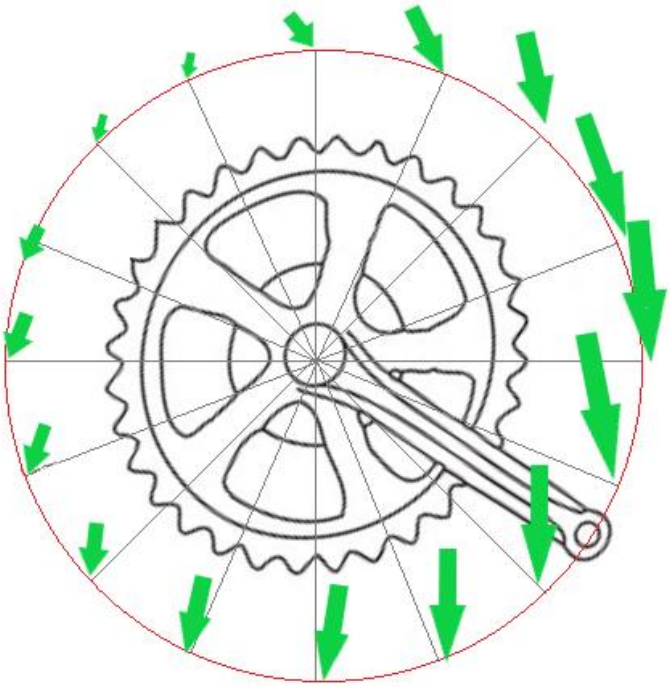

Figure 2.6 Pedal vector force. Visualisation of the resulting pedal forces during one complete cycle. Arrow lengths represent the magnitude and directions of the applied force. Figure is adapted from Broker (2003).

Muscular forces accelerate the legs whilst the foot-pedal connection ensures that the resulting movement of the foot follows a constrained, circular path around the crank axis. Consequently, pedal forces not only reflect muscular activity, but also depend on external forces. As a result, the applied pedal force cannot be understood independent of the dynamics of the cycling movement. With this in mind, researchers presented a method of separating these distinct components of pedal force (Kautz and Hull, 1993), and, as such, enhancing the understanding of the mechanical cost of cycling. Consequently, two further force components have been identified, separating the total pedal load into muscular-based torque production which leads to moments generated in the hip, knee and ankle joints; and naturally occurring non-muscular forces which may influence pedal or crank forces (e.g centripetal, Coriolis and gravitational; Fregly and Zajac, 1996). The relationship between these components is highlighted in Figure 2.7.

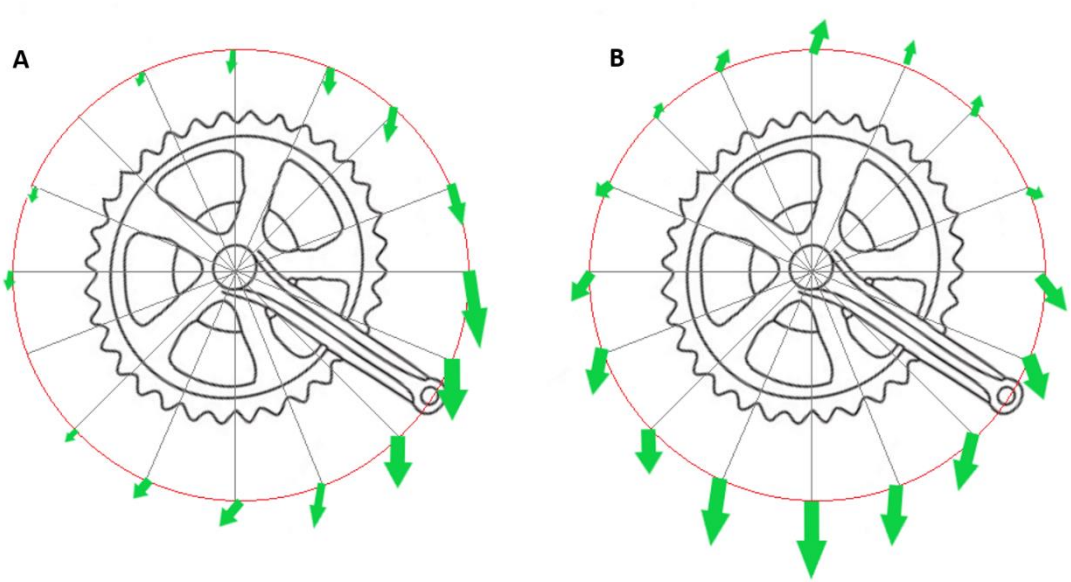

Figure 2.7 Muscular and non-muscular pedal loading vectors. Visualisation of the (A) muscular and (B) non-muscular pedal forces during one complete cycle. Arrow lengths represent the magnitude and directions of the applied force. The muscular and non-muscular components sum to create the total pedal load depicted in Figure 2.6. Figures are adapted from Broker (2003).

Further to this, muscular forces have been found to reduce as pedal speed increases owing to the contractile properties of the muscle, while non-muscular pedal forces increase linearly with pedal rate (Neptune and Herzog, 1999). Given that gravitational forces have been found to be largely unaffected by cadence transitions (Brown et al., 1996), the augmented contribution of non-muscular components to total pedal forces at increased cadences could be attributed to the influence of crank inertial load ($kg \cdot m^2$), creating a centripetal force about the crank (Baum and Li, 2003) and interacting with the muscular components in, what could best be described, as a quadratic relationship (Figure 2.8). Crank inertial load has the effect of dampening changes in the crank angular velocity over the course of a pedal cycle (Edwards et al., 2007) and given that during steady state cycling with conventional drivetrain kinematics, fluctuations in the velocity of the cranks exist (Gregor et al., 1991); the effect of this component should be carefully considered when employing alternate task mechanics which might seek to manipulate crank angular velocity (Rankin and Neptune, 2008). This is could be of great importance within the context of understanding the mechanics of drivetrain kinematics as altered crank inertial loads have been found to impact propulsion biomechanics as noted by Hansen and colleagues (2002), with peak torque being found to be greater at higher inertial loads.

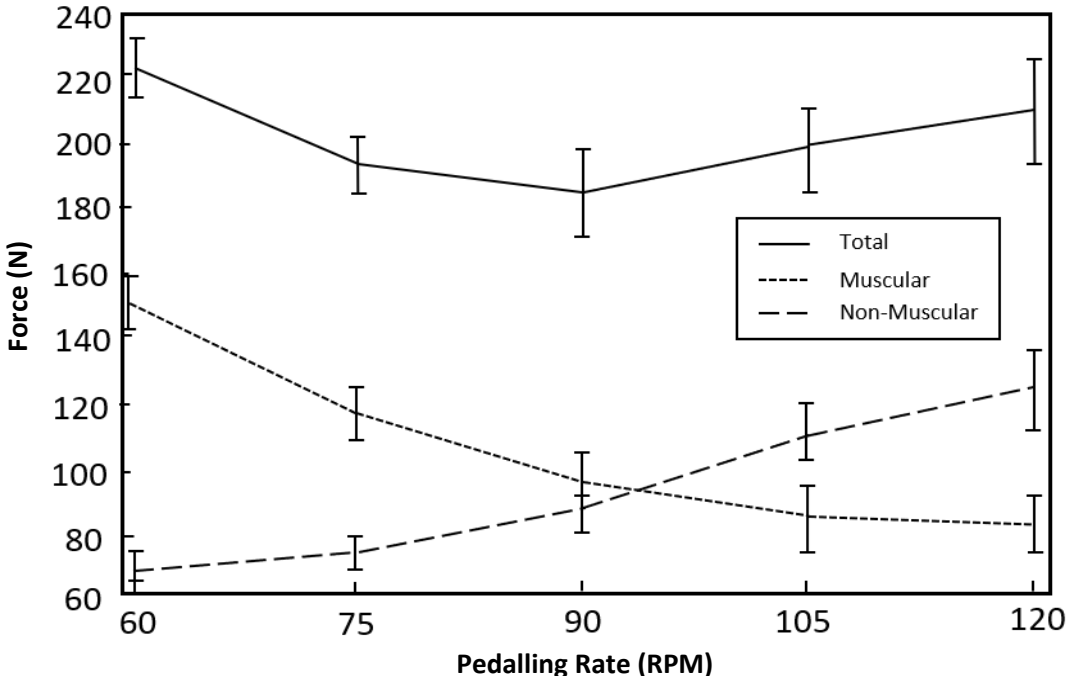

Figure 2.8 Relationship between pedal force components and cadence. Diagram to show the quadratic relationship between cadence and muscular and non-muscular components and their contribution to total pedal force when at fixed power outputs. Adapted from Neptune and Herzog (1999).

2.4 Skeletal muscle contractile properties

An individual's ability to perform functional movements is determined by a range of mechanical properties, including the force and power producing capabilities of the skeletal muscle and the interaction of how the force and power outputs are coordinated between different muscle groups. The ability of whole muscle to generate force is dependent on its architecture and size. This is because a muscle's effective physiological cross-sectional area (PCSA; calculated using muscle volume, fascicle length and pennation angle) is representative of its total area of muscle fibres, which is directly proportional to the maximum force that it can produce and is therefore indicative of force-generating capacity (Powell et al., 1984). Meanwhile, the ability of the individual muscle fibres to generate force is governed by the principles of activation, length and velocity (Gordon et al., 1966; Hill, 1953). Fascicle length influences the distance over which muscles can contract to do work [work (J) = distance (change in length; m) × force (N)] and therefore the contractile ability (excursion and velocity) of the muscle. These concepts are well understood in isolation,

however, may not be representative of how the muscle behaves *in vivo* and in unison with tendinous tissue (tendons and aponeuroses). Whilst it is typical for voluntary movements to occur when the muscle undergoes concentric contraction and shortens, other muscles may actively lengthen during eccentric contractions, allowing energy to be dissipated for control of inertial movements, or to undergo brief periods of active stretch prior to shortening, acting to enhance force development and the amount of work performed. Additionally, muscles may develop force isometrically, consequently performing little mechanical work but providing greater and more economical force generation and allowing for tendon elastic energy recovery. Under each of these conditions, muscle force and velocity are affected by the timing of muscle activation and deactivation, as well as the variance in external load during the locomotive activity, making force and velocity time varying entities, which rarely remain constant. Therefore, it is important to understand how these properties function in relation with each other (Biewener and Roberts, 2000).

For a given mass of muscle, fascicle length and PCSA are inversely proportional, and based upon their limb location and primary function, they typically specialise towards a greater working range or force production, and a trade-off exists between these two entities (Lieber and Friden, 2000). Within vertebrate species, general pattern has been established that many proximal limb muscles are specialised for doing mechanical work (with long parallel-fibred muscles), whilst distal muscles are specialised in the generation of large forces and storing and recovering mechanical energy as an energy saving mechanism due to their pennate architecture and compliant tendons. This is because parallel fibres cause a larger muscle shortening than pennate fibres (Biewener and Roberts, 2000), and consequent to then acting at a lower part of the length tension relationship, have higher force depression (Burkholder and Lieber, 1996), while a muscle with pennate fibres with a larger PCSA has a higher peak force (Wilson and Lichtwark, 2011). Joint torque is produced by the force exerted by these muscle fibres and the tendinous tissue is deformed in the process. The relationship between length of muscle-tendon unit complex and muscle fibres is consequently altered by the variation in moment arm. Therefore, taking into account that fibre length and contraction velocity affect the force development capacity in line with force-length and force-velocity relationships, tendon mechanical properties can impact the relationship of muscle force to joint angle and/or to angle velocity (Muraoka et

al., 2001).

The characteristic force-length relationship demonstrates that the greatest force production occurs at a specific length (Figure 2.9A), defined as the optimal fibre length (L_O), dictating that at shorter or longer lengths the muscle's ability to generate force depreciates in accordance with a reduction in the effective overlap of contractile proteins (Huxley and Simmons, 1971). More recently, it has also been proposed that, under isovolumetric conditions, radial forces occurring during contraction require alterations in myosin and actin dynamics through changes in the lattice spacing that also augment the effects of variations in length and the length-tension curve (Williams et al., 2013). The effects of muscle shortening velocity on muscular force production were first reported by A.V. Hill (1938). The hyperbolic equation primarily presented force as decreasing with increased shortening velocity (Figure 2.9B). These traditional force- and power-velocity relations are determined from protocols that allow the muscle to become fully excited before shortening, and therefore, are not influenced by activation-deactivation dynamics. Additionally, despite these relations typically being portrayed as continuous functions, they are formed from isolated contractions in which the muscle shortens against several discrete loads. Conversely to the discrete velocities and loads used to determine traditional force-velocity properties, a variable muscle shortening velocity is associated with most functional movements. During locomotion, velocity will generally be at zero at the start and end of a movement (i.e., maximal and minimal joint extension) and peak velocity will be reached at some intermediary point within the movement. Movements such as this will often produce a sinusoidal length trajectory, and therefore, velocity will follow a cosine function. Because velocity varies substantially within a given movement variation, relationships between average muscle force and average shortening velocity may not be immediately apparent (Martin, 2007). At slow shortening velocities, muscles are still capable of producing relatively large forces, however, an exponential decrease in force generating capacity is observed as the speed of shortening increases until the muscle reaches its maximum shortening velocity (V_{max}) (Caiozzo and Baldwin, 1997).

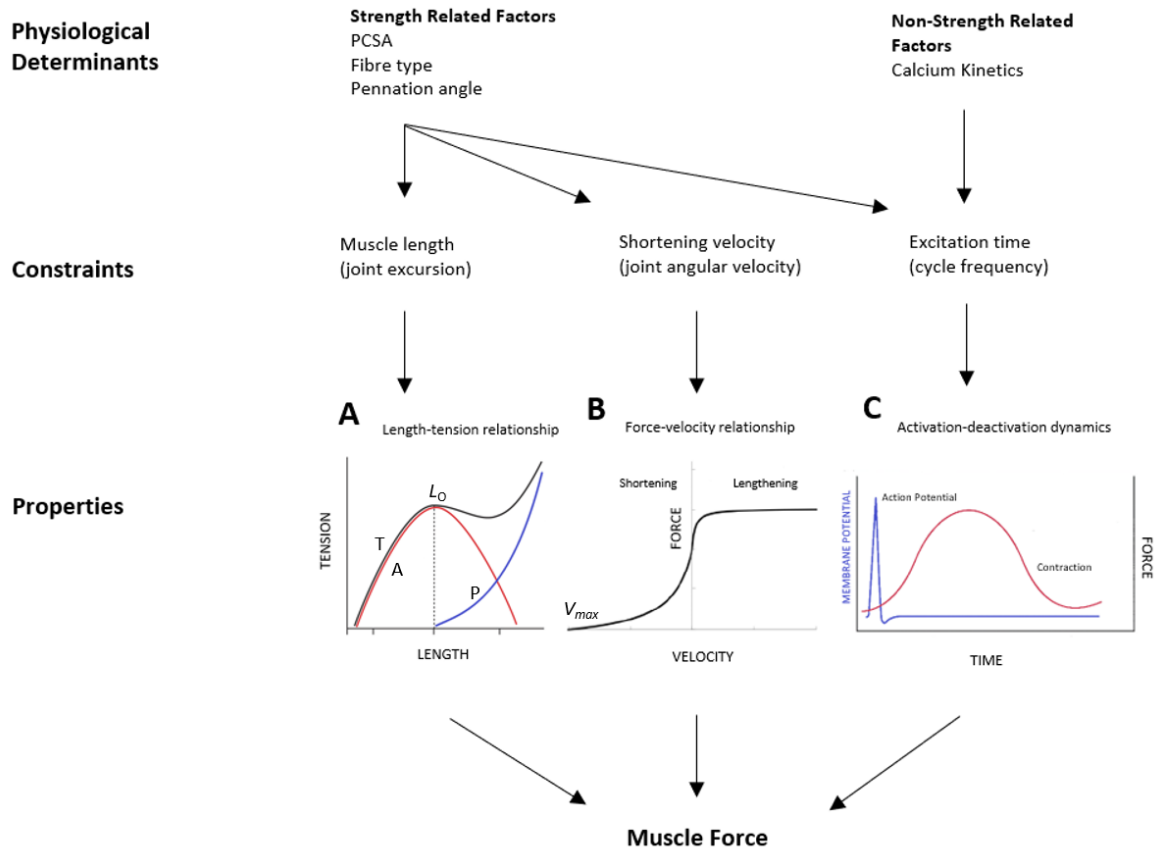

Figure 2.9 Schematic illustrating the relationship between contractile properties and the production of muscle force. A hypothetical length-tension relationship of skeletal muscle, where the active tension (A; red line) generated by the muscle reaches a maximum at the optimum contractile element overlap (L_o) and decreases as the muscle is shortened or lengthened. Passive tension (P; blue line) is generated by the connective tissue with and around the muscle, increasing as the muscle is stretched to longer lengths. The total muscle tension (T; black line) is determined by the contributions of both the active and passive elements. (B) A hypothetical force-velocity curve for skeletal muscle, where eccentric (lengthening) and concentric (shortening) contractions are capable of producing muscle forces. As the velocity of shortening increases, there is an exponential decrease in maximum force capacity of the muscle until reaching the maximum shortening velocity (V_{max}). (C) A hypothetical action potential and subsequent contraction for skeletal muscle, where the electrical signal of depolarisation of the fibre leading to the peak in muscle tension is met with a delay during the rise in muscle stimulation (excitation dynamics) followed by the delay during the build-up of tension (contraction dynamics).

Additionally in the muscle-tendon unit (MTU), a ratio between the MTU velocity (V_{mtu}) and fibre velocity (V_f) represents a phenomenon known as MTU gearing. Here, the compliance and stretch of the tendons can result in an uncoupling and displacement between the velocities, allowing the muscle belly to shorten at rates in keeping with the muscle fibres optimal velocity. This indicates that focusing entirely on the shortening velocity of the fibres might not give an accurate depiction of what is happening in the muscle as a whole in the process of translating muscle fibre forces into joint torques (Wakeling et al., 2011). Wakeling and colleagues (2011) reported increases in MTU gearing ratios occurring at

higher cadences, postulating that this allowed the slowest fascicles in the muscles of the triceps surae to contribute more usefully to contractile force at faster pedalling rates. A thorough understanding of the length and velocity properties of the muscle are therefore imperative, given they may constrain force production, and the subsequent impact this has on the ability to generate mechanical power in dynamic movements such as running and cycling (Biewener, 2016).

2.5 Implications of mechanical muscle properties during cyclic locomotion

During cyclic locomotor tasks, the intrinsic properties of the muscles impose constraints that the nervous system overcomes by activating and deactivating at a suitable point in time, whilst controlling the magnitude of force (de Koning et al., 1991; Jacobs & van Ingen Schenau, 1992). The coordination requirements that this places on the muscle highlights why mechanical interactions observed during maximally activated, isolated muscles do not always translate across to locomotion. Subsequently, optimal coordination strategies are task dependent. The outcome during a submaximal task might be to optimise the patterns toward energy expenditure conservation (Anderson and Pandy, 2001) or minimise neuromuscular fatigue (Neptune and Hull, 1999). Alternatively, during maximal locomotion, it is probable that the optimal intermuscular coordination strategy would exploit the mechanical properties of the muscle (activation and deactivation dynamics and force-velocity-length relationships) (Jacobs & van Ingen Schenau, 1992; van Soest and Casius, 2000).

Cycling provides an ideal paradigm to study these principles as the foot-pedal interface ensures that the lower limbs remain kinematically constrained over a repetitive motion, with an amenability to manipulation and modelling, therefore allowing researchers to investigate mechanical muscle properties via altered joint kinematics (Martin and Spirduso, 2001). Utilisation of cycling as a model for such investigations allows for movements to be performed under both submaximal and maximal conditions, yet remain predictable and consistent, whilst considering mechanical muscle properties (Dick et al., 2017) and intermuscular coordination patterns (Wakeling et al., 2010; Blake et al., 2012).

Over the course of a pedal cycle, the leg undergoes a cyclic action of flexion and extension, with the course of the joints being predominately dictated by the fixed entities which are

bicycle geometry, pedal spindle path and leg segment length. Despite this, a certain level of freedom is available for the cyclist to alter the movement of the leg through manipulating motion at the ankle and hip joints. These biomechanical 'degrees of freedom' allow the cyclist to choose to position their ankle in a heel up or down pedalling style, and to modify the amount of side-to-side rocking at the pelvis. Despite this allowing for some degree of variation over the course of the pedal cycle, the possible movement patterns during cycling are far fewer than those in other movements such as swimming, running or walking.

During the downstroke, when the leg is extending, the hip and knee joints go through the largest ranges of motion, and it is the muscles which act upon these joints which provide the largest contribution to overall cycling power (Ericson, 1988) and generate the largest joint moments (Mornieux et al., 2007). The largest and most powerful hip extensor muscle is the gluteus maximus. The most important knee extensor muscle group is the quadriceps femoris, which is comprised of four separate muscles, with the vastus medialis and lateralis having the largest impact on force production. The knee extensors and hip extensors consist of two of the largest muscle groups in the human body and are consequently well suited to produce high power outputs. During the leg extension phases, there is a significant power contribution from the ankle extensors (plantar flexors), the most important being the gastrocnemius and soleus muscles. Nonetheless, joint velocity is much lower at the ankle joint, and consequently joint powers and muscle force contribution to mechanical power production is lower than that of the hip or knee (Ericson, 1988). In addition to production of power, this muscle group also play an important role in stiffening the ankle joint so that the power created at the knee and hip extensors can be transferred to the pedal (Martin and Nichols, 2018). Due to the constrained nature of the cycling motion, joint powers are only responsible for propulsive action during certain portions of the pedal cycle, which remains relatively constant regardless of changes in cadence and power output (Mornieux et al., 2007). Despite this, it is possible to implement an alteration in joint moments and powers, adopted through a change in position (Caldwell et al., 1999) or bicycle geometry such as seat height (Sanderson and Amoroso, 2009) or crank length (Too, 1990), ultimately manipulating strain and strain rates for given joint motions (Rome et al., 1988).

Considering the whole muscle in detail generates an ability to discern the type of functionality they allow for, as their ability to produce power is dependent on the volume and architecture. Parallel fibred muscles (such as the bicep femoris and semitendinosus of the hamstring group) are arranged so that the fibres run along the length and in the direction of force transmission. Pennate fibred muscles (such as rectus femoris and vastus lateralis of the quadriceps groups, classified as bipennate and unipennate respectively) have shorter fibres, packed at an angle that does not correspond with the main axis of force transmission. The significance of this is related to the length of fascicles such formation allows for. The majority of muscles in the leg are responsible for either eliciting or resisting movement, and so joint angle changes that ensue during muscle lengthening or shortening help in fulfilling their function, which is subject to change at different points of a locomotive action (da Silva et al., 2016). Muscles with long fibres and short moment arm can produce large angular displacement and a high angular velocity with a small torque and initial acceleration (Biewener and Roberts, 2000). Conversely, short fibred muscles with long moment arms produce larger joint torques and movement forces.

One of the primary requirements of a muscle is shortening to generate tension and leading to the performance or absorption of mechanical work. Peak power is developed at around one third of maximum contraction velocity and peak efficiency of performing mechanical work at a lower velocity (Woledge et al., 1985). Where exactly this value falls is dependent on the shape of the power-velocity curve. Therefore, a muscle's PSCA needs to be sufficient at generating forces at appropriate velocities and adequately long fibres to operate at a strain rate around or below that corresponding to peak efficiency or peak power. Those muscles needing to generate both high force and perform work such as the knee extensors are subject to a trade-off which limits the L_O. Short fibres reduce the costs associated with the generation of high forces; however, long fibres reduce sarcomere shortening velocity for a given fibre shortening speed and thus reduce the cost of performing mechanical work. It is also important to consider that larger muscle volumes also increase limb inertia and muscle inertia as during submaximal contractions the actively contracting fibres must work to accelerate both their own mass, and the mass of the remaining inactive fibres (Ross and Wakeling, 2016).

Muscle force is also dependent on the activation state, which is determined from the electrical signals, elicited by the nervous system via the motor neurons. When the signal is above a certain threshold, an action potential occurs and results in the depolarisation of a muscle cell. Such an event initiates the release of calcium ions from the sarcoplasmic reticulum and triggers a cascade of events culminating in the binding of myosin heads to nearby actin filaments allowing cross bridges to form and generate force (Huxley and Simmons, 1971; Neptune and Kautz, 2001). The delay between the neural excitation arriving at the muscle and the development of force (Figure 2.9C) and the subsequent relaxation when muscle force returns to zero is encompassed within activation-deactivation dynamics, and primarily results from calcium kinetics and cross bridge attachment and detachment rates (Zajac, 1989). The summation of these principles are outlined in Figure 2.9.

To achieve functional movement, the appropriate number and combination of motor units and hence muscle fibres, must be recruited. Most skeletal muscles contain a mixture of fibre types. These can be classified by their characteristic movement rates, neural inputs and metabolic properties, and consequently can be distinguished into “slow twitch” (type I) and “fast twitch” fibres (type II), of which there are two major subtypes in humans: types IIA and IIX; depending on cellular metabolic programming (Schiaffino and Reggiani, 2011). The response to stimuli varies significantly between the fibre types, and whereas fast twitch fibres fatigue more rapidly, they possess a higher maximum shortening velocity and faster activation-deactivation rates compared to slow twitch fibres. Some contention has arisen concerning the way in which they are recruited. Whilst the ‘size principle’ is the generally accepted rule, which purports that the neural recruitment of motor units is governed by their size, recruiting the smallest α-motoneurons first and following sequentially with the recruitment of increasingly larger motor units until the force demands are met (Henneman et al., 1965). This is then reversed, as motor units are de-recruited from largest to smallest as the force demands decrease (Henneman et al., 1965). Orderly recruitment of slow to fast twitch muscle fibres provides a convenient method of ensuring the more fatigue resistant fibres are enlisted first, and therefore allowing faster motor units to be reserved for high intensity tasks and an overall smooth increment in force production (Zajac and Faden, 1985).

Since this pivotal work in motor unit recruitment patterns was proposed, there have been reports that orderly recruitment may not always be favourable, and variance might actually occur in some cases to meet specific task mechanical needs, with evidence provided in animal studies (Hoffer et al., 1987; Hodson-Tole and Wakeling, 2007) and human locomotion (Von Tscharner and Goepfert, 2006; Blake and Wakeling, 2015). When considering the impact this has on cycling performance, it is conceivable that cycling at a low cadence with a constant power output will require high muscle forces to be obtained per cycle, which could be achieved through progressive recruitment of higher threshold motor units to meet this demand. However, the mechanical demands of high cadence cycling dictate that faster twitch muscle fibres contribute more to maximum power given their force-velocity-power properties (Beelen and Sargeant, 1991; Blake and Wakeling, 2015).

2.6 Situational specificity

Just as the recruitment of muscle fibres cannot be generalised across all locomotive situations, studies examining joint level mechanical outputs during cycling have highlighted how maximal cycling is not simply a scaled-up version of submaximal cycling. The extent of this can be seen in the significant differences in joint kinematics between submaximal and maximal cycling; and more specifically, a greater proportion of the pedal cycling is spent in extension rather than flexion during maximal cycling as compared with submaximal (Martin and Brown, 2009; Elmer et al., 2011). Additionally, maximal cycling places greater reliance on hip extension and knee flexion as well as greater contribution for the upper body (Elmer et al., 2011; Mcdaniel et al., 2014). In addition to the way in which fibres are recruited at augmented pedal speeds, muscle force is also affected by cycle frequency via excitation state. More specifically, muscle excitation has been found to be incomplete at high cadences in association with a shift in activation-deactivation dynamics seen in the muscle in accordance with the altered joint actions, which consequently reduces force output in comparison with a muscle in a fully activated state (Caiozzo and Baldwin, 1997; Martin, 2007). This effect is joint dependent (Elmer et al., 2011), and the extent of phase shift (timing of the activation) is different across muscles (Blake and Wakeling, 2015). Further, research from Blake and Wakeling (2015) suggests that

adaptation in the timing of activation is sensitive to cadence increments rather than workload. This is an important consideration when procuring insight into any alteration in mechanical demands during cycling, and results from one paradigm may not be generalisable to the other.

During the course of a pedal cycle, the movement pattern represents the nervous system's attempt to resolve the specific constraints it is confronted with, such as speed requirements, load variations and task imposed alterations in movement patterns (resulting from changes in external mechanical properties), whilst optimising neural and muscular parameters (activation, force, power, efficiency). Despite this, the movement pattern which minimises metabolic cost is not automatically selected during human cycling (Marsh and Martin, 1997), and it appears that more than the neuromuscular component is responsible for selecting the preferred cadence (Neptune and Hull, 1999). Taken together, care must be taken when interpreting results; selection of cadence is complex and the parameters that control performance under a variety of conditions remain poorly understood. However, the implementation of a mechanical interface in cycling makes manipulating singular variables a more accessible option than other forms of locomotion when exploring optimal control models. As such changing the mechanics of the pedalling task can offer insight into how offsetting the movement pattern of the lower limb can affect muscle-tendon mechanics and intermuscular coordination patterns. There is currently a lack in understanding of how perturbing traditional movement patterns during *in vivo* cycling can change muscle-tendon unit behaviour across a range of medium to high cadences and configuring such a design could offer significant insight into how the central nervous system and musculoskeletal system interacts during functional movements. One way that this can be achieved could be through the use of non-circular chainrings.

2.7 The use of non-circular chainrings

Since the invention of the derailleur in 1905, and consequently the ability to change gears, the mechanics of the drivetrain has remained relatively unchanged. However, there remains apparent constraints with the transfer of power from the body to the drivetrain, which are reliant upon a series of components such as crank length (Martin and Spirduso, 2001; Barratt et al., 2016), anterior-posterior foot position on the pedal (Van Sickle and

Hull, 2007), seat height (Sanderson and Amoroso, 2009) and seat tube angle (Verma et al., 2016). All of these factors are responsible for affecting the moment about the ankle and/or hip, and ultimately the ability to apply maximum effective force. Yet, torque production remains a near sinusoidal entity, when 'power vacuums' are created at the top and bottom of the pedal cycle, known as "dead spots" and effective force production is severely compromised (Figure 2.7). With this in mind, multiple optimisation analysis studies have tried to identify a shape for the most effective application of force throughout the pedal cycle through altering the drive radius of the chainring (Kautz and Hull, 1995; Purdue et al., 2010; Rankin and Neptune, 2008) and consequently manipulating the crank angular velocity (Hull et al., 1992). This can be achieved on the basis that as the chainring rotates with the crank, the chainring radius encountered by the chain varies depending on which pedal cycle quadrant it is in (Figure 2.10). Altering the orientation of the crank against the major and minor axes enables the user to manipulate where in the cycle the smallest and largest radii are met. An optimal orientation has been identified as allowing the largest radius to be utilised during the downstroke, providing a greater propulsion around the crank.

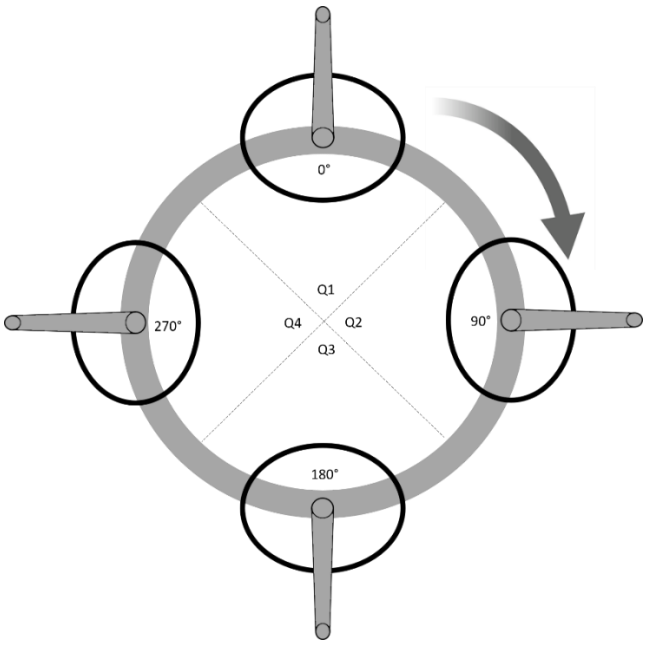

Figure 2.10 Schematic of the positioning of elliptical chainrings throughout the pedal cycle. The position of the crank angle is labelled on the inside of each chainring and the crank is moving in a clockwise direction.

Simulation based approaches of these chainring systems have indicated that an increase in net joint torques may occur when using a non-circular chainring (Kautz and Hull, 1995),

however, this study failed to include muscle mechanics within their model, which likely would have reduced the torques predicted at the joints. Miller and Ross (1980) developed a theoretical model of crank torque developed by muscles as a function of crank angle and velocity and used an optimisation approach to identify the crank angular velocity profile that might maximise average crank power. The result of this was a velocity profile that slowed down the crank during the downstroke to allow muscles to generate power for longer, and an increase in power delivered to the rear wheel. However, this model included just one degree of freedom, thus does not adequately present a precise geometric representation of the musculoskeletal system. The implications of this are important, particularly in a situation where muscle forces are being predicted within a system that does not account for force sharing behaviour across muscles and joints (Jinha et al., 2006), and results should be interpreted accordingly.

Rankin and Neptune (2008) built further onto the model of Kautz and Hull (1995) by including individual muscle actuators and using a dynamic optimisation framework to identify an optimal chainring shape that maximises average crank power. This work predicted that an eccentricity (see Figure 2.12 for definition) of 1.29 would increase average crank power by 3.0% at 90 rpm. The authors dismissed the contribution of intrinsic muscle properties to this finding, in that the fibre lengths and velocities of their musculoskeletal model remained almost identical during their active states between the optimal and circular chainrings across all the pedalling conditions. Instead, they attribute increases in crank power to the slower crank angular velocity predicted to occur during the downstroke (Figure 2.11B). They therefore proposed that the muscles would have more time to generate power and transfer it to the pedal, and hence greater external power would be produced. In particular, hip and knee extensors, and ankle plantar flexors produced increased muscle work in the downstroke, whilst in the upstroke, there was a small increase in iliacus psoas and tibialis anterior work (Rankin and Neptune, 2008). It is important to note that Hill-type muscle models were used in this study, which neglect history dependent effects such as force enhancement following stretch shortening (Herzog et al., 2000); force depression following shortening contractions (Huijing, 1998); the heterogeneity of muscle fibres and subsequent impact on recruitment patterns and force predictions (Lai et al., 2018); and activation-deactivation adaptations during fast cyclical

motions (Askew and Marsh, 1998; Blake and Wakeling, 2015). However, using a first order differential equation to couple muscle activation and neural excitation pattern (Raasch et al., 1997), Rankin and Neptune (2008) did account for the activation-deactivation dynamics. They consequently found activation-deactivation dynamics were a key determinant of optimal chainring eccentricity, meaning that the higher and lower pedalling rates resulted in a requirement for different eccentricities and crank orientations (Figure 2.11A), which yielded different crank angular velocities (Figure 2.11B).

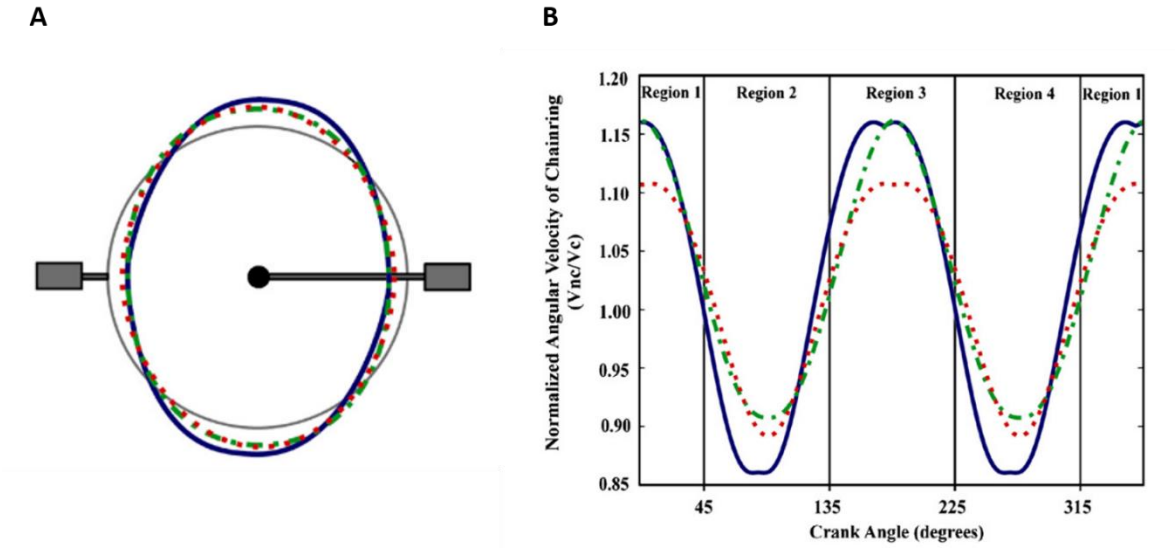

Figure 2.11 (A) Optimal chainring shapes and (B) angular velocity profiles for each pedalling rate normalised to the constant velocity of a circular chainring over the course of a complete pedal cycle. Chainring shape was predicted using dynamic optimisation to identify the shape that maximises average crank power. The solid, dash-dot and dotted line represent the optimal chainring shape/velocity at 60, 90 and 120 rpm, respectively. Reprinted from J Biomech, Vol 41, Rankin JW and Neptune RR. 'A theoretical analysis of an optimal chainring shape to maximise crank power during isokinetic pedalling.' pp 1494-1502, 2008 (Figure 4 & Figure 3, respectively).

The principle of altering crank angular velocity with the use of non-circular chainrings has been incorporated into chainring design by multiple companies, in the hope of successfully applying theory into practice and improving performance. Three major design elements are utilised (Figure 2.12): orientation, which is the determination of angle between the centreline of the cranks and the major axis of the chainring; the eccentricity value, which is the ratio of largest to smallest diameter of the chainring and determines; and the form factor, which defines the perimeter of the chainring through the presence of arcs, ovals, angles, flat sections and ellipses (Malfait et al., 2010). Such geometries cause a shift in gear ratio throughout a single pedal cycle, as the chainring rotates with the crank, making the top and bottom dead centres seemingly amount to that of a smaller diameter chainring.

Additionally, more teeth are available for connection with the chain during the downstroke, and theoretically in a position to generate greater force whilst the joint-action power is high and a more effective downstroke.

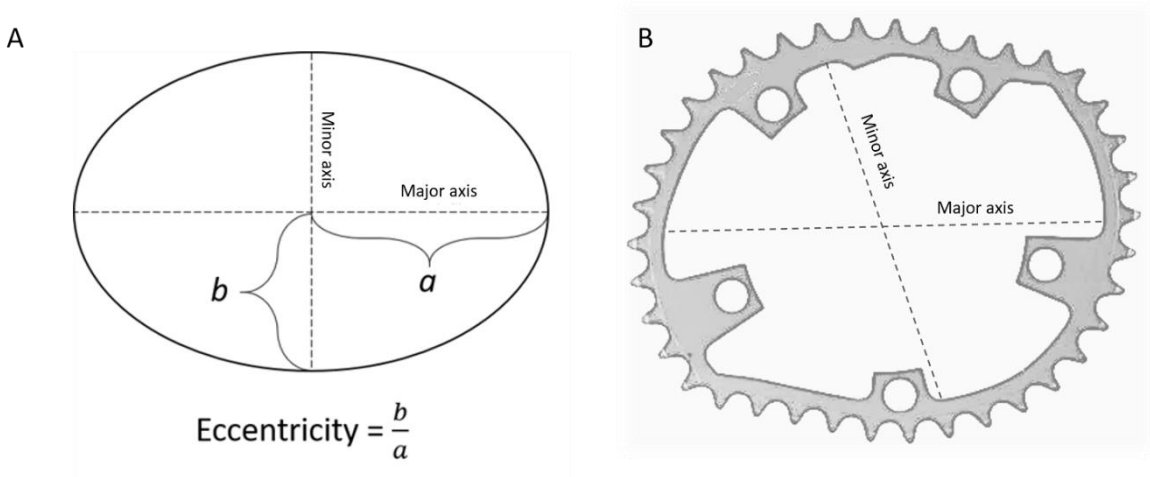

Figure 2.12 Schematic highlighting the degrees of freedom available in the design of non-circular chainrings. (A) Is a reflection of the ratio of eccentricity available within the system which is dependent on the radii of the major and minor axes, and (B) the skew, which is a reflection of the perpendicularity of the major and minor axes.

Despite the modelling-based evidence for increments in average power for complete cycles (Rankin and Neptune, 2008), significant results from empirical studies are elusive, with some studies finding enhanced power production (Hue et al., 2008; O'Hara et al., 2012), whilst others report no change (Horvais et al., 2007; Leong et al., 2017). The source of these inconsistencies probably lies in the array of methodologies employed. There is very much a trend towards empirical, performance driven studies, concentrating on augmenting a particular parameter of performance, be it metabolic (Hue et al., 2001), average power production (O'Hara et al., 2012), or maximal cycling power (Leong et al., 2017). Additionally, the study of power production is broad and dependent on whether load is held constant or open to manipulation; if cadence is constant or freely chosen; and if peak or average power is desired, all factors that differ amongst studies evaluating the effects of chainring geometry on performance. A summary highlighting the diversity of some of these approaches can be found in Table 2.1.

Table 2.1 Selected references on comparisons between circular and non-circular chainrings.

Author	Chainring	Eccentricity	Orientation	Symmetry	Study design	Subjects	Variable	Outcomes
Hansen et al. (2009)	Shimano Biopace II	1.04	-8°	Point symmetry	10-min bout at 70% VO_2 peak with freely chosen cadence. Two 2-min bouts at 180 W at cadences of 65 and 90 rpm	Competitive cyclists	Peak and minimum crank torque, blood lactate, freely chosen pedal rate, $\dot{V}O_2$, RER, heart rate, RPE	Blood lactate was significantly lower in the Biopace condition.
Hintzy et al. (2016)	O'symetric	1.215	78°	Bi-radial	Four maximal 8-second sprints	Competitive cyclists	Instantaneous force, velocity, optimal power and optimal velocity	Significantly higher maximal average power, optimal force & instantaneous max force in the downstroke.
Horvais et al. (2007)	O'symetric	1.215	78°	Bi-radial	8-min submaximal test at 100 W and 200 W. Two maximal 8 second sprints. Repeated four weeks later.	Competitive triathletes	Mechanical parameters at the crank. Muscle activation.	Lower net crank torque at 0° and 180°; higher net crank torque at 90° in submaximal test. Higher burst duration in bicep femoris in sprint test.
Hue et al. (2001)	Unspecified. Inner elliptical cam increases crank length during downstroke and decreases it during upstroke.	Unspecified	Unspecified	Unspecified	Maximal 1 km sprint	Competitive cyclists and triathletes	Metabolic parameters	Faster performance time elicited in the elliptical group. No changes in metabolic variables
Hue et al. (2008)	Unspecified. Inner elliptical cam increases crank length during downstroke and decreases it during upstroke.	Unspecified	Unspecified	Unspecified	1 km track cycling sprint	Competitive cyclists.	Metabolic parameters, blood lactate, heart rate	No significant difference between performance or physiological measurements. Individuals with greater muscle volume correlated positively with increases in performance with the elliptical chainring.
Hull et al. (1992)	Shimano Biopace I; Hull Eng10; Hull Eng 90	1.09; 1.36; 1.36	-8°; 10°; 90°	Bi-radial	15 minutes at 60% $\dot{V}O_{2max}$, 10 minutes at 80% $\dot{V}O_{2max}$	Endurance trained cyclists and triathletes	Metabolic parameters, lactate, heart rate, RPM	No significant differences between chainrings and collated variables.
Leong et al. (2017)	Rotor Q-Ring; O'symetric	1.1; 1.215	61°; 78°	Bi-axis symmetry; Bi-radial	Inertial load cycling test ~4 second maximal test at 90 rpm; ~3 second maximal trial at 120 rpm	Competitive cyclists	Pedal and joint kinematics and powers, Maximal cycling power, optimal pedalling rate	Peak ankle angular velocity lower in the O'symetric than circular. No significant difference between maximal cycling powers, eccentricity of ankle joint centre, trajectory or peak linear velocities of joints during extension.
Neptune & Herzog (2000)	Hull Eng10; Hull Eng 90	1.36; 1.36	10°; 90°	Biradial	10 minutes at 90 rpm and 200W	Competitive cyclists	Kinetic, kinematic and muscle activity	EMG onset and offset minor significant timing shifts in some muscles and increase in magnitude using Eng10.
O'Hara et al. (2012)	Rotor Q-Ring	1.1;	61°	Bi-axis symmetry	Five week Q-ring training intervention and 1 km time trial pre and post.	Competitive cyclists and triathletes	Time trial performance, Average power, max power, average speed, max speed, blood lactate	Significantly faster time trial performance using Q-rings with a higher average power and average speed. No significant difference in lactate concentrations
Rankin & Neptune (2008)	Optimised chainring shape	1.24 – 1.35 cadence dependant	84.9° - 91.9° cadence dependant	Bi-axis symmetry	Optimisation study	Musculoskeletal model simulation	Average power, muscle excitation timing, muscle mechanical work, intrinsic muscle properties	Increase in average power

Note: Outcomes are in comparison with the circular chainring employed in the study. Studies are listed in alphabetical order.

In summary, the range of methodologies utilised, and consequential mix of results makes it impossible to generalise and leaves unanswered questions regarding exactly what effect the altered chainring geometry has on the neuromusculoskeletal system. The force generated by the muscle is dependent not just on its size and architecture, but also its activation state and force-length and force-velocity properties. We do not currently understand the effects of chainring design on joint behaviour, muscle contractile and activation-deactivation dynamics, but with information of these fundamental properties, we will be in a better position to predict how elliptical chainrings might influence performance and provide future direction to the study of non-circular chainrings.

2.8 Measuring muscle behaviour *in vivo*

As previously eluded to, little is known about the *in vivo* behaviours of skeletal muscles during human locomotion as opportunities for directly measuring the forces placed on muscles, bones and joints are severely limited in humans. Primary properties such as force-velocity, force-time and force-length relations are typically investigated using reductionist techniques, by controlling all external factors and the variable of interest in manipulated whilst force is measured. For example, force-velocity relationships are typically established using data collated from protocols which allow the muscle to become fully excited (eliminated force-time) before shortening across some predetermined range of length (controlling for force-length). Such techniques have been instrumental in forming foundations of understanding surrounding muscle function. Nonetheless, their direct application to voluntary movement is flawed considering the highly controlled nature the results were achieved under (Martin, 2007). They are unable to determine where exactly during functional movements excitation may occur on a force-time basis, influences of variable shortening velocities and resistive forces, and shortening from one length to another. Concomitant to this, the properties associated with the force-time, force-length and force-velocity paradigms are known to be influenced by history dependent effects, such as stretch-induced force enhancement (Edman et al., 1978), and shortening-induced force depression (Herzog et al., 2000).

In order to explore the influences of non-circular chainring design on the neuromusculoskeletal system, alternate approaches must be taken to avoid the need for extrapolation from studies on isolated muscle. Other techniques have been enlisted to evaluate animal muscle behaviour *in vivo* through the use of implanted sensors such as sonomicrometry, tendon buckles and intramuscular electromyography (EMG) to record fascicle lengths, forces and excitation respectively. As such, valuable insight has been gained into how the energetics and performance of muscle is determined by the mechanical and physiological properties through activities such as hopping (Biewener et al., 1998; Azizi and Roberts, 2010), running (Roberts et al., 1997) and flying (Berg-Robertson and Biewener, 2012). Due to the ethical and technical issues implicated by the invasive nature of these procedures, optic-fibre techniques and tendon buckles are not replicated

in humans as easily, although some research laboratories have been successful in performing locomotor tasks using such apparatus during running (Komi, 1996) and cycling (Gregor et al., 1987).

Instead, human movement has been analysed using other tools such as force plates, motion capture and intramuscular and surface EMG, allowing for quantitative descriptions of the kinematics, kinetics and muscle coordination patterns behind body-segmental movement. From this, methods of deducing muscle and tendon function have been introduced to overcome some of the gaps in our understanding. Joint level analyses can provide insight to the physiologically relevant mechanical muscle properties across multiple joints (Martin and Brown, 2009), and allows researchers to observe how force and power are generated by various muscle groups, transferred across the limb and exerted. There are issues with this form of investigation, given that muscle fibre strain and strain rates are difficult to predict from joint movements alone given the role of tendinous structures in uncoupling the strain and strain rates of muscle fibre from the whole MTU (Wakeling et al., 2011). Additionally, the rotation of muscle fibres in pennate muscles during contraction means that muscle fibre velocities can also be uncoupled from the shortening velocities of the MTU (Randhawa et al., 2013).

Muscle function is dependent on the principles of the force-length-velocity relationship, however, as this cannot be measured directly *in vivo* it must be estimated using alternative techniques. Modelling is an attractive method, as the model can be made as simple or as complex as the research question requires, given that the body can be split into a system of anatomical segments, connected by joints and acted upon by the muscles, tendons and other internal structures. This is a controlled way of obtaining a system that can interact with the environment and produce a purposeful movement. In this way, musculoskeletal models can provide an avenue for estimating the internal loading of anatomical structures and advancing our understanding of energetics and the control of movement. Although these models can vary in complexity, ranging from a single degree of freedom (DOF) and its corresponding actuator, to multiple DOF models with several body segments and muscles. Notwithstanding this, models of varying intricacy should continue to represent the skeleton anatomy, inertial characteristics of the body segments and properties associated with the muscular and neural systems with an adequate level of accuracy

needed to answer the specific question in mind. To achieve this level of detail, the fundamental parts of the musculoskeletal model can be represented in software via mathematical expressions used to determine the dynamics of motion. One open-source simulation software available is OpenSim (Delp et al., 2007), and enables the users to model lower and upper extremities to examine the biomechanical consequences of movements such as walking (Arnold et al., 2013), running (Lai et al., 2016), and cycling (Lai et al., 2017).

There are certain flaws associated with this approach given the accuracy of a simulation is dependent upon the accuracy of the mathematical model underpinning the neuromusculoskeletal model. As previously alluded to, the *in vivo* empirical evidence driving this is limited, and more needs to be collated in terms of musculoskeletal geometry and joint kinematics to influence predictive models. Models are only as good as the understanding of the system it is attempting to explain and the data which drives it, consequentially, synergistic approaches combining computational modelling used in conjunction with experimental cycling data would allow kinematic data to be coupled with the muscle-tendon behaviour and allow for a better understanding of the association between the two.

2.9 Summary

The implementation of an altered chainring geometry, and subsequent modification of angular velocity can impact the leg during cycling, thus having consequences for the contractile state of the muscles. The muscle's ability to exert power is dependent on its intrinsic properties, and a manipulation of pedal velocity could have implications for the timing of muscle activation and deactivation, muscle tendon unit and joint kinematics, therefore affecting the muscle's ability to produce power. However, such detailed experimental data have never previously been reported and it remains unclear what effects, if any, chainring geometry has on cycling performance. This could be a result of the varying techniques used to assess their impact, using both *in vivo* performance based tests (Hue et al., 2007; Hull, 1992; Leong et al., 2017) and modelling based studies (Rankin and Neptune, 2008). The gap which currently exists between the theoretical and empirical suggests a need to explore the effects of altered chainring geometries with a different approach, moving away from performance-based approaches by first uncovering the

mechanisms affected by alterations in task mechanics. Elucidating muscle function is not straightforward, however, combining the techniques discussed above can offer insight into the relationships between the complex dynamic systems involved in cycling tasks.

2.9.1 Outline and specific aims of this thesis

The overall goal of this thesis was to assess the acute responses of the neuromusculoskeletal system to alterations in chainring eccentricity and the orientation of the crank against their major and minor axes, with the underlying aim of using the elliptical chainrings as a platform to understand more about how the human neuromuscular system behaves *in vivo*. The specific research objectives were therefore to determine whether manipulations of chainring geometry and crank orientation would alter:

(a) patterns of crank angular velocity through the pedal cycle;
(b) the components of force expressed at the crank;
(c) the kinematics of the hip, knee and ankle joints;
(d) behaviours (length and velocity) of muscle-tendon units of the leg; and
(e) muscle activation patterns across proximal and distal leg muscles.

The data One experimental study was performed, using instrumented cranks, electromyography and motion capture, to collect a large biomechanical data set, required to address these objectives. The 3D marker trajectories were incorporated within a subject-specific scaled musculoskeletal model, allowing smoothed anatomically constrained joint kinematics and muscle-tendon unit lengths to be generated. Chapter Three assesses changes in the crank angular velocity, reactive forces and joint kinematics caused by the use of elliptical chainrings over a range of cadence and load conditions. Chapter Four assesses the alterations in MTU lengths and velocities of the soleus, medial gastrocnemius and vastus lateralis. Chapter Five, assesses how muscle activation patterns change in response to the altered joint and MTU behaviours recorded in previous chapters. Chapter Six integrates all these results and critically appraises the new findings, discussing potential consequences for understanding neuromusculoskeletal function and cycling performance.

Chapter 3. Effects of chainring geometry on crank kinematics and kinetics, and kinematics of lower limb joints during cycling

3.1. Introduction

Optimisation of movement strategies during cycling is an area that has gathered a lot of attention over the past decade. Interventions to augment performance have included alterations in saddle height, seat tube angle, crank length, crank-pedal mechanics and manipulation of chainring geometries (Gonzalez and Hull, 1989; Rankin and Neptune, 2008; Sanderson and Amoroso, 2009). A musculoskeletal model devised by Yoshihuku and Herzog (1990) suggests that pedalling with a fixed value of crank angular velocity does not allow for maximal power production. Consequently, manipulations of drivetrain technology aimed at forcing the path of the foot along a non-constant angular velocity profile have been developed. One method of doing this is to alter the geometry of the chainring. Specifically, it has been proposed that pedalling with a circular chainring evokes a quasi-constant crank angular velocity (owing to the equidistant radius from the crank centre to the chain driving the rear wheel). However, non-circular chainrings (both skewed and ellipses), will promote a more varied crank angular velocity profile, as a result of the varied radius from the crank centre to the chain driving the rear wheel. Non-circular chainrings therefore have the potential to produce slower crank velocities during the downstroke and provide greater time for cyclists to apply forces to the crank (Rankin and Neptune, 2008).

Using an optimisation framework, preliminarily theoretical work by Hull and colleagues determined that implementing a variable angular velocity profile, congruent with that of an elliptical shape, could promote a 48% reduction in muscle mechanical work relative to a constant angular velocity profile (Hull et al., 1991). This was in keeping with an earlier simulation-based study from Miller and Ross (1980), which highlighted that a varying crank angular velocity was optimal for delivering power to the rear wheel. Subsequent studies attempted to validate these optimisation observations using empirical evidence, however, after failing to distinguish any metabolic differences between a circular chainring, their custom designed elliptical chainrings and the skewed ellipse associated with the Shimano Biopace (devised by Okajimi, 1983), the authors did not take their work any further (Hull et

al., 1992). Since then, more work has attempted to understand the performance effects of using non-circular chainrings, with mixed results (Hue et al., 2007; O'Hara et al., 2012; Hintzy and Horvais, 2016). This lack of clear evidence supporting an *in vivo* performance advantage has dominated the study of non-circular chainrings for the past 20 years and left the area stagnated.

A possible explanation for the equivocal results surrounding the use of non-circular chainrings may be the lack of adequate preliminary work in the area, as there is a jump from theoretical work (Kautz and Hull, 1995; Rankin and Neptune, 2008) to *in vivo* performance-based studies (Horvais et al., 2007; Leong et al., 2017). While the overarching aim of intervention-based *in vivo* studies is to optimise performance (Weinberg and Burton, 2000), this is a complex parameter to target, given the ambiguous nature of what constitutes 'good performance'. In cycling, performance optimisation is mainly related to the measurement of time or distance. Depending on the event (i.e. endurance, time trial, sprint), cycling demands predominately dictate the need to cover a fixed distance as quickly as possible, or to go as far as possible in a fixed amount of time. Performance improvements are then determined as being when the athlete is able to surpass previous attempts via an improved time or cycling further. Owing to the etymology, a literature search in the optimisation of cycling performance finds different points of view emerge, with an almost equivalent meaning. As such, it is possible to uncover results pertaining to cycling efficiency (Hansen et al., 2002; Korff et al., 2007), muscular efficiency (Neptune and Herzog., 1999; Zameziati et al., 2006; Carpes, Diefenthaeler et al., 2010), mechanical efficiency (Umberger et al., 2006; Wakeling et al., 2010) and mechanical effectiveness (Zameziati et al., 2006; Korff et al., 2007; Mornieux et al., 2010), all of which are related to alterations in cycling 'performance'.

Consequently, a new approach was deemed important if we are to better understand the effects of elliptical chainrings on the cyclist and cycling performance. To this end, a clear understanding of the neuro-mechanical effects of elliptical chainrings seems important, if their uses are to be directly related to consequences for cycling performance. Quantifying the responses of lower limb kinematics and crank kinematics and kinetics is a required first step for better understanding of the effects of altered chainring geometry. Such data have, however, yet to be reported in the literature, and therefore represents a significant gap in

understanding the effects of elliptical chainrings on pedalling technique and how cyclists interact with the bike.

The purpose of this chapter is therefore to evaluate how acute use of different elliptical chainrings influences crank angular velocity, kinematics of the lower limb joints and patterns of force application at the crank. I hypothesise that there will be greater variation of crank angular velocity within the pedal cycle when using elliptical compared to circular chainrings, with the degree and magnitude of changes dependent on the degree of eccentricity and orientation of the crank to the elliptical chainring's major axis. Additionally, it is predicted that altered crank angular velocity profiles will impact pedalling technique, altering the time spent in the downstroke of the pedal cycle and consequentially providing a longer time for F_E to be applied, and a reduction in F_{IN} at the top and bottom dead centres.

3.2. Methods

3.2.1 Protocol and Data Acquisition

Four well-trained male cyclists (age: 39.5 ± 17.7 years, mass: 78.9 ± 11.4 kg, height: 184.8 ± 11.9 cm) and four well-trained female cyclists (age: 36 ± 15 years, mass: 61.2 ± 5.1 kg, height: 167.4 ± 2.3 cm) volunteered for the study. All participants met at least five of the ten-point criteria system developed by Jeukendrup and colleagues (2000) for the classification of trained, well-trained, elite and world class cyclists, as determined by a questionnaire completed prior to taking part. All but one participant were from road cycling training backgrounds, the remaining participant competed in triathlon events. All participants gave informed consent to take part in the study, which was approved by Manchester Metropolitan University, Faculty of Science and Engineering, Local Ethics Committee and complied with the principles laid down by the *Declaration of Helsinki.*

Participants reported to the laboratory at Manchester Metropolitan University and performed the trials on a stationary cycling ergometer (Indoor Trainer, Schoberer Rad Messtechnik (SRM), Jülich, Germany). The geometry of the cycle trainer was matched to the participant's own bicycle, and they brought their own shoes with cleats and pedals. Cadence, effective and ineffective forces applied to the crank arms were recorded using instrumented cranks (Powerforce, Radlabor, Freiburg, Germany) allowing the bilateral

recording of reaction forces at 2000 Hz. A manual calibration of the cranks was performed using a known weight, rotated over a pedal cycle, to determine the necessary offset and correction values for the precise calculation of each force component. The crankarm length used was the same for all participants (172.5 mm). Participants were presented with three different chainring geometries, a 61-tooth circular chainring and two elliptical chainrings of two different levels of eccentricity (i.e., the ratio of major to minor axes lengths), 1.13 (E_1) and 1.34 (E_2), each with 52 teeth and in which the major and minor axes were perpendicular. E_1 and E_2 were also fitted at two different orientations to the crank arm as identified in Figure 3.1, one orientation had the arm closer to the minor axis (E_{1-}, E_{2-}) typical of the orientation used for cycling; the other orientation had the arm closer to the major axis (E_{1+}, E_{2+}). This altered positioning reduced and increased the distance between the crank centre and the drive chain at different points in the pedal cycle, included to manipulate the location of any crank angular velocity effects and facilitate study of neuromuscular mechanics in this and later thesis chapters. The elliptical chainrings were designed and manufactured specifically for the study (Hope Technology, Barnoldswick, UK; Figure 3.1).

Three-dimensional kinematics were acquired using a Vicon optical capture system (Vicon Nexus version 2.5, Vicon Motion Systems LTD, Oxford, UK) with ten high-speed cameras (Vicon Nexus) sampling at 100 Hz. Reflective markers were positioned bilaterally over the following specific anatomical landmarks of the pelvis and lower limbs: iliac crest, anterior superior iliac spine, greater trochanter, lateral and medial epicondyle, lateral and medial malleolus, calcaneus, and at the anterior aspect of the I metatarsophalangeal joint and lateral aspect of the V metatarsophalangeal joint (secured to the shoe). Five markers were positioned on the pelvis and rigid marker triads were secured to the thigh, shank and an ultrasound probe in order to obtain time histories of their positions.

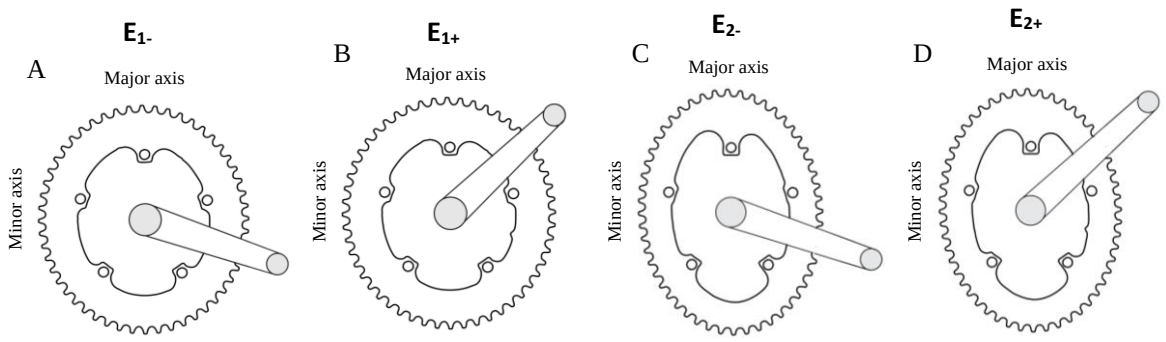

Figure 3.1. Geometries of elliptical chainrings. A. E_{1-} has an eccentricity (deviation from circularity) of 1.13 and the crank arm was orientated 67° behind the major axis and 23° forward of the minor axis. B. E_{1+} 40° forward of the major axis and 50° behind the minor axis. C. E_{2-} has an eccentricity of 1.34 and was orientated 65° behind the major axis and 25° forward of the minor axis and, (D) E_{2+} 51° forward of the major axis and 39° behind the minor axis.

On the left lower limb, surface electromyography (EMG) electrodes were placed over the mid-bellies of the soleus, medial gastrocnemius, lateral gastrocnemius, tibialis anterior, vastus medialis, rectus femoris, vastus lateralis, bicep femoris, semitendinosus and gluteus maximus. EMG signals were also collected from the right lower limb over the vastus medialis, vastus lateralis, bicep femoris, and semitendinosus. The skin overlying these muscles was carefully prepared. Hair was shaved off, the outer layer of epidermal cells was abraded, and oil and dirt were removed from the skin with an alcohol swab. Surface electrodes (Trigno Wireless EMG, Delsys Inc, USA) with a fixed inter-electrode distance of 10 mm were placed on the muscle site using strong adhesive tape and further secured using stretchable adhesive bandages to minimise the movement of artefacts during the trials. Signals from both EMGs and instrumented pedals were sampled at 2000 Hz through a 16-bit data acquisition card (USB-6210, National Instruments Corp, Austin, TX) linked to a host computer equipped with data acquisition software (Vicon). Data sources were synchronised in Vicon using a common trigger signal. The data collected from the EMG electrodes is presented in Chapter Five.

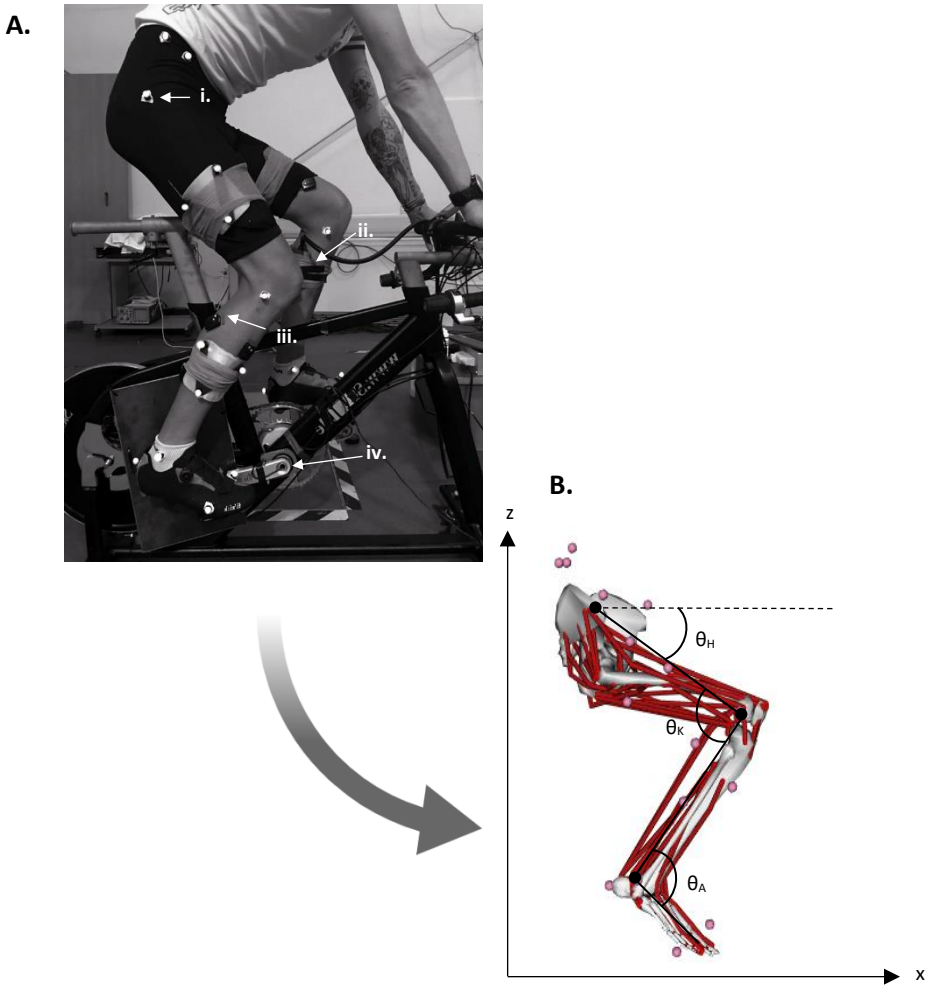

Figure 3.2 Experimental set-up. This thesis integrates *in vivo* experimental data: i. motion capture; ii. B-mode ultrasonography; iii. EMG and; iv. instrumented cranks (A) and a subject-specific scaled musculoskeletal model using inverse kinematics to calculate joint angle changes, with joint kinematic definitions (B). Angle definitions: θ_H – Hip angle; θ_K – knee angle; θ_A – ankle angle.

Participants warmed up using the circular chainring at a self-selected power output and cadence for five minutes before commencing the data collection protocol. Participants performed the first of the experimental trials with the circular chainring. Individual trials randomised first by the cadence and load combinations, were set at cadences of 90, 110, 130 and 150 rpm and power outputs of 200, 250 and 300 W, with the exception that no trial of 150 rpm was conducted at 300 W because of the difficulty of achieving this combination. Feedback for the cadence control was provided to the participant via a digital power meter (Power Control 7, SRM) positioned within their line of sight on the bike handle bars. Once the target cadence was achieved in a given trial, data collection was initiated and continued for 30 seconds. Between consecutive trials, the load was decreased, and participants were requested to continue pedalling for a minimum of 1 minute at

approximately 100 W. Participants were instructed to maintain a seated position with hands on the drop handlebars throughout the data acquisition. The next trial was not initiated until the participant self-reported that they had recovered enough from the previous trial to continue.

Following completion of all cadence × load conditions with the circular chainring, participants were asked to dismount the ergometer whilst the chainring was changed. The two elliptical chainrings and crank orientations were introduced in a randomised, counterbalanced design with four ordering sequences. The randomisation was designed to minimise the impact of fatigue on the measurements obtained in the study. Participants pedalled for two minutes on a low load prior to the condition being commenced to become accustomed to the chainring. This was deemed sufficient by Neptune and Herzog (2000) who proposed that 10 – 20 crank cycles was enough to promote muscle coordination adaptation in response to altered task mechanics. The participants did not perform familiarisation sessions with the elliptical chainring as it was deemed important to record the acute neuromusculoskeletal responses resulting from an altered chainring geometry. It is unclear whether neuromuscular coordination would adapt with training. O'Hara and colleagues (2012) found increases in mean power and mean speed during a 1km time trial using elliptical chainrings following a five week training plan and owing to the ambiguity surrounding the nature of the mechanisms promoting these results, it was deemed a viable precaution to employ. The same cadence-power output protocol was followed for each of the elliptical chainring conditions as the circular chainring condition. The respective load used to achieve the required mechanical power output was different between the circular and elliptical rings to account for the known alteration in drivetrain kinematics induced by having different size chainrings (i.e. 61 vs 52 teeth) (Hansen et al., 2002).

3.3. Data Analysis

3.3.1 Crank kinetics and kinematics

The top dead centre (T_{DC}) of the crank revolution was defined as 0°, and the bottom dead centre (B_{DC}) was defined as 180°. Crank angle was defined using the position of known markers and shoe and cleat dimensions to predict a "virtual" pedal centre and the entire pedal revolution was used to analyse pedal force. Crank angular velocity was calculated as the first-time derivative of the crank angle over the course of the pedal cycle. Resultant

force (F_R) was calculated from the recorded effective force (F_E) and the ineffective force (F_{IN}) at each degree of the crank angle (θ) for both left and right pedal forces:

$$F_R(\theta) = \sqrt{F_E(\theta)^2 + F_{IN}(\theta)^2} \quad \text{Eq. 3.1}$$

Examining the effective force (F_E) acting to propel the crank relative to the resultant force (F_R) provides an index of force effectiveness (IFE), an established method of quantifying pedalling technique (Korff et al., 2007). Therefore, IFE was calculated for the complete crank revolution (IFE_{0-360}) according to Korff and colleagues (2007).

$$\text{IFE} = \frac{\int_0^{360} F_E(\theta)}{\int_0^{360} F_R(\theta)} \times 100\% \quad \text{Eq. 3.2}$$

IFE was further quantified in four quadrants of the pedal revolution sections: Q1 (315° - 45°), Q2 (45° - 135°), Q3 (135° - 225°), and Q4 (225°-315°).

3.3.2 Musculoskeletal Simulation to Calculate Leg Joint Angles

Using the open-source software OpenSim v3.3 (Delp et al., 2007), a musculoskeletal model (Lai et al., 2017) was scaled to each participant's anthropometry. Musculoskeletal models offer the ability to smooth the kinematics data obtained under experimental conditions and produce a consistent, anatomically constrained, representation of the movement that occurred. For this simulation, the left leg segment of the model was removed, along with its corresponding actuators (Figure 3.2B). A multi-stage process was used to scale the mass and inertia tensor of the model and the dimensions of the body segments (Delp et al., 2007). This involved measurement-based scaling to compute the scale factors for each segment using the experimentally measured marker positions recorded from a static calibration trial taken on the ergometer. In this procedure, virtual markers were created and placed on the model based on the anatomical location of the experimental markers. Following this, the model's geometry was adjusted in accordance with the anatomical segment length, width and depth. The mass properties of the body segments were also adjusted proportionally in this process, allowing the total mass of the participant to be reproduced. Total actuator length percentages were preserved through accordant scaling of the muscle fibre lengths and tendon slack lengths.

Hip, knee and ankle kinematics were calculated using OpenSim's inverse kinematics function, to find the best matching values for the generalised coordinates of the model by minimising the error value between the experimentally derived data and model-based markers (Lu and O'Connor, 1999) in three-dimensional space. For the musculoskeletal model, recorded iliac crest positioning was used to determine hip joint angles, which is reported to provide a more accurate approximation of hip joint centre than tracking the superior aspect of the greater trochanter or assuming a fixed hip joint centre (Neptune and Hull, 1995). Joint kinematics from the inverse kinematics were exported from OpenSim and all secondary analysis of joint angle behaviour was completed using custom-written programs in Mathematica 11 software (Wolfram Research, Champaign, IL). Joint excursion was defined as the difference between maximum and minimum joint angle for the corresponding joint.

3.3.3 Principal component analysis to quantify the main features of kinetic and kinematics data

Dominant patterns in the kinetic (crank forces) and kinematic (crank angular velocity; joint angles) datasets were decomposed using principal component (PC) analysis into a series of orthogonal patterns of variability in all analysed pedal cycles (Deluzio et al., 1997). In short, data were arranged into a $P \times N$ matrix **A**, where waveforms observations from the collated data were interpolated to 100 time points per cycle (P) and multiplied by the number of time points analysed (8 participants × 5 conditions × 11 trials × 26 pedal cycles; N).

To determine the PC of the data, the covariance matrix **B** was calculated from the data of matrix **A**, and the PC weightings were determined from the eigenvectors ζ of covariance matrix **B**. The ranking of each PC was given by the eigenvalue for each eigenvector-eigenvalue pair with the greatest absolute eigenvalues corresponding to the main PCs. The relative proportion of the crank forces and kinematic data explained by each PC was given by $\zeta' \mathbf{B} \zeta$. The PC analysis did not include subtraction of the mean before calculation meaning the eigenvectors did not describe the set of orthogonal components that maximise the variance of data from the mean (Ramsey and Silverman, 1997). Instead, this approach allowed the eigenvectors to describe the set of orthogonal components that maximise the variability of the entire data with the first PC (PC I) representing the mean (Wakeling and Rozitis, 2004).

The loading scores for each PC for the *P* time points were given by $\zeta'\mathbf{A}$. To interpret the biomechanical meaning of each PC, the joint kinematic and crank force and angular velocity waveforms were reconstructed from the vector product of the PC weighting and their loading scores. This was done for each pedal cycle using the first three PCs in accordance with the 90% trace criterion; which dictates that when the cumulative percentage of the total variation that is explained by the retained PC exceeds 90%, all further principal components are discarded (Chau, 2001). PC analysis and reconstruction of data was carried using a custom-written program in Mathematica 11 software (Wolfram Research, Champaign, IL).

3. 4 Statistics

General linear model analysis of variance (ANOVA) was used to identify the effect of chainring eccentricity, cadence and load on the loading scores for the first three PCs from the lower limb kinematics and force data. The interactions between chainring condition, cadence and power output, with subject as a random factor, were also determined. A *post hoc* Tukey test was performed to determine the location of the significant differences between chainring condition for a given cadence or power output. Where significant interactions were found between chainring conditions and cadence, the loading scores were separated into cadences and reconstructed independently to enable visualisation of the effects of chainring eccentricity on the dependent variables.

Descriptive statistics (mean, standard deviation and effect size) were used to describe how far PC loading scores differed for crank forces and joint excursions when using an elliptical chainring in comparison to a circular ring. Effect sizes allow for the quantification of the difference between two groups (the circular chainring in comparison to the elliptical chainring condition) and emphasises the magnitude of this difference (Cano-Corres et al., 2012). Effect sizes were corrected for bias using Hedges and Olkin's factor (1985). Effect sizes were interpreted on the basis of Cohen's (1988) classification scheme: effect sizes <0.5 were considered to be small, effect sizes between 0.5 and 0.8 were considered to be moderate and effect sizes >0.8 were considered to be large. Statistical analyses were processed using Minitab version 18 (Minitab Inc., State College, PA). All data are presented as means ± SD, and statistical tests were deemed significant at $\alpha = 0.05$.

3.5 Results

3.5.1 Cadence Selection

Although cadence was prescribed to the participants prior to each trial, within the 30 second data collection window, there was margin for human error, causing the actual cadence to deviate slightly. Table 3.1 contains the mean cadences attained during each condition. There was no significant effect of chainring condition on cadence (P = 0.698). All participants were able to complete all cycling conditions across the range of cadences between 90 and 150 rpm, and power outputs of 200-300 watts and cadence was comparable across the different chainring conditions.

Table 3.1. Cadences achieved across the 11 conditions

Prescribed Cadence	90	90	90	110	110	110	130	130	130	150	150
Power	200 W	250 W	300 W	200 W	250 W	300 W	200 W	250 W	300 W	200 W	250 W
Circular	90±1	91±1	90±1	110±1	111±1	110±1	131±1	130±1	130±2	151±1	149±2
E_{1-}	91±1	90±2	90±1	110±1	109±1	110±1	130±1	129±1	128±1	150±2	149±0
E_{1+}	91±1	91±2	90±1	109±1	109±1	110±1	129±1	129±1	129±1	149±1	149±1
E_{2-}	91±1	91±1	90±1	110±1	110±1	109±1	128±1	129±1	129±1	151±1	149±1
E_{2+}	90±1	90±0	90±1	110±1	110±1	110±1	130±1	129±1	129±1	150±2	148±3

Note: data represented as mean ± SD rpm. Number presented in the first row denotes the prescribed cadence (rpm); and in the second row, the power (watts) in which the trial was completed at.

3.5.2 Crank angular velocity fluctuations

The circular chainrings were associated with a 3% change crank angular velocity over the course of the pedal cycle, with respect to peak to nadir differences. The elliptical chainrings effectively manipulated peak crank angular velocity (Figure 3.3B), where there was a 8% change in peak to nadir difference between the E_{1-} condition and circular chainring. In the E_{2-} condition this difference increased to 18%. When examining the non-optimal crank orientations, peak to nadir differences in crank angular velocity increased by 14% in the E_{1+} condition and 40% in the E_{2+} condition. The crank orientations placed ahead of the major axes (E_{1+} and E_{2+}), and thus at a 'non-optimal' angle, increased the downstroke and upstroke velocity, allowing less time to be spent in these quadrants (Q2 and Q4). Additionally, they slowed crank velocity in Q1 and Q3 and so it took more time to travel through the top and bottom of the pedal cycles (Figure 3.3A).

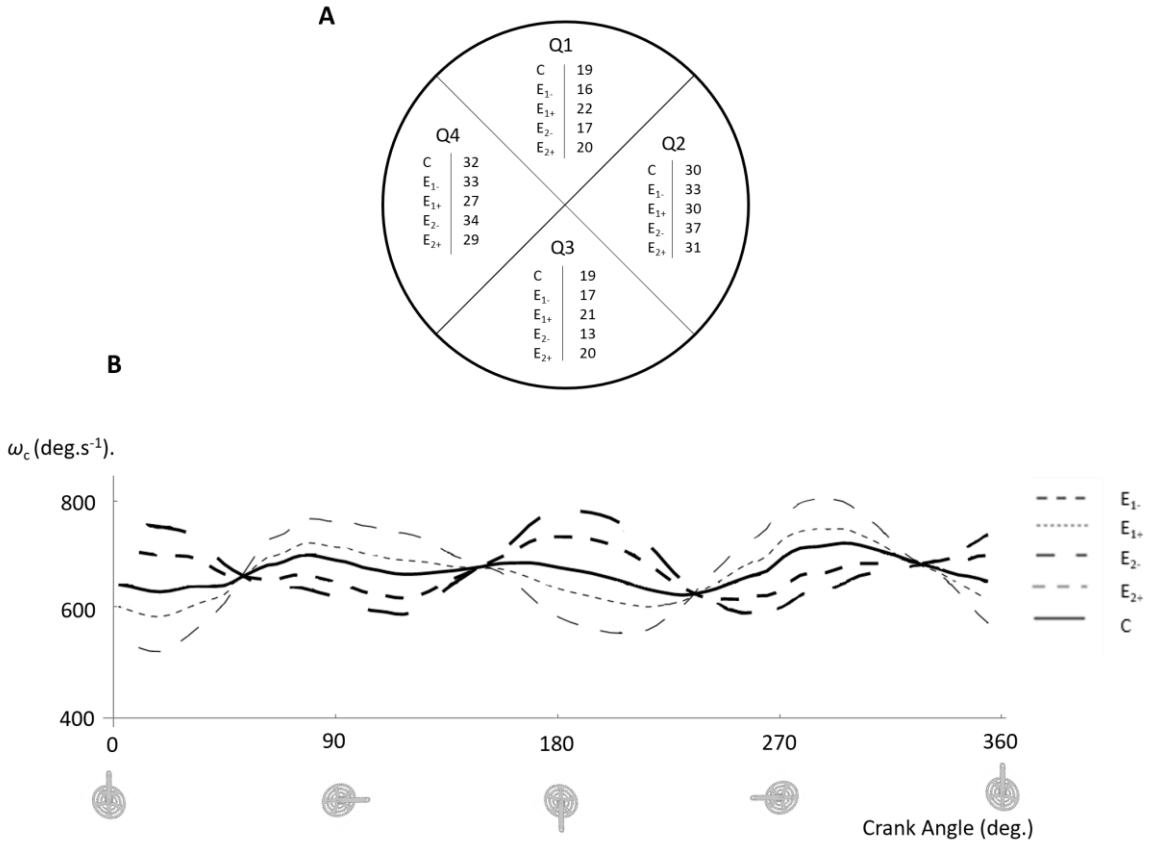

Figure 3.3 Crank speed variations during the pedal cycle. (A) Percentage of time to complete the pedal cycle devoted to each quadrant where Q1 denotes top of the pedal cycle, Q2 denotes the downstroke, Q3 denotes the bottom of the pedal cycle, and Q4 denotes the upstroke, and; (B) visual representation of the for crank angular velocity (ω_c),reconstructed from the first three principal components (deg.s^{-1}). Chainring conditions are represented in grey scale.

3.5.3 Crank forces

The PC-based waveform reconstruction revealed distinct features in both frequency and timing of the crank force variable in the different cycling conditions (Figure 3.4; Column II). The first PC weight for crank forces, representing the mean, explained more than 94% of the signal variability (Figure 3.4), and so, the results below focus primarily on this component. Statistical analysis showed that the F_E and F_{IN} loading scores were significantly affected by chainring condition ($P < 0.001$), and these differences are highlighted in the reconstructed waveforms (Figure 3.5). However, the crank force responses were also different between the left and right pedals. Subsequent *post hoc* analysis revealed that all five chainring conditions elicited significantly different effective force for the right crank, with chainring condition E_{2-} (Figure 3.5) displaying the largest increment in peak F_E compared with the circular and E_{1-} and E_{1+} chainrings conditions. Changing the crank angle

to the opposing orientation (E_{1+} and E_{2+}) significantly decreased peak F_E as compared to E_{1-}, E_{2-} and circular conditions across all pedal speeds (Figure 3.5). Broadly speaking, larger degrees of chainring eccentricity were associated with larger peak F_E during the downstroke and a similar F_E in the upstroke (Figure 3.5), whilst the same degrees of eccentricity when placed at a non-optimal crank orientation resulted in a lower peak F_E output, but larger degrees of phase shift.

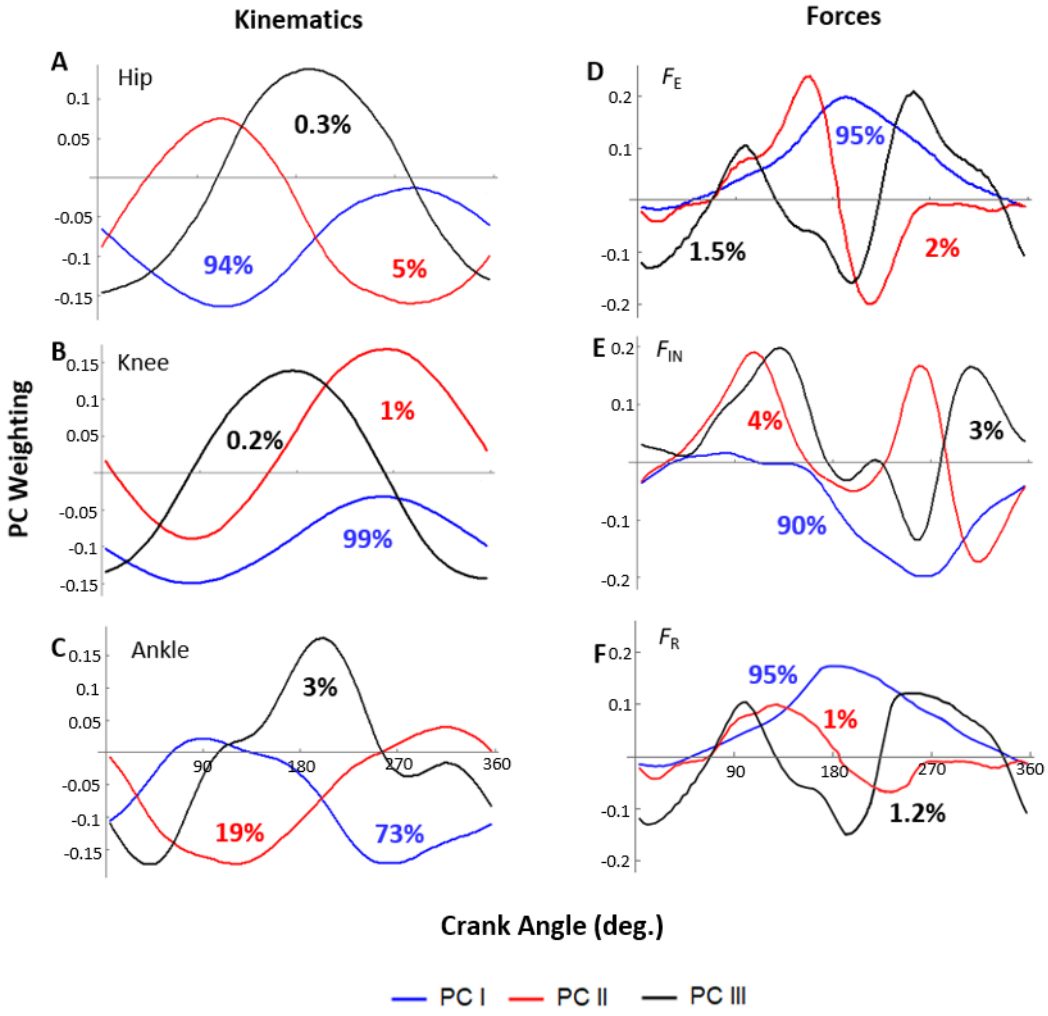

Figure 3.4 Principal component weighting for (A) the hip joint, (B) the knee joint (C) the ankle joint (D) effective force (E) ineffective force, and (F) resultant force. Embedded values depict the proportion of the signal that this component describes. Where PC I describes the mean of the data.

There was also a significant interaction between chainring condition and cadence, and as such, the loading scores for F_E and F_{IN} have been broken down into individual cadence conditions to highlight the distinct variability (Figure 3.5). Using the PC reconstructions to visualise the crank force waveform, it is possible to discern that the E_1 condition had a smaller effect on F_E in both left and right pedals compared to E_2. Nevertheless, with

increasing pedal speed, there is an observable trend of increased peak F_E ($P < 0.0001$) in the elliptical chainrings, and *post hoc* analysis of the different cadence conditions shows that E_{1-} only began to elicit a significantly greater F_E at 110 rpm and 130 rpm in comparison to the circular chainring.

A stark observation made clear in the reconstructions is that the bilateral asymmetries in F_E are particularly evident with increasing cadence. That is, at 110 rpm a subtle phase drift in the decline of positive F_E application begins to occur in the left pedal, this effect increases through 130 rpm and was substantial at 150 rpm, where peak F_E was achieved at 145° in the left pedal as opposed to 97° in the right pedal (Figure 3.5; Column I). The extent of the asymmetries is more convoluted when considering the effect sizes as shown in Table 2.2. For example, at 90 rpm, the left F_E changes are related to an effect size of 0.01 in PC I as compared to -0.08 for the right pedal (small effects). However, PC II (which indicates phase shifts in the application of force) has an effect size of -1.1 for the left (large effect), whilst the right pedal was small at -0.03. These opposing trends are pervasive across the cadences and chainrings, and larger effect sizes alternate between the left and right pedals.

Analysis of the F_{IN} components also shows a significant effect of chainring condition ($P < 0.001$), and again a chainring × cadence interaction ($P < 0.001$), so this variable has also been broken down by cadence (Figure 3.5; Column II). Analysis of the PC-reconstructed waveform shows decrements in F_{IN} with the elliptical chainrings when presented at the E_{1+} and E_{2+} crank angles. However, when at the E_{1-} and E_{2-} crank orientations, there was an increase in F_{IN}. This pattern is present in both left and right pedals, an effect that increases with eccentricity, up until 130 rpm; at this point the effect decreases and at 150 rpm, there is an increase in F_{IN} with chainring eccentricity. F_{IN} also displayed differing results between the two pedals; the circular, E_{1-} and E_{2-} chainring were all significantly different to one-another in the right pedal, but only E_{1-} was significantly different to the circular chainring in the left pedal.

Peak maximum and minimum F_R also displayed a parabolic relationship with cadence. Forces shifted later in the pedal cycle as cadence increased, into a wider peak in the right pedal at 150 rpm in comparison to a narrow peak in the left pedal in addition to a shift in F_R magnitude. There was a significant effect of chainring condition ($P < 0.001$), where elliptical rings E_{1-} and E_{2-} led to an increase in peak F_R, which was prevalent across cadence

conditions. In contrast with the F_E pedal force profiles, E_{2+} displayed a direct relationship with cadence in the left pedal which culminated in a significantly higher peak resultant force at 150 rpm.

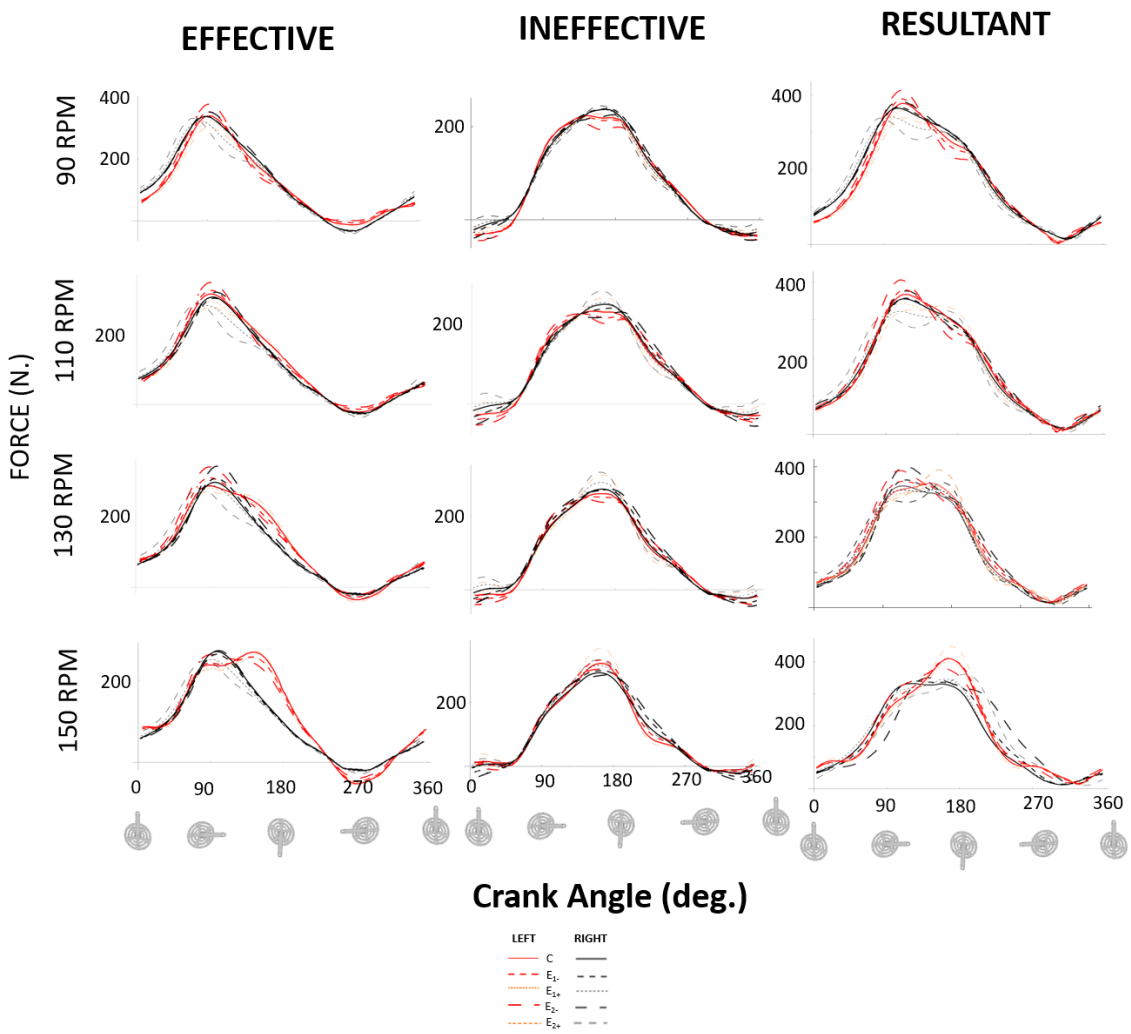

Figure 3.5 Principal component reconstruction of pedal forces. Visual representation of the first three principal component loading scores for the effective (first column), ineffective (second column) and resultant (third column) pedal forces for each chainring; broken into cadence blocks over the course of a pedal cycle regardless of resistance. The chainring conditions for the right pedal forces are represented in grey scale and are represented in red for the left pedal forces.

Table 3.2 Effect sizes describing how far the mean pedal force principal component loading score for each experimental chainring condition is from the circular chainring.

		90 rpm		
Condition	LE_{PCI}	LE_{PCII}	RE_{PCI}	RE_{PCII}
E_{1-}	0.01	-1.10	-0.08	-0.03
E_{1+}	0.22	0.22	-0.25	0.98
E_{2-}	-0.52	-2.39	0.38	-0.47
E_{2+}	0.49	1.21	-0.57	2.21
		110 rpm		
Condition	LE_{PCI}	LE_{PCII}	RE_{PCI}	RE_{PCII}
E_{1-}	0.00	-1.2	-0.19	-0.48
E_{1+}	0.46	0.24	-0.59	0.82
E_{2-}	-0.22	-2.44	0.15	-0.96
E_{2+}	0.81	1.02	-0.89	2.6
		130 rpm		
Condition	LE_{PCI}	LE_{PCII}	RE_{PCI}	RE_{PCII}
E_{1-}	-0.11	-0.54	0.01	-1.05
E_{1+}	0.31	0.03	-0.1	-0.09
E_{2-}	-0.42	-1.94	0.6	-1.37
E_{2+}	0.36	0.53	-0.46	2.37
		150 rpm		
Condition	LE_{PCI}	LE_{PCII}	RE_{PCI}	RE_{PCII}
E_{1-}	0.01	-0.25	-0.34	-0.02
E_{1+}	0.53	-0.35	-0.57	0.64
E_{2-}	0.04	-1.15	-0.21	-0.31
E_{2+}	0.16	0.26	-0.53	1.34

Note: Left effective principal component I (magnitude; LE_{PCI}); Left effective principal component II (phase; LE_{PCII}); Right effective principal component I (magnitude; RE_{PCI}); Right effective principal component II (phase; RE_{PCII}).

3.5.4 Index of Force Effectiveness

The IFE data are presented in Figure 3.6. Here there was a significant effect of chainring condition on IFE in two of the pedal cycle quadrants in the right pedal (Q1: $P < 0.001$; Q2: $P = 0.088$; Q3: $P = 0.302$; Q4: $P < 0.001$; Figure 3.6A), and no significant result in the left pedal (Q1: $P = 0.355$; Q2: $P = 0.957$; Q3: $P = 0.676$; Q4: $P = 0.065$; Figure 3.6B).

Post hoc analysis in the right pedal revealed different relationships between the chainrings at different portions of the pedal cycle. During Q1 in the right pedal E_{2-} IFE was significantly lower than the other chainrings across all cadences, and E_{1+} and E_{2+} had significantly higher IFE than E_{1-}. In Q3, there was a significant cadence × chainring interaction ($P < 0.001$), and at 130 rpm, E_{1-} and E_{2-} had significantly greater IFE than the circular chainring, whilst E_{1+} was significantly lower. In Q4, as cadence surpassed 130 rpm, E_{2-} had a significantly greater IFE than the other chainrings whilst the significant difference between E_{2+} and the other chainring closed at cadence increased (Figure 3.6A).

Whilst there were no significant effects of pedal cycle quadrant on IFE with the different chainring conditions, there were significant interactions ($P < 0.001$). At 90 rpm in Q1 and Q3, E_{2-} had a significantly greater IFE than the other conditions, which was not present in the other cadences; at 110 rpm in Q1, the circular chainring had a significantly greater IFE; and in Q3, there were no further interactions. In Q4, E_{2-} had a significantly greater IFE at cadences 90 and 130 rpm than the circular chainrings, and E_{1-} was significantly lower at 130 rpm than other conditions.

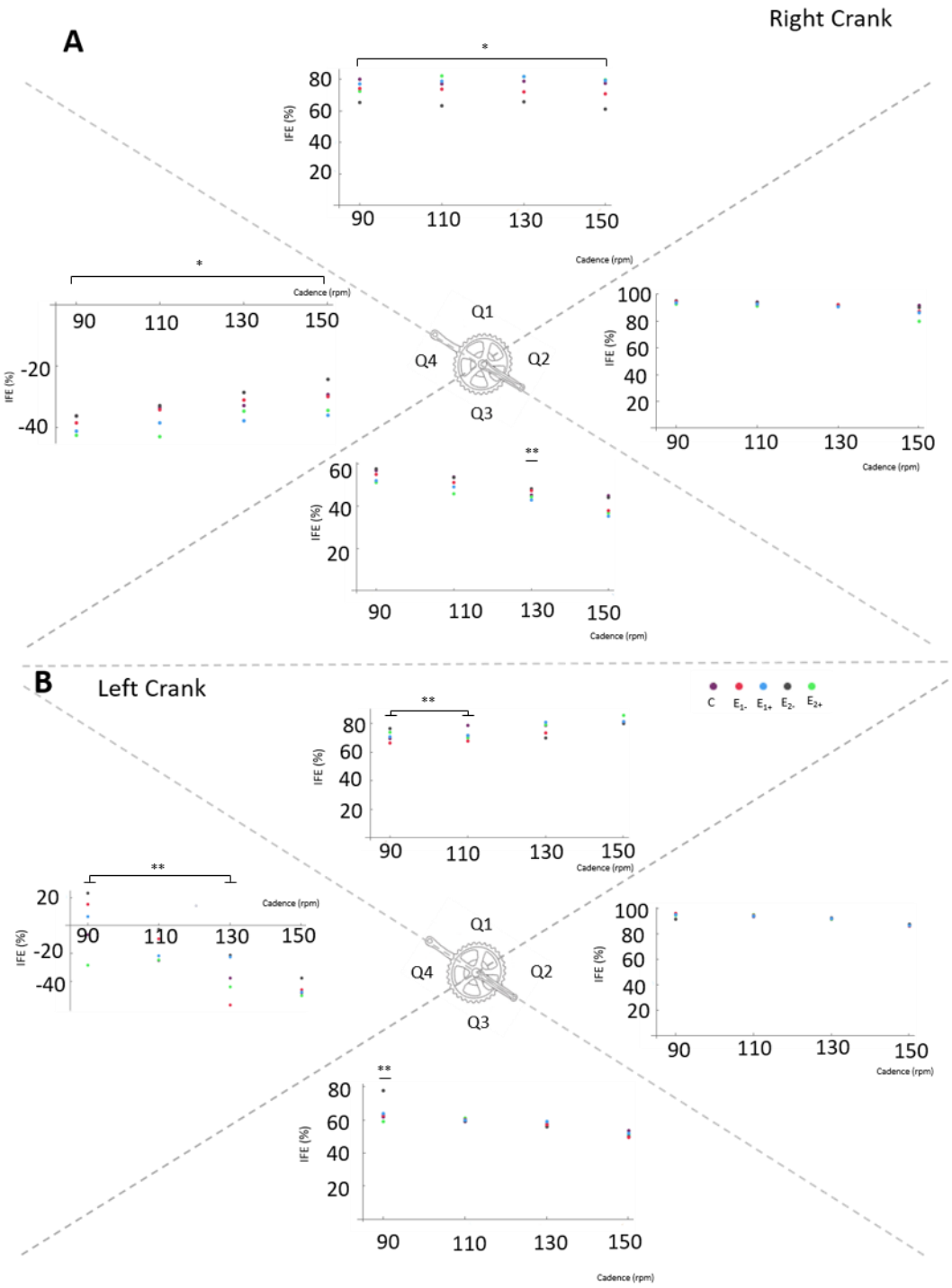

Figure 3.6 Representation of the index of mechanical effectiveness at the four quadrants in the pedal cycle for the five chainring conditions in the right (A) and left (B) pedals. Q1 (from 315° to 45°), Q2 (45° to 135°), Q3 (135° to 225°), and Q4 (225° to 315°) in a clockwise direction. * denotes a significant main effect of chainring condition on IFE across the quadrant; ** denotes a significant cadence × chainring interaction at the identified pedal speed.

3.5.5 Joint kinematics

The PCs from the joint kinematics are shown above in Figure 3.4. In the ankle joint kinematics there was a large amount of inter-subject variation, indicating that participants adopted different patterns of ankle motion; however, PC I still captured 73% of the variability in the waveforms (Figure 3.3C). There was a significant effect of chainring on the ankle joint PC I loading score ($P < 0.001$). PC II weighting in the ankle explained 19% of the variability and captures a phase shift occurring across conditions (Figure 3.3C). Differing biomechanical features (e.g. magnitude and timing) encapsulated by each PC loading score were determined during the reconstruction of the waveforms, where individually including each loading score allowed for the visualisation of the altered waveform and subsequent detection of the feature it was responsible for describing. There was a significant effect of chainring condition on PC II loading score ($P < 0.001$). The extent of ankle flexion and extension were visualised using PC reconstruction (Figure 3.7C). An increase in ankle excursion during Q2 and Q4 was observed, which was evidenced as an increase in ankle extension at the B_{DC} and a larger degree of flexion at T_{DC} in the elliptical chainrings. This was seen to the largest extent in E_{2+}, whilst E_{1-} had a significantly greater extension than the circular chainring ($P < 0.001$). Owing to a significant cadence × chainring interaction in PC I and II loading scores ($P < 0.001$), the loading scores were further dissected into their cadence groupings and reconstructed accordingly (Figure 3.8). The effect of the different chainring conditions varied depending on the cadence, however E_{2+} was associated with the largest ankle joint excursion throughout. There was a significant effect of chainring condition on PC I and PC II loading scores for 90, 110 and 130 rpm ($P < 0.001$), however there was no significant effect of chainring at 150 rpm ($P = 0.072$; Figure 3.6D). At the slowest cadence, this effect was associated with increased ankle plantar flexion in the E_{1-} condition, and to a lesser extent E_{2-} than the circular chainring (Figure 3.6A). When cadence increased to 110 rpm, there was no significant difference between the circular and the largest elliptical chainring when presented in the E_{2-} orientation, but E_{1-} was associated with a significantly greater degree of ankle extension than the other chainrings. Greater excursions in ankle angle were observed in conditions E_{1+} and E_{2+} (Figure 3.8B). When cadences reached 130 rpm, there was a significant decrease in ankle excursion with in the E_{1-} condition, and no significant difference between the circular and E_{2-} chainrings, whilst

E_{2+} maintained the largest joint angle (Figure 3.6C). These relationships are highlighted further in Table 3.2, which presents the degree of ankle joint excursions and the *post hoc* comparisons.

The PC weightings displayed in Figure 3.3 show that PC I captured 94% and 99% of the variability in joint range of motion in the hip and knee respectively. There was a significant effect of chainring condition on the PC I and PC II loading scores for the knee joint angle ($P < 0.001$) and hip joint angle ($P < 0.001$), in addition to significant effects of cadence ($P < 0.001$) and interactions between condition and cadence ($P < 0.001$) in both variables, and a significant effect of load in the hip joint angle ($P < 0.001$). In the reconstruction of the hip joint kinematics (Figure 3.7A), the significant effect of elliptical chainring condition represented an increased rate of extension during the downstroke (Q2), concurrent with the altered crank angular velocity (Figure 3.3B). Increased extension of the hip was observed at B_{DC} (Q3) with the elliptical chainrings in comparison to the circular ring (E_{1-}: +7°; E_{2-}: +5°), and a greater proportion of the pedal cycle was spent with the hip extending. Conversely, the effects of chainring condition on knee joint kinematics are not as visible in the PC reconstructions (Figure 3.7B), however, *post hoc* analysis suggests that there is a significant difference between the three chainrings and the manipulation of crank orientation, but no significant difference between the conditions with the crank oriented ahead of the major axes (E_{1+} and E_{2+}).

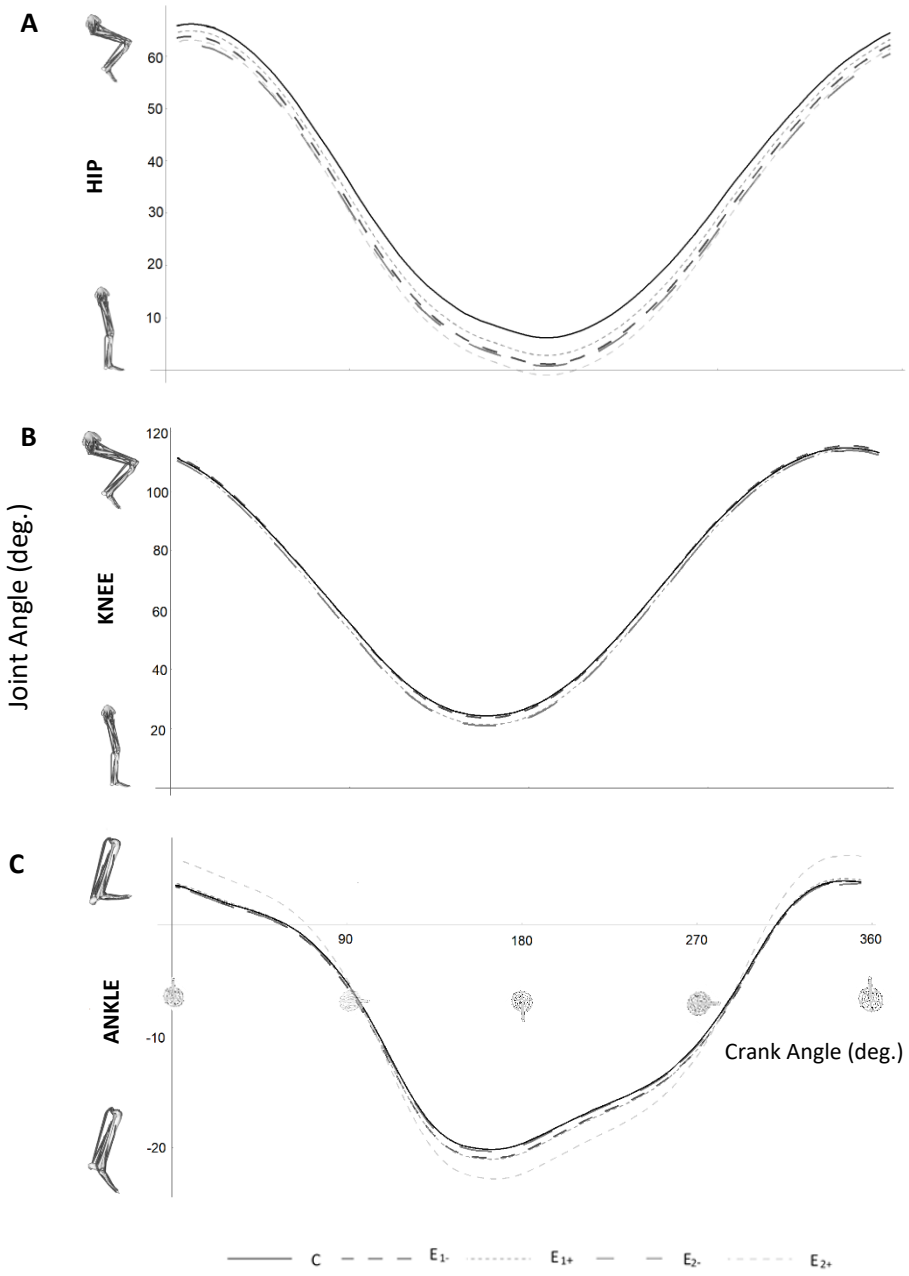

Figure 3.7 Principal component reconstructions of lower limb joint kinematics. Visual representation of the first three principal components for the hip (A), knee (B) and ankle (C) joint angles containing all cadence and resistance combinations. Chainring conditions are represented in greyscale.

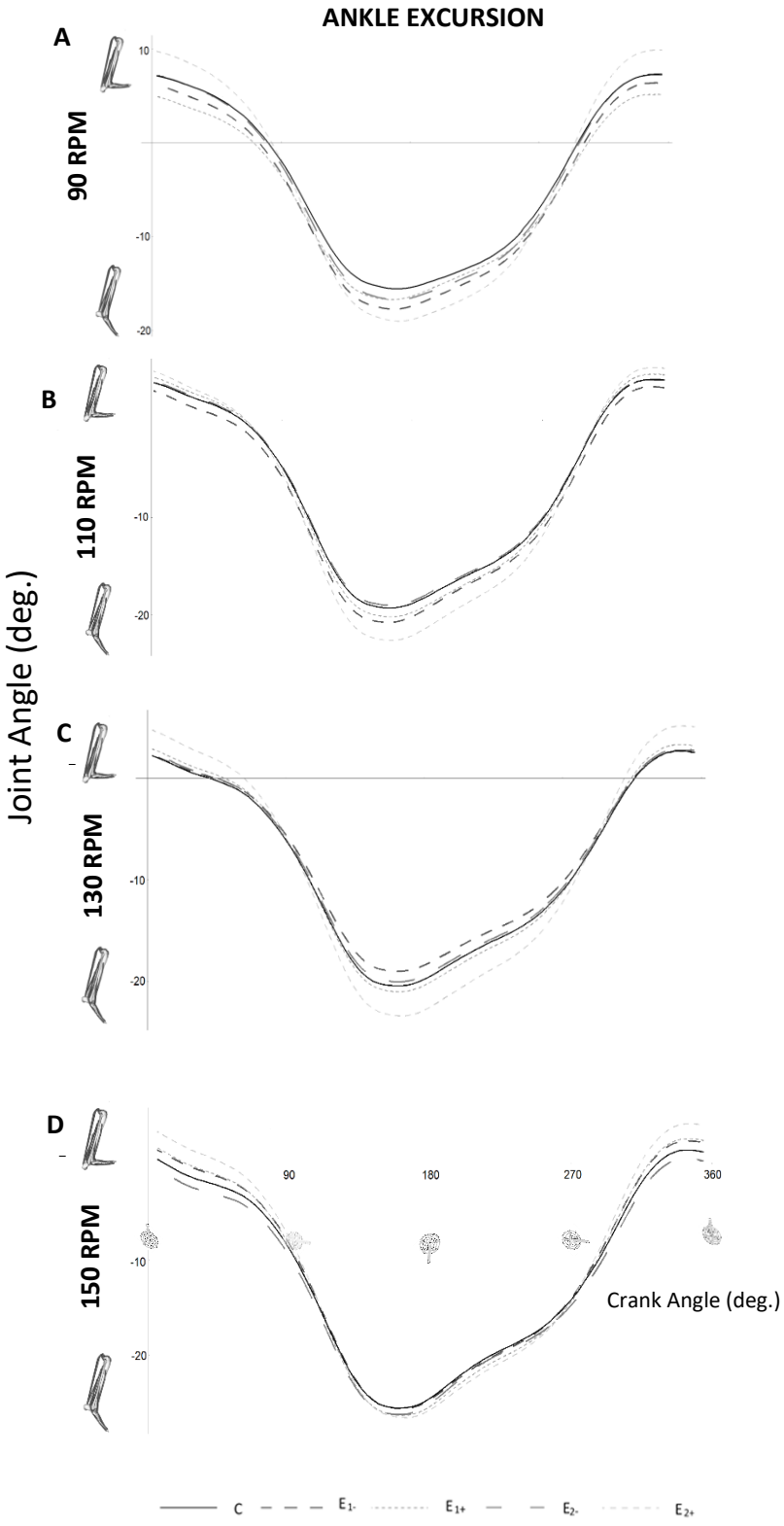

Figure 3.8 Principal component reconstructions of ankle joint excursions. Visual representation of the first three principal components for ankle joint, separated to show the effects of chainring condition at each cadence setting. Chainring conditions are represented in greyscale.

Table 3.3 Ankle joint excursions from the principal component reconstructions and post-hoc analyses of principal components one (magnitude) and two (phase). Letters presented in third and fourth column denote post-hoc analysis results. Conditions that do not share a letter are significantly different.

90 RPM			
Chainring Condition	Joint Excursion (°)	PC I	PC II
E_{1+}	22.0	A	C
Circular	22.8	B	A
E_{1-}	23.8	C	B
E_{2-}	24.0	A	A
E_{2+}	28.6	D	D
110 RPM			
Chainring Condition	Joint Excursion (°)	PC I	PC II
E_{2-}	22.9	A	A
Circular	23.2	A	A
E_{1-}	23.7	B	B
E_{1+}	24.6	C	A C
E_{2+}	27.7	D	C
130 RPM			
Chainring Condition	Joint Excursion (°)	PC I	PC II
E_{1-}	21.2	A	A
Circular	22.6	B	A
E_{2-}	22.7	B	A
E_{1+}	23.8	B	A
E_{2+}	28.1	C	B

150 RPM	
Chainring Condition	Joint Excursion (°)
E_{2-}	25.7
Circular	26.0
E_{1-}	27.0
E_{1+}	28.0
E_{2+}	29.9

3.6 Discussion

The objectives of this study were to determine the effects of changing the geometry and crank orientation of the chainring on (1) crank angular velocity, (2) lower limb kinematics, and (3) crank force profiles and pedalling technique. It was found that elliptical chainrings with an eccentricity of 1.13 and above significantly altered the crank angular velocity profile (Figure 3.4B). As predicted, the changes in crank angular velocity slowed the downstroke and upstroke (Q2 &Q4) and lessened the time spent in the top and bottom of the pedal cycle (Q1 & Q3). In association with this, lower limb segments were found to differ with chainring condition, with larger excursions about the ankle and hip joints, observed when the elliptical chainrings were used than with a circular chainring (Figure 3.7), and to a lesser extent in the knee. With respect to the crank force profiles, the most notable finding suggests that the effect of chainring eccentricity is cadence dependant, with more prominent increments of peak F_E observed at 110 and 130 rpm. Additionally, striking asymmetries in force application patterns were found between left and right pedals at the faster cadences, which was an unexpected finding.

3.6.1 Elliptical Chainrings alter Crank Angular Velocity Patterns

The hypothesis that chainring eccentricity and crank orientation would alter crank angular velocity in both phase and magnitude was supported (Figure 3.3). This finding is in agreement with research by Miller and Ross (1980), who developed a theoretical model of crank torque developed by muscles as a function of crank angle and velocity profile. They used optimisation to identify the crank angular velocity profile that maximised average crank power. This resulted in a velocity profile which slowed the crank during Q2, allowing for the muscles to generate power for a longer duration. The elliptical chainrings were found to have significant effect on crank angular velocity, altering the timing within the pedal cycle (Figure 3.4A), and when used in positions E_{1-} and E_{2-}, more time was spent in the power producing portion of the pedal cycling, and less time was spent in Q1 and Q3. This finding confirms the association between elliptical chainrings and a variable crank angular velocity as identified in previous theoretical work (Hull et al., 1991; Rankin and Neptune, 2008). The experimental data analysed here therefore confirms that elliptical chainrings do influence crank angular velocities *in vivo* and therefore do have the potential to affect force application at the pedal through altered musculoskeletal mechanics.

3.6.2 Elliptical Chainrings Alter Joint Kinematics

There were clear effects of the elliptical chainrings on lower limb joint excursions. The joint angle kinematics from the hip, knee and ankle were significantly altered (Figure 3.7) by changes in chainring eccentricity and crank orientation. This supports Rankin and Neptune (2008), who proposed that altering crank angular velocity using non-circular chainrings could be used to manipulate the leg kinematics throughout a pedal cycle. There were however differences in the magnitude of changes observed in each of the joints, and the interactions with cadence found in each joint. This indicates a complex response in limb mechanics occurs to the different chainring conditions studied here that could have implications for the resulting muscle mechanics.

When interpreting the reconstructions of principal components presented in Figure 3.7, it is notable that a comparison across the joints shows that the hip and ankle joints underwent the largest change in range of motion as a result of altered chainring geometries. However, the ankle kinematics were subject to the largest degrees in variability, as evidence by the PC weighting attributed in Figure 3.4C. In order to meet the task requirement during cycling, the neuromuscular system has been found to freely choose combinations of joint actions, made possible by the multiple degrees of freedom available between the pedal platform and the lower limb segments (Boyd et al., 1997). Martin and Brown reported that during maximal cycling, cyclists exploited ankle movement to increase the time spent extending the leg during the downstroke and thus increasing average power. This action was proposed to decrease fatigue during a 30 s maximal cycling trial (Martin and Brown, 2009). Here, the longer time spent in the downstroke (Figure 3.3A) was also associated with altered ankle angle kinematics, although the range of motion associated with each chainring condition was seen to vary across the different cadences (Figure 3.8). A reduction in ankle range of motion in conditions E_{1-} and E_{2-} in comparison to the circular chainring was observed in Figure 3.8C, and could be attributed to a strategy for simplifying the cycling task in conjunction with an increased cadence which may have caused fatigue (Murian et al., 2008). Little change was observed at the knee and it could be argued that knee joint actions were preserved as the dominant power producing muscle which cross this joint (the vasti complex) required conservation of its length

characteristics (Martin and Brown, 2009). This will be explored in greater detail in the next chapter.

3.6.3 Elliptical Chainrings Alter Crank Kinetics

Significant differences in the pattern of force application at the pedal were also found to occur between chainring conditions, suggesting that the alterations in crank angular velocity do influence force production and transfer to the crank. This follows from an earlier study in which the proportion of the pedal cycle occupied by the leg extension phase during maximal single leg cycling power was manipulated through the employment of a 20mm off-centre drive sprocket with a conventional circular circumference (Martin et al., 2002). It was shown that both instantaneous power and average power over a complete revolution were 12% and 8% greater, respectively when the leg extension phase occupied 58% of the cycle time *vs.* the traditional 50%. The increase in instantaneous power resulted from increased muscle excitation allowed by the increased time and reduced crank velocity for the leg extension phase (Martin et al., 2002). Interestingly, although the theoretical premise for the use of non-circular chainrings has been the argument that altered crank angular velocity provides a longer period for power production in the downstrokes and upstrokes, this study demonstrated that the timing of force application throughout the peak cycle does not change. Instead the work here highlights that the magnitude of peak F_E is affected during Q2 which is in keeping with earlier work by Strutzenberger and colleagues (2014) who reported an increase in magnitude of tangential force during the downstroke; an effect which in the current study, is sensitive to cadence (Figure 3.5; Column I). Additionally to this, as crank angular velocity increased through Q3 during the E_{1-} and E_{2-} conditions (Figure 3.4; Column I), there was a reduction in the negative work performed by the left crank across all cadences (as observed in the reconstructions in Figure 3.4; Column I), allowing for an increase in work production. Therefore, while changes in crank angular velocity were similar to those predicted the concomitant effects on force application are not as initially predicted.

Cadence alterations have previously been found to affect pedal forces and joint kinematics (Kautz and Hull, 1993; Marsh and Martin, 1995). In corollary with this, the enhanced F_E in the E_{1-} and E_{2-} conditions with increasing cadence justifies further consideration of how the

internal pedal forces interact with the bicycle. Muscular forces accelerate the legs while the foot-pedal connection constrains the resulting movement so that the pedal axis follows a circular path about the crank. Consequently, the applied pedal force cannot be understood independent of the dynamics of cycling movement, and in particular to how gravitational and inertial forces contribute to how the foot travels about the axis (Kautz and Hull, 1993). Decomposing the pedal kinetic measurements into muscular and non-muscular components would further substantiate the understanding of the mechanisms controlling the alterations in peak F_E observed here in response to cadence.

Pedal forces are understood to have a quadratic relationship when plotted as a function of cadence (Figure 2.8). Whilst activation based muscular forces contributing to force development and transfer to the crank have been found to decrease linearly from approximately 155 N at 60 rpm to 85 N at 120 rpm; non-muscular forces, such as gravitational and inertial forces, increase linearly with increasing cadences from near 70 N at 60 rpm to about 125 N at 120 rpm (Neptune and Herzog, 1999). Moreover, gravitational effects remain fairly constant across cadence conditions at the same body position (Brown et al., 1996), the increase in the non-muscular component reflects an increase of the inertial influence on pedal forces at greater cadences (Baum and Li, 2003).

Previous work into the consequences of increased crank inertial loads on freely chosen pedal speed and gross efficiency have observed increases in peak crank torque and changes in torque (Fregly et al., 2000; Hansen et al., 2002), which is thought to arise as a result of amplified stimulation of mechanoreceptors in the legs. Additionally, increased torque changes would require an enhanced rate of force development to occur within the active muscles (Hansen et al., 2002), possibly to allow torque to be produced within the appropriate portion of the pedal cycle. In relation to results presented within this chapter it is reasonable to draw similarities between Hansen and colleagues (2002) work and the results presented here. Figure 3.5 highlights that the F_E profiles in conditions E_{1-} and E_{2-}, were affected significantly only in terms of their magnitude, which was represented as an increase in peak force application over pedal speeds of 110 rpm, with no significant impact on negative work during the pedal cycle (in Q4). Thus, it could be argued that principles governing the efficaciousness of non-circular chainrings are centred around centripetal force, and the altered velocities within the drivetrain kinematics.

Similarities between the cadence interactions with crank forces reported in this chapter can be drawn with the unpublished theoretical work from Malfait et al. (2012), showing eccentricity and crank orientation dependent alteration in the hip and knee joint moments and powers that were found to increase exponentially with pedalling rate (up to 140 rpm). Also of note were the increases in the dynamic peak muscle power, particularly affecting the hip extensors (hamstring complex) and knee extensors (vasti muscle complex). This finding may in part explain why previous studies, using submaximal (i.e. slow cadence) cycling protocols, found equivocal results pertaining to physiological and performance variables of cycling with non-circular chainrings. Most of these studies use cadences ranging between 60 – 120 rpm and therefore do not test conditions under which the chainrings have an appreciable effect on force development. This is further supported by the fact that although Rankin and Neptune (2008) predicted no such cadence effect, despite including pedalling rates of up to 120 rpm in their SIMM (Musculographics, Inc) constructed musculoskeletal model, the model used did not take into account the inertia and gravitational forces affecting the leg muscles. Equally, Hue and colleagues (2006) found no differences in the time taken to complete a 1 km time trial between non-circular and circular chainrings. However, they did note that subjects with the highest lower limb muscle volumes produced their fastest times with the non-circular chainrings, suggesting a benefit to having greater mass about the crank, which could increase the effects of crank inertial properties with greater benefits seen with the non-circular chainrings.

Although there is evidence of enhanced sprint-style cycling performance owing to the employment of a non-circular chainring (Hue et al., 2001) the work presented here is seemingly the first to connect non-muscular components of force production and potential performance benefits of elliptical chainrings. As such, future work should consider a thorough analysis of decomposed force components when considering the implications of altered chainring geometry. An association between augmented crank inertia and elliptical chainrings does not seem inconceivable, given the equation to calculate crank inertia proposed by Fregly and colleagues (2000) considers the rotational inertia of entities affecting drive chain kinematics and gear ratio (Eq 3.3). As such, it appears important to explore this notion further within a controlled laboratory environment if we are to understand how best to exploit the biomechanical prospects of such systems.

$$\underbrace{\{\mathrm{I_X} + (\mathrm{R_X}/\mathrm{R_Y})^2(\mathrm{I_Y} + \mathrm{I_Z})\}\theta_1}_{(I_{Eff})_{\text{Ergometer}}} = T_C - \underbrace{\{(R_X/R_Y)R_Z F_Z\}}_{(T_{Eff})_{\text{Ergometer}}} \quad \text{Eq. 3.3}$$

where

I_{Eff} = effective rotational inertia about the crank due to rigid bodies about the crank axis (i.e., chainrings, pedals and crank arms) and about the flywheel or rear wheel axis (e.g., the freewheel)

$\mathrm{I_X}$ = combined rotational inertia of the chainring, pedals and crank arms about the crank axis

$\mathrm{I_Y}$, $\mathrm{I_Z}$ = rotational inertia of the ergometer freewheel and fly-wheel, respectively, about their axis of rotation

θ_1= angle of the crank measured with respect to top dead centre

T_C = crank torque due to the pedal forces produced by both legs

R_X/R_Y = gear ratio

R_Z = radius of the ergometer flywheel

F_Z = frictional resistance force applied to the flywheel by the band brake

T_{Eff} = effective resistance torque about the crank axis

Within this equation, there is the possibility of elliptical chainrings altering the outcome at $\mathrm{I_X}$, whereby mass or size of the ellipse could cause an altered mass distribution relative to the crank axis; and also at R_X/R_Y as elliptical chainrings have been described as being a ratio of crank-angle dependent effective radius of the front chainring to the rear cog. Quasi-elliptical chainring have been found to substantially manipulate the gear ratio over the course of the pedal cycle in comparison to small variations detectable with a circular chainring, and consequentially alter the effective chainring radius via a fluctuation in the number of teeth in contact with the chain (van Soest, 2014). Therefore, altering chainring geometry would have the ability to manipulate I_{Eff} and/or T_{Eff}, and consequently crank

inertia. However, the effects of the elliptical chainrings may not just be non-muscular as the orientation of the crank relative to the major axis (which is not represented in Eq 3.3) also influenced forces measured and therefore, any effects that varied with chainring orientation are additional to these.

It is important to bear in mind the possible bias in these responses, given that the musculoskeletal model used in this study was unilateral. Nonetheless, it is possible that elliptical chainrings could exacerbate differences in imbalances in leg dominance and as they are contrary to the participant's formal training of pedalling technique initiating an imbalance in ankle stiffness between left and right joints, a notion supported by the asymmetries observed between left and right F_E (Figure 3.5; Column I). As such, even larger joint excursions could have been seen in the contralateral side, causing a change length and velocity characteristics of the plantarflexor muscles, and consequently, an alteration in force production seen at that pedal. However, it does raise validity issues in that generalising joint kinematics to the opposing leg may not be appropriate.

3.6.3 Effects of Elliptical Chainrings on Index Effectiveness

The breakdown of mechanical effectiveness into quadrants within a pedal cycle (Figure 3.6) offers further perspective into the effects of both chainring eccentricity on force application and also left/right discrepancies in pedalling technique. A surprising result is that within Q4 the bilateral asymmetries appear to be particularly large. This discrepancy is most likely related to the fact that IFE is a calculation based upon ratios between F_E and F_R. When considering the negative F_E and low F_R present during Q4, calculating ratios when using negative values can lead to major fluctuations appearing, despite the possibility that the different chainring conditions might only be responsible minor deviations in IFE values. As a result, this quadrant may not give the most representative feedback and must be interpreted with caution.

However, when referring to the crank force results presented (Figure 3.5) the peak F_E occurs between 90° and 180° in both the left and right crank, thus Q2 and Q3 (Figure 3.6) could give the best indicator of pedalling technique when the IFE is used as a measure, and the results in these quadrants, do indicate some degree of asymmetry. At 130 rpm in the right pedal Q3, the IFE in the E_{1-} and E_{2-} conditions were significantly greater than the

circular chainring, suggesting that through the B_{DC} (Q3) at 130 rpm, the participants were better able to orient the expressed crank forces into contributing toward a propulsive action when the elliptical chainrings were used. Interestingly, commercially available non-circular chainrings, such as the "Shimano Biopace" (Okajima, 1983) and "Eng 10" (Hull et al, 1992), orient the smallest chainring radius toward the major axis, making the design similar to the non-optimal conditions, E_{1+} and E_{2+} in this study. These have been shown to be unsuccessful in reducing the time spent by the foot in the top (Q1) and bottom (Q3) of the pedal cycle and increase maximal crank angular velocity through the downstroke (Malfait et al., 2010). The commercially available non-circular chainrings are typically used with the crank orientation that is detrimental to their aim. They may be more successfully used if the crank orientation was altered to be nearer the one used here. As such, the elliptical geometry of the chainrings presented in this thesis allowed maximal crank angular velocity to be achieved at 0° and 180° in conditions E_{1-} and E_{2-} (Figure 3.3B). This was achieved through precise alignment of the smallest radius of the chainring and minimises the mechanical constraints of pedalling through this Q3 and adds further evidence that position against the crank when using elliptical chainrings is important within the context of IFE.

3.6.4 Pedalling Asymmetries

Much of the research quantifying kinetics and kinematic variables in cycling has focused on a single leg (Sanderson and Black, 2003), however, questions of asymmetry are an important consideration when assessing the implications of implementing a change in mechanical behaviour, as identifying differences is vital for reducing knee loads transmitted by the dominant leg, which could lead to overuse injuries. When examining the effects of chainring geometry on the patterns of force production (Figure 3.5), there are bilateral differences, the size of which are affected by cadence. For example, a larger peak F_E occurs in the left pedal at 90 rpm and 110 rpm in the E_{2-} condition, which is supported in terms of effect size as presented in Table 3.3. As such, the PC I loading score denotes a higher effect size in the left pedal (-0.52) than the right (0.38) at 90 rpm, and again to a smaller extent at 110 rpm (-0.22 and 0.15, respectively; Table 3.3).

An interesting observation is the bilateral asymmetries in pedal forces with increments in cadence. That is, as cadence increases, there is a clear shift in phase in the left pedal, and

the peak F_E occurs closer to 180°, than to 90°. The asymmetries between the left and right crank force responses are pervasive throughout the conditions studied. There is a consistent overall pattern; in that E_{2-}, and to a lesser extent E_{1-}, creates the larger changes in peak F_E compared to the circular. E_{1+} and E_{2+}, conversely amounted to a degradation in peak F_E development (Figure 3.5), and as previously suggested that when presented at alternative crank angles, it was not possible to effectively orient the force around the crank when pedalling in conjunction with an increased angular velocity. A pedalling rate induced bilateral asymmetry is not uncommon (Cavanagh et al., 1974; Sargeant and Davies, 1977), however, there issues of etymology whereby this can cover a variety of differences such as applied pedal forces, mean pedal forces or total work output. There is a tendency among humans to preferentially use one side of the body in voluntary motor acts, known as lateral preference (Carpes et al., 2007a). Previous studies indicate there is an advantage of the preferred limb to that of the contralateral in terms of neuromuscular control, and lower muscle activation and frequency during dynamic tasks (Adam et al., 1998), and imbalances in bilateral force production are known to be in the region of 5 – 20 % (Carpes et al., 2010). It has also been reported that the dominant leg might also not contribute as much positive average power as the contralateral leg during pedalling, perhaps owing to a greater hip extensor moment in the non-dominant leg (Smak et al., 1999). In the study conducted by Smak and colleagues they highlight one subject in particular who displayed a minor shift in phase in crank torque in their non-dominant leg when cycling at 120 rpm. To explain this, they propose a contribution from altered differences in knee and hip moment patterns, rather than the ankle joint, perhaps resulting from differences in strength and/or motor control deficits in the non-dominant side (Smak et al., 1999).

Shifts in phase just as the one reported by Smak and colleagues (1999) and the one reported here are unusual and scarcely identified elsewhere. However, it is important to acknowledge that PC analysis is capable of detecting dominant patterns in the data that may be overlooked by other forms of analysis. PC analysis specifically allows for the assessment of waveform data and subsequent reconstruction, allowing for fuller details than is typically reported in experiments investigating cycling asymmetries, which typically focus on mean variables and the use of asymmetry indexes (Carpes et al., 2007a) allowing the result to be described as percentage values (Robinson et al., 1987). However, PC have

successfully been utilised in the past to detect asymmetries in time-dependent kinematic responses to walking in amputee subjects (Crenshaw and Richards, 2006) suggesting that is a viable method of deducing differences. Given the prevalence of disproportionality well documented in lower limb work in gait studies (Cuk et al., 2001; Herzog et al., 1989), it is perhaps not surprising that such asymmetries exist. What may be of interest is that as the demands of the task increased through increments in cadence, the asymmetry was exacerbated, an effect which is typically attributed with running and augmented muscular effort (Cavagna, 2006). The opposite has seen to be apparent in other cycling studies as Carpes and colleagues previously demonstrated by increasing the demands of the task by increasing power output was found to have the opposite effect during an incremental maximal test and a reduction in pedalling asymmetries was observed (Carpes et al., 2007b). Similarly, Carpes and colleagues also found that increases in voluntary crank torque output during a simulated 40 km time-trial competition were associated with increases in pedalling symmetry (Carpes et al., 2007a). The authors attribute the symmetry observed during high intensity cycling to the influence of fatigue on motor unit recruitment, and that as intensity of the cycling task increases, there is an increase of common bilateral input (Boonstra et al., 2008), promoted by augmented excitability and neural coupling by inter-hemispheric cortical communication and part of the multi-factorial strategies which minimise lateral differences (Anguera et al., 2007; Teixeria & Caminha, 2003).

In contrast with this, Bini and Hume (2015) reported large inter-limb asymmetries for the F_R (11-21%) and F_E (36-54%) in competitive cyclists (n =10) during a 4-km time trial, which was performed maximally and at a self-selected cadence. Also of note in this study, was a strong correlation (r = -0.72) between the asymmetry index results and F_E, and participants who displayed larger asymmetries had an enhanced cycling performance than those with smaller asymmetries. As per this study, asymmetry indices were smaller for the F_R compared with that of the F_E (Figure 3.5). This is postulated to occur due to a coupling effect between kinetics and kinematics in measures of F_E, but not so F_R, which is in line with results put forward by Carpes and colleagues (2007a), who found direct links between asymmetry, peak torque output and limb dominance. This seemingly contests popular notions of asymmetries leading to reductions on performances, however, it is important to note that conceptually at least, during cycling, total power production likely results in a

superior performance.

One factor that could have an influence on asymmetry in cycling performance is fatigue of the participant. As the protocol used here was demanding and data were collected within a single session, the effects of fatigue were considered in the design of the study. More specifically, well-trained cyclists were used and the ordering of pedalling/resistance combinations and chainring conditions were randomly assigned within each subject. A further ANOVA test was run for each test to determine whether joint angles and pedal forces loading score values were affected by the progression of pedal cycles during the test, and for each variable the test returned a non-significant value ($P > 0.999$).

3.6.6 Summary

This chapter investigated how altering chainring eccentricity would affect crank angular velocity over the course of the pedal cycle, and how this would in turn impact the joint kinematics and crank force patterns. The findings demonstrate that manipulating chainring eccentricity and orientation of the crank relative to the major axis of the chainring is an effective method of altering crank angular velocity over the course of the pedal cycle. The impact this has on crank force was found to be dependent on cadence. When pedalling at 130 rpm, an eccentricity of 1.13 (E_{1-}) was enough to elicit an increment in peak F_E, with concomitant alterations in joint kinematics and mechanical effectiveness. Larger eccentricities of 1.34 (E_{2-}) promoted an even larger response in peak force production at this cadence. The cadence dependent effects in these data support speculations that the effects of chainring geometry is a product of non-muscular components of force production, namely increased crank inertia. In addition to this finding, large asymmetries in left/right pedal kinetics arose which may impact the way in which these results are interpreted and generalised due to altered interactions in either limb.

When splitting the leg into its respective segments of thigh, shank and foot, the pedalling motion determines both segment orientation and rate of joint angle change, thus segment kinematics are determined by the drivetrain kinematics, which in turn affects the intersegmental moments (Hull and Jorge., 1985). The skeletal muscles spanning the leg joints are primarily responsible for developing these moments, thus it might be predicted that the muscle force requirements are altered. This has previously been shown to be the

case for joint moments (Marsh et al., 2000), negative muscle work (Neptune and Herzog, 1999) and muscle activation (Neptune and Hull, 1999). The results presented here show that patterns of joint excursion were altered across the leg joints. Changes in joint range of motion are known to be a marker of muscle length and torque producing capabilities (Charteris and Goslin, 1986), and therefore suggesting muscle-tendon unit lengths and velocities and muscle activation patterns could be affected by use of elliptical chainrings, factors that will be discussed in detail in Chapters Four and Five.

Chapter 4. Are muscle-tendon unit kinematics affected by chainring eccentricity at different pedalling cadences and loads?

4.1 Introduction

In the previous chapter, employing different chainring geometries was shown to evoke changes in both the crank angular velocity and the kinematics of the lower limb joints. It could therefore be suggested that the working lengths and contraction velocities of the muscle-tendon unit (MTU) complexes acting upon the leg joints would be altered as well (Too, 1990). Although MTU dynamics have not been previously investigated in respect to non-circular chainrings, this is an important element of neuromuscular control given the potential interactions between the muscle fibre force-length and force-velocity properties, tendon dynamics and excitation patterns (Lieber and Friden, 2000). Therefore, to better understand the implications of alterations in hip, knee and ankle joint kinematics as well as variations in crank angular velocity profiles, the resultant behaviour of the muscles acting on these joints needs to be considered in greater depth.

Skeletal muscle's capacity for force production depends upon the length and shortening velocities over which the fibres operate during the task. The fibres of each muscle have an optimum length (L_o) for force production and at shorter or longer lengths, the fibre's capacity to produce force is constricted owing to a reduced effective overlap of its contractile proteins (Huxley and Hanson, 1954) and changes in the lattice spacing (Williams et al., 2013). The velocity of active fibre lengthening and shortening also influences the force producing capacity of the muscle fibres. When acting at slow shortening velocities, the muscles are capable of producing relatively large forces (Hill, 1938). However, when the velocity of shortening increases, there is an exponential decrease in the force until reaching maximum shortening velocity (Figure 2.9; V_{max}). These intrinsic properties influence the way force can be produced and the ability to generate the necessary mechanical power during dynamic movements such as running and cycling (Biewener, 2016). As changes in MTU kinematics could have an impact of fibre behaviour, quantifying differences in MTU length and velocities related to altered chainring geometries is therefore an important first step to understanding potential neuro-mechanical effects of the chainrings.

Previously, Rankin and Neptune (2008) implemented a musculoskeletal model and simulation with the aim of using a dynamic optimisation framework to identify the chainring shape that might maximise average crank power. An elliptical chainring with an eccentricity of 1.29 (Figure 2.11) was identified as being the optimal shape by allowing crank power to increase by 3.0% when pedalling at 90 rpm relative to a circular chainring. This alteration in power was attributed to increased mechanical work from the vasti muscle complex, gluteus maximus, soleus and gastrocnemius during the downstroke and the iliopsoas and tibialis anterior during the upstroke. However, the authors dismissed any contributions of altered force-length-velocity relationships, given that fibre lengths and velocities were predicted to remain nearly identical between optimal and circular chainrings across all the experimental cadences (Rankin and Neptune, 2008). Rankin and Neptune (2008) employed a Hill-type model to represent the behaviour of the 15-lower extremity MTUs under observation, however, only the fibre lengths and velocities were reported in their findings. Whilst this provides valuable insight, it raises more questions. The authors postulated that the optimal chainrings evoked a longer amount of time for the downstroke (Q2, Figure 3.3A), increasing power generated in the muscles and resulting in an increase in external work. However, increases in muscle work must be generated somehow, such as an increase in force. Given the uncoupling in velocities that can occur between the MTU and fascicles (Wakeling et al., 2011) the effects of tendon stretch on force and power production should not be overlooked. Furthermore, joint kinematics were not reported by Rankin and Neptune (2008), aside from mentioning that hip motion was fixed in the model. As established in Chapter Three of this thesis, alterations in kinematics of the hip, knee and ankle were associated with changes in chainring geometry and crank orientation (Figure 3.7). The evidence presented here therefore suggests that MTU trajectories behave differently to the intrinsic muscle adaptations reported by Rankin and Neptune (2008).

The primary aim of this study was to explore the associations between chainring eccentricity and crank orientation on the behaviour of the MTU in the lower limb muscles for pedalling at different cadences and loads. More specifically, due to the previously observed changes in timing and magnitude of crank angular velocity (Figure 3.3B) and kinematics (Figure 3.7), it was predicted that alterations in the length and velocity of the

soleus (SOL), medial gastrocnemius (MG) and vastus lateralis (VL) MTUs would occur. Significant differences in ankle joint plantar and dorsiflexion angles were reported in Chapter Three between the different chainring conditions (Figure 3.7C), consequently it was hypothesised that the SOL and MG MTU lengths and velocities would vary significantly between these conditions. In contrast, smaller differences in knee joint kinematics were observed (Figure 3.7B), and as such, it was hypothesised that VL MTU lengths and velocities would not differ between chainrings.

4.2 Methods

This chapter utilises data from eight well-trained cyclists (4 male, 4 female; age: 37.8 ± 15.3 years, mass: 70.1 ± 12.5 kg, height 176.1 ± 12.2 cm). Data acquisition is described in Chapter Three, but briefly, participants performed eleven 30 second trials as various power (200 W – 300 W, in steps of 50 W) and cadence (90 – 150 rpm in steps of 20 rpm) on an indoor cycling ergometer indoor trainer (Schoberer Rad Messtechnik (SRM), Jülich, Germany). They were presented with elliptical chainrings (Hope Technology, Barnoldswick, UK) of two levels of eccentricity (E_1: 1.13 & E_2: 1.34) and fitted at an optimal (E_1- & E_2-) and non-optimal (E_1+ & E_2+) crank orientation (Figure 3.1) whilst three-dimensional kinematic data (100 Hz, Vicon, Oxford, UK) were recorded.

4.2.1 Muscle-Tendon Unit Modelling

Kinematics data were used to drive a subject-specific musculoskeletal model (Lai et al., 2017) in OpenSim v3.3 (Delp et al., 2007), as detailed in Chapter Three. Each model was scaled to each subject's height and weight, allowing muscle fibre and tendon slack lengths to remain the same percentage of the scaled total actuator length. The top dead centre denoted the start of each pedal cycle, with joint angles calculated using inverse kinematics analysis, and consequently muscle-tendon unit lengths were calculated from each model (Figure 4.1).

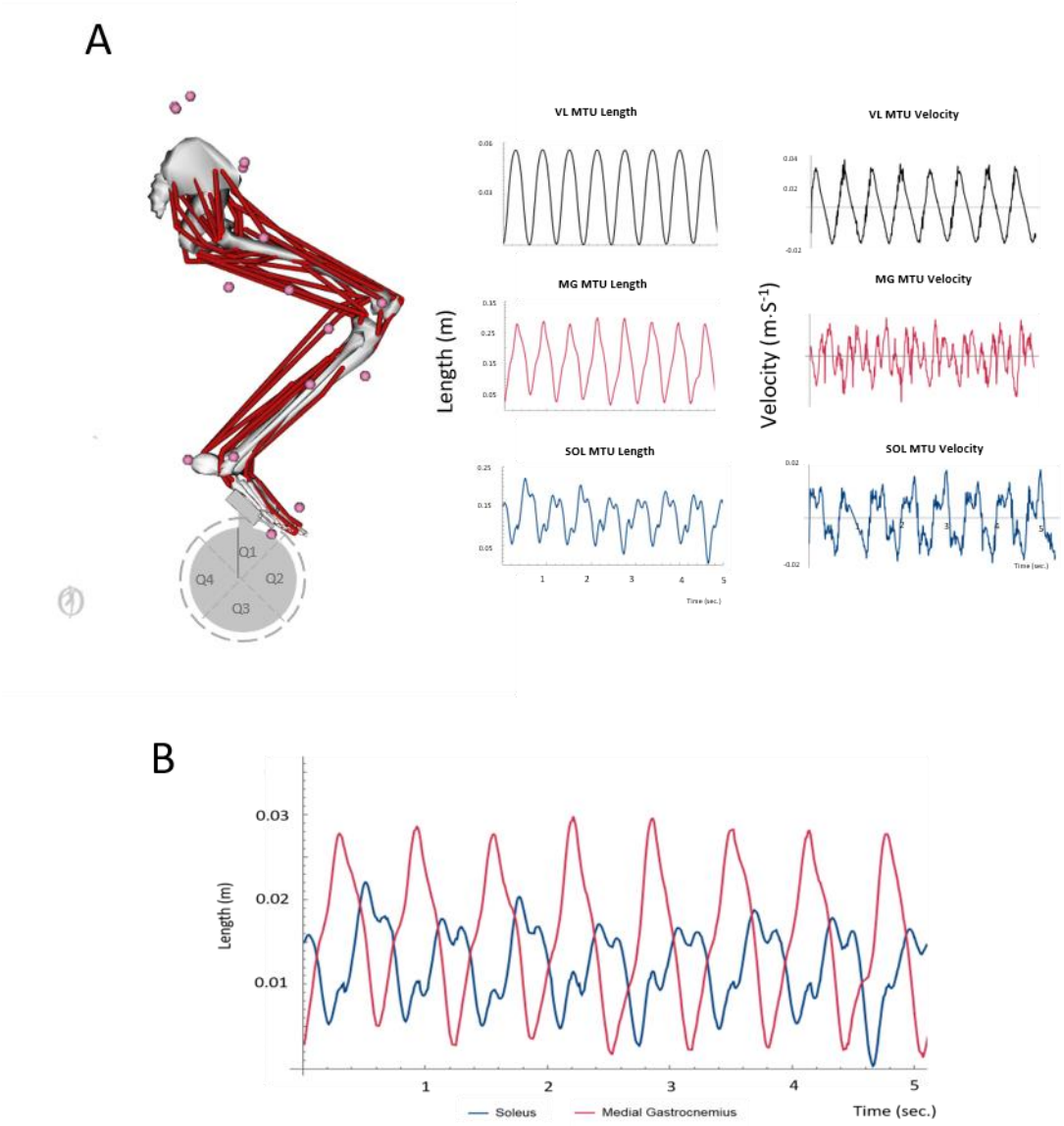

Figure 4.1 Example MTU length and velocity data from a representative participant cycling with a circular chainring. **(**A) The model is positioned with crank at the top dead centre, and the four zones of the pedal cycle depicted (Q1 top; Q2 downstroke; Q3 bottom; Q4 upstroke). The muscles are represented as red lines, and raw MTU lengths for the soleus (SOL), medial gastrocnemius (MG) and vastus lateralis (VL) are highlighted for the first 5-seconds of data acquistion from a single trial of one participant, with calculated MTU velocities also provided and, (B) Plot shows the raw MTU length traces from the musculoskeletal model highlighting the timing differences in soleus (blue) and medial gastrocnemius (Red). Data are for five seconds at 90 rpm and 250 Watts.

4.3 Data Analysis

The inverse kinematics analysis in OpenSim was used to predict SOL, MG and VL MTU length, and subsequently MTU velocity was calculated as the first-time derivative of MTU length across the pedal cycle using custom written code (Mathematica 11 software, Wolfram Research, Champaign, IL). The monoarticular (soleus; SOL) and biarticular (medial gastrocnemius; MG) ankle plantar flexor muscles were selected to observe the impact of

the altered ankle joint kinematics. Vastus lateralis (VL) was selected, as one of the largest contributors to total power production in cycling, to identify whether external alterations at the crank produced musculotendon adaptations in proximal segments despite the small changes in knee joint kinematics observed.

MTU lengths and velocities were interpolated to 100 points per pedal cycle. The primary patterns in MTU behaviour over the pedal cycle were determined using principal component (PC) analysis. Data were arranged into a $P \times N$ matrix **A**, where the interpolated MTU length or velocity data points per cycle (P = 100) were organised into N = 8 participants × 5 conditions × 11 trials × 26 pedal cycles rows. The mean was not subtracted beforehand, as has been described previously (Wakeling and Rozitis, 2004), so that it was represented by the first PC. In order to visualise the primary differences in MTU length and velocity waveforms for each condition, they were reconstructed from the vector sum of the MTU weightings and loading scores for the first PC for SOL, MG, VL length and VL velocity and the first five PCs for SOL and MG shortening velocity. The number of PCs included for each variable was chosen to ensure >90% of the variability were accounted for within the reconstructions (Chau, 2001). PCA was completed using custom written code in Mathematica (Mathematica 11 software, Wolfram Research, Champaign, IL).

4. 4 Statistics

General linear model analysis of variance (ANOVA) was used to identify the effects of chainring eccentricity, crank orientation, cadence and load on the loading scores for the first PC (PCI_{LS}) for MTU length and VL MTU velocity and first five PCs ($PCI\text{-}V_{LS}$) for SOL and MG MTU velocity. Additionally to the main effects, the model included two-way interaction terms between chainring condition, cadence and load on SOL, MG, and VL MTU length and velocity, with subject defined as a random factor. A *post hoc* Tukey test was performed to determine where the significant differences between chainring condition for a given cadence or load occurred. Statistical analyses were completed using Minitab version 18 (Minitab Inc., State College, PA). All data are presented as means ± SD, and statistical tests were deemed significant at $\alpha = 0.05$.

4.5 Results

4.5.1 Principal Component Loading Scores

The number of PC loading scores (PC_{LS}) used to reconstruct the MTU length and velocity waveforms (Figure 4.2) was in accordance with 90% trace criterion (Chau, 2001), whereby the cumulative percentage of PC weightings explained 90% of the total variability. This percentage varied depending on which muscle and whether they were explaining MTU lengths or velocities.

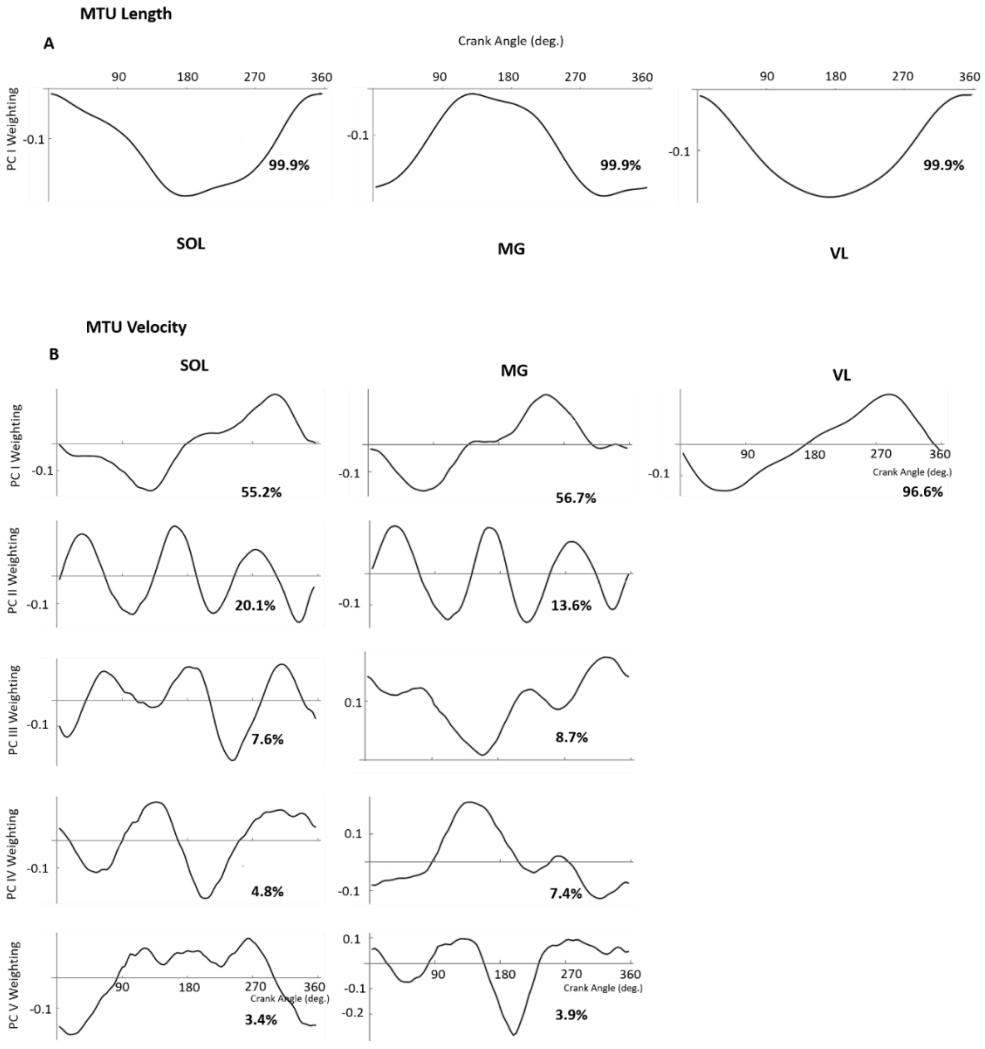

Figure 4.2 Principal component weightings for the patterns of (A) MTU lengths and (B) MTU velocities for each muscle. The embedded value represents the percentage of the signal explained by each component. Where PC I explains the mean of the data.

4.5.2 Soleus MTU lengths and velocities

The soleus MTU shortened during the downstroke of the pedal cycle, whilst the ankle was plantar flexing, prior to lengthening after the pedal went past 180°. There were no

significant main effects of chainring eccentricity or crank orientation on the PCI_{LS} for SOL MTU length (P = 0.097; Figure 4.3A&B). There was a significant effect of cadence (P < 0.0001) and load (P < 0.0001) on SOL MTU length.

There was significant effect of cadence across all five SOL shortening velocity PC loading scores (P < 0.0001) and as could be expected, SOL MTU shortening velocities tended to increase systematically with cadence. Chainring eccentricity (Figure 4.3; column I) and crank orientation (Figure 4.3; column II) significantly affected the first five SOL MTU velocity PC loading scores (P < 0.0001), and a chainring condition × cadence interaction (P < 0.0001) was also found. As such, the MTU velocity waveforms were separated and reconstructed in their respective cadence groups, presented in Figure 4.2. Over the course of the pedal cycle, there was an increase in both maximum lengthening velocity (E_{1-} = +0.017 $m \cdot s^{-1}$, E_{2-} = +0.05 $m \cdot s^{-1}$, E_{1+} =+ 0.037 $m \cdot s^{-1}$, E_{2-} = + 0.083 $m \cdot s^{-1}$) and maximum velocity of shortening (E_{1+} = -0.019$m \cdot s^{-1}$, E_{2+} = -0.045$m \cdot s^{-1}$, E_{1+} =-0.032$m \cdot s^{-1}$, E_{2-} = -0.054$m \cdot s^{-1}$) in the elliptical chainrings compared to the circular chainring (0.102 $m \cdot s^{-1}$ and -0.109 $m \cdot s^{-1}$, for lengthening and shortening velocities, respectively; Table 4.2). Additionally, the chainring eccentricity resulted in the peaks of shortening and lengthening velocities occurring at different points in the pedal cycle than the circular chainring (Table 4.3 & Figure. 4.3C-J), with the optimal crank orientation leading to peaks occurring later in the pedal cycle and the alternate crank orientation resulting to the peaks occurring earlier in the pedal cycle.

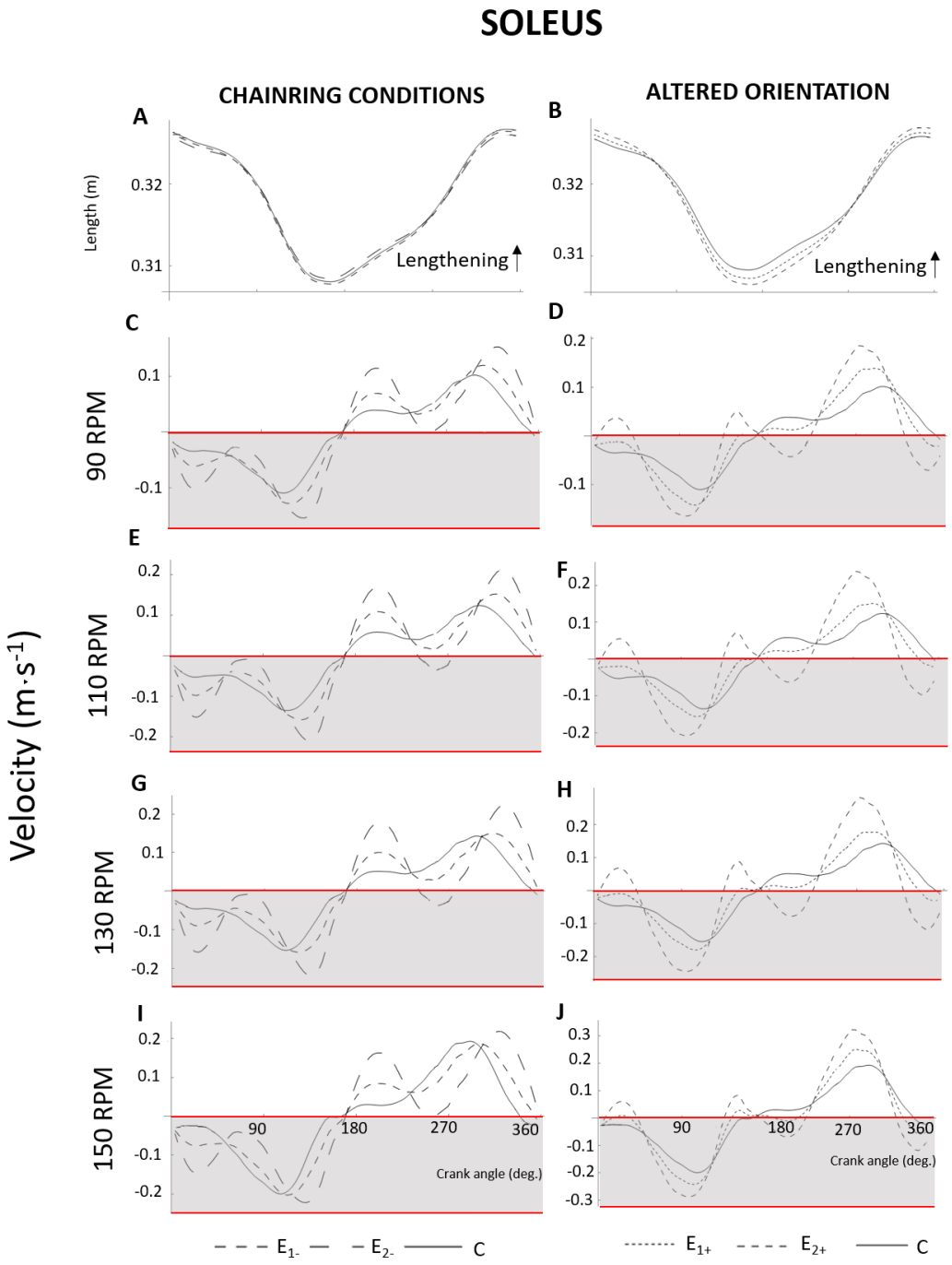

Figure 4.3 Principal component reconstructions of soleus muscle-tendon unit lengths and shortening velocities. Visual representation of the soleus MTU length using the first PC loading score (A & B), and velocity using the first five PC loading scores (C - J) when using three different chainring eccentricities presented at an optimal crank angle (first column) and chainrings presented at an alternate crank angle (second column). MTU lengths reconstructions are pooled across cadences and loads, whilst shortening velocity reconstructions are completed independently for respective cadences, pooled across loads. The shaded portion indicates shortening velocity.

4.3.3 Medial gastrocnemius MTU lengths and velocities

Figure 4.4 shows reconstructed MG MTU lengths and velocity waveforms. In contrast to the SOL, the MG MTU was lengthening during the first 90° of the pedal cycle, before beginning to shorten in the second phase of the downstroke (Q2, 45^{o} – 135^{o}). It then continued to shorten past peak plantar flexion of the ankle (at 180° of the pedal cycle), until the ankle had almost returned to a neutral position just after 270° of the pedal cycle (Figure 4.4 A, C, E & G).

There was a significant effect of cadence on PCI_{LS} ($P < 0.0001$) with the MG MTU functioning at shorter lengths with increasing cadence. A significant cadence x chainring interaction ($P = 0.015$) was also found for MG MTU lengths (Figures 4.4 & 4.5). Specifically, at 90 rpm there was a significant effect of chainring condition on MG MTU length ($P < 0.0001$), *post hoc* analysis revealed that whilst the circular chainring and E_{2-} had no significant difference between them, E_{1-}, E_{1+} and E_{2+} were all associated with a significantly shorter length than the aforementioned conditions. Despite this, there was a similar range of lengths across all of the chainring conditions at each of the cadences, with a total MTU length change of 0.02 ± 0.001 m within a pedal cycle (Figure 4.4 & Figure 4.5; column II). There was a significant effect of chainring condition on MG MTU length when cycling at 130 rpm ($P < 0.0001$), where the elliptical chainrings resulted in longer MG MTU lengths (Figure 4.4), (circular < E_{1-} < E_{2-}). The peaks and nadirs did however occur at the same point in the pedal cycle and the total range of lengths were the same for each condition (0.02m; Figure 4.4; column I). The alternate crank orientations (E_{1+} and E_{2+}) at 130 rpm were associated with a small, but significant decrease in total length change across the pedal cycle, and *post hoc* analysis showed this decrease was significantly different from the circular, E_{1-} and E_{2-} trials, but not between each other (Figure 4.5; column I). There was no significant effect of chainring condition when pedalling at 110 rpm ($P = 1.57$) and whilst a significant effect was present at 150 rpm ($P < 0.002$), *post hoc* analysis did not reveal the location of these differences. Further details of this are highlighted in Table 4.1.

MG MTU velocities are shown in Figure 4.4; column II, where it can be seen that lengthening velocity peaked between 0° and 90° of the pedal cycle, and peak shortening occurred between 180° and 270° of the pedal cycle. The elliptical chainrings were associated with delayed attainment of peak lengthening or shortening velocity of MG

(Figure 4.4; column II), and the alternate crank orientation led to the peak lengthening and shortening velocities occurring earlier in the pedal cycle (Figure 4.5; column II). There was an increase in the magnitude of shortening and lengthening velocities when the elliptical chainrings were employed, however, there was a larger effect on maximum shortening velocity than maximum lengthening velocity. Aside a continued alteration in timing, once the cadence reached 150 rpm, there was no significant effect of chainring condition on the magnitude of shortening and lengthening velocity (Figure 4.4H). The main effects of the chainring conditions on lengthening and shortening velocities are summarised in Table 4.2. There was a significant effect of chainring condition on the timing of peak lengthening and shortening velocity ($P < 0.0001$), which was variable across cadences. The timing effects are highlighted in Table 4.3.

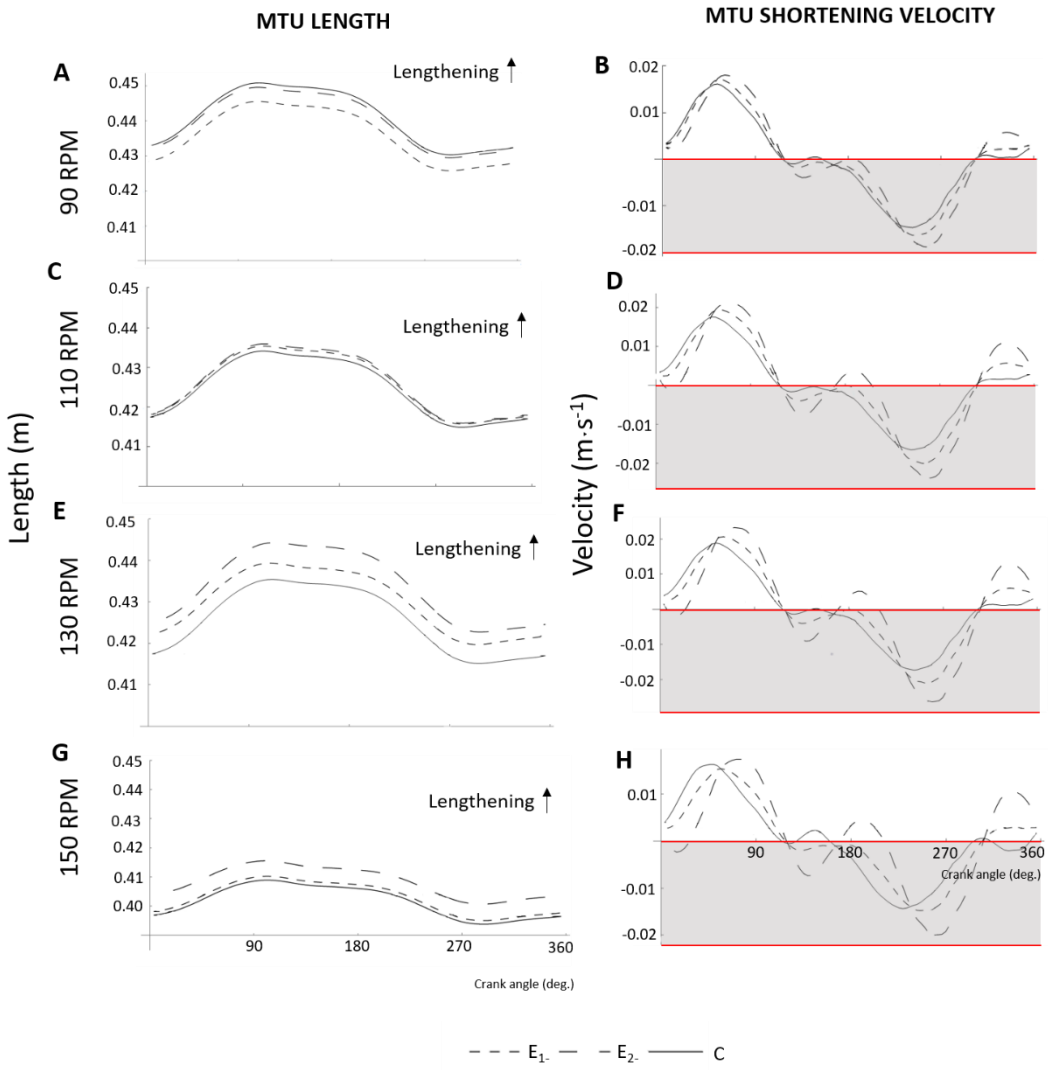

Figure 4.4 Principal component reconstructions of medial gastrocnemius MTU lengths and velocities for optimal crank orientation. Reconstructions used the first principal component for MTU length (first column), and the first five principal components for MTU shortening velocity (second column) when using three different elliptical chainrings presented with the optimal crank orientation. Reconstructions are completed independently for respective cadences, pooled across loads. The shaded portion of graphs in the second column indicates shortening velocity.

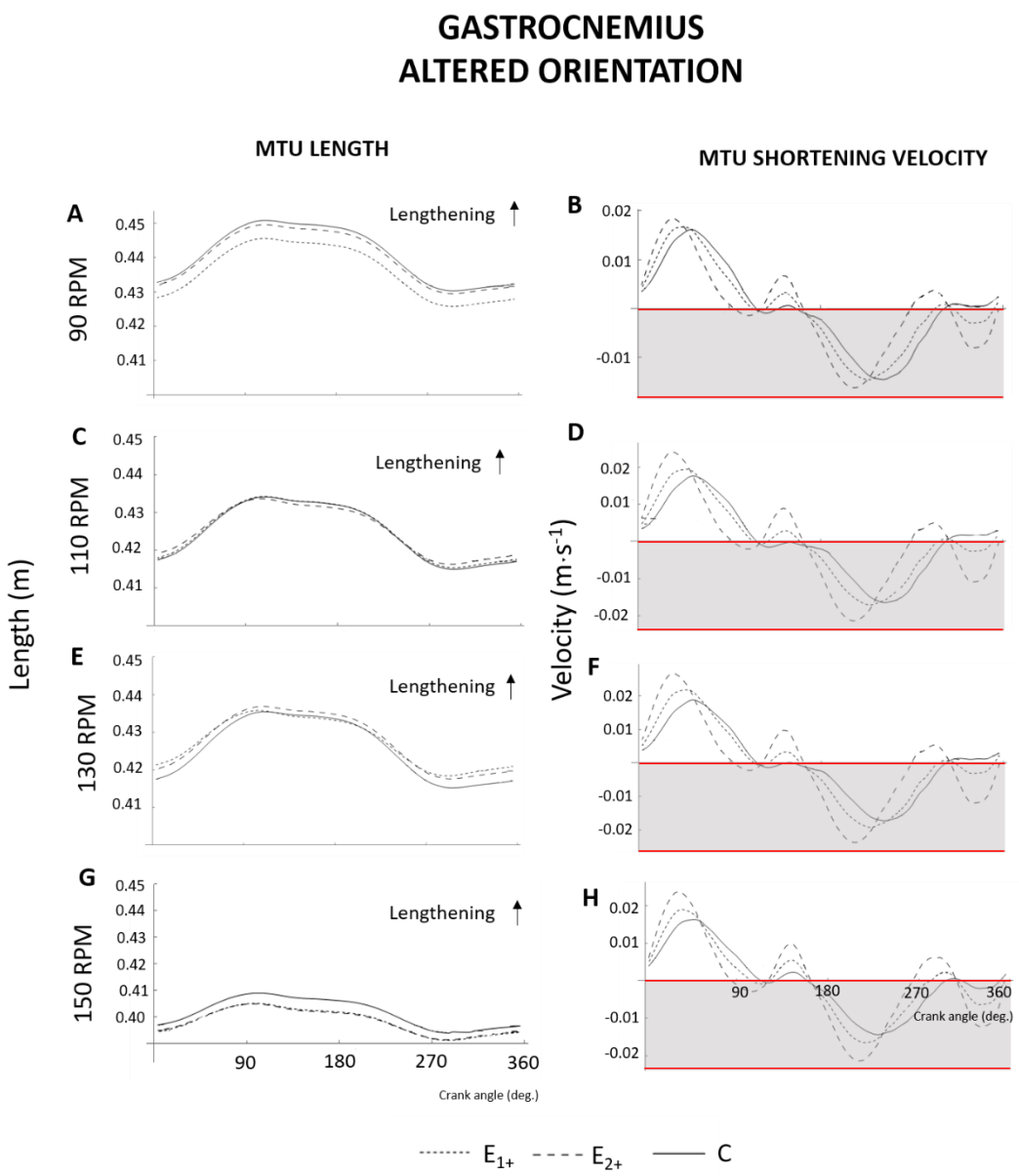

Figure 4.5 Principal component reconstruction of medial gastrocnemius MTU lengths and velocities, for alternate crank orientation. Reconstructions used the first principal component for MTU length (first column), and the first five principal components for MTU shortening velocity (second column) when using three different elliptical chainrings presented with the alternate crank orientation. Reconstructions are completed independently for respective cadences, pooled across loads. The shaded portion of graphs in the second column indicates shortening velocity.

4.5.4 Vastus lateralis MTU lengths and velocities

Figure 4.6 shows reconstructed VL MTU lengths and velocity waveforms. VL underwent a period of shortening through the downstroke, reaching minimum length in all chainring conditions at 160° of the pedal cycle. There was a significant effect of chainring condition on PCI_{LS} for VL MTU lengths ($P < 0.0001$), where the degree of eccentricity was associated with a decrease in minimum length (Figure 4.6; Column I). A significant chainring × cadence

interaction in PCI_{LS} was also found ($P < 0.0001$), indicating the shortest MTU length varied with cadence (Figure 4.7; column I). At 90 rpm, there was a significant difference in MTU length between the circular and elliptical chainrings; and observing the reconstructions (Figure 4.6A), it is possible to see a 0.001 m difference between the conditions at bottom dead centre. At the same time point, the E_{2+} condition was associated with a 0.004 m shorter length in comparison to the circular chainring. At 110 rpm, E_{2-} was associated with a significant difference in length ($P < 0.0001$), and the reconstructions in Figure 4.5C highlights a decrease in maximum length over top dead centre and a decrease in minimum length over bottom dead centre. *Post hoc* analysis showed that E_{1-} also significantly differed from the circular chainring, and a decrease in minimum length over the bottom dead centre was visible (Figure 4.6C). Orientating the crank to a non-optimal angle (E_{1+} and E_{2+}) increased the peak-to-peak length change of the VL MTU to 0.048 m, compared with 0.045 m in the circular condition, 0.044 m in E_{2-} and 0.046 m in E_{1-}.

There was a significant effect of chainring condition on PCI_{LS} in the VL MTU velocity ($P < 0.0001$), and a cadence × chainring interaction ($P < 0.0001$). The reconstruction of the waveforms (Figure 4.6; Column II) allows subtle differences to be observed between the chainrings when used at different cadences. Unlike the SOL and MG MTU shortening velocities, only the PCI_{LS} was needed to reconstruct these data, given the amount of variability explained within the first PC (Figure 4.1C), and subsequently, there was no phase effect in the VL velocity given that the main characteristics are explained in a single PC. At 90 rpm (Figure 4.6B), *post hoc* analysis revealed a significant increase in magnitude of shortening and lengthening velocities between the elliptical chainrings and the circular. *Post hoc* analysis showed no significant difference between the crank orientations and elliptical chainrings at 90 rpm. There was a systematic increase in lengthening velocity as cadence increased to 110 rpm across all chainrings (Figure 4.6D), however, the overall effect of PCI_{LS} across the chainrings was similar to the previous cadence. When cadence increased to 130 rpm, there was a significant chainring effect, which resulted in the circular chainring having a lower peak shortening and lengthening velocity than the four other chainring conditions, which had no significant difference between each other. At 150 rpm, all chainring conditions were significantly different from each other, and elliptical chainring conditions were associated with increased shortening and lengthening velocities.

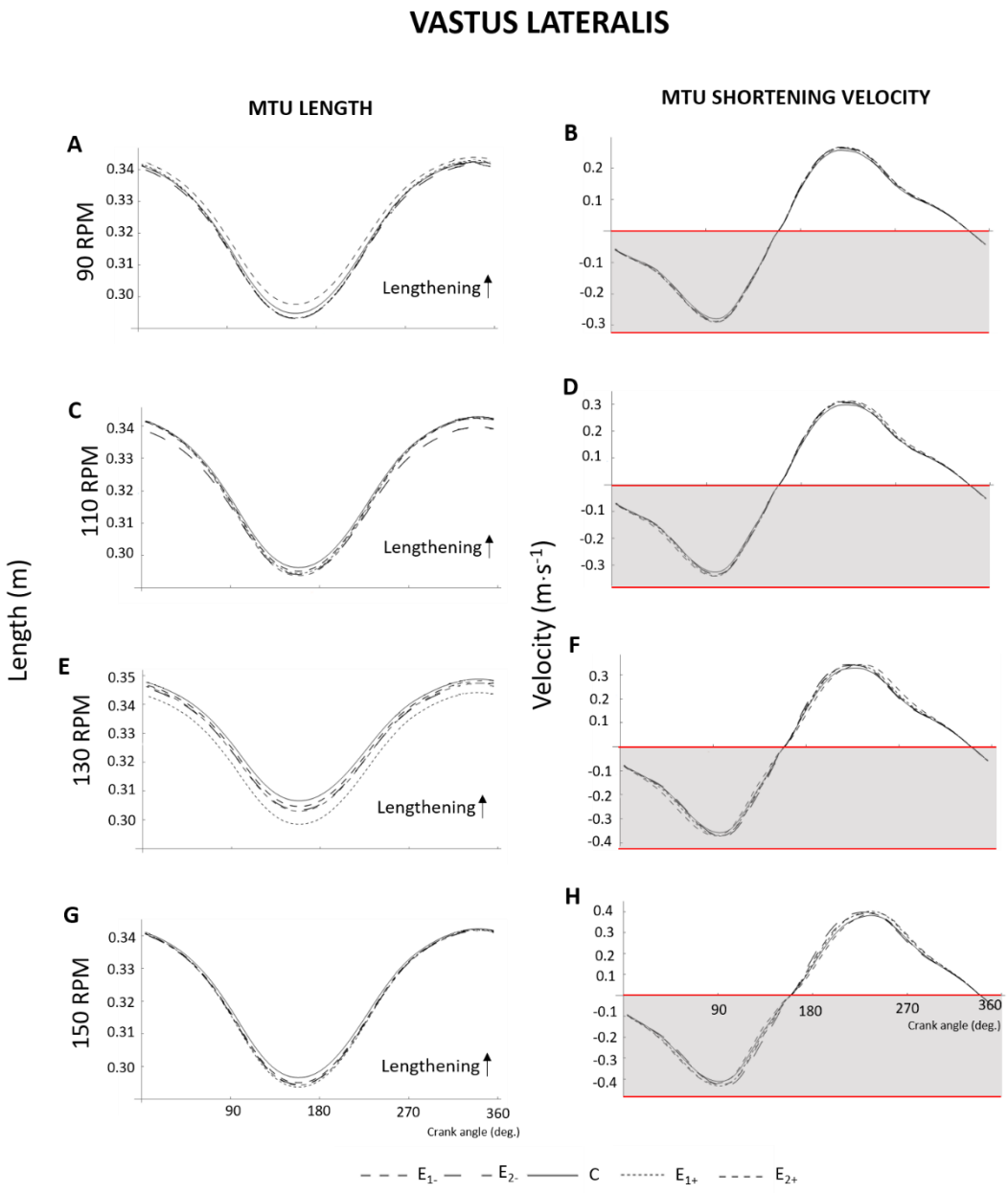

Figure 4.6 Principal component reconstructions of vastus lateralis MTU lengths and shortening velocities. Reconstructions used the first principal component for MTU length (first column) and MTU shortening velocity (second column) when using three different elliptical chainrings presented with the optimal and alternate crank orientations. Reconstructions are completed independently for respective cadences, pooled across loads. The shaded portion of graphs in the second column indicates shortening velocity.

4.6 Discussion

In the previous chapter, crank angular velocity was identified as being altered by the different chainrings, such that altering the chainring eccentricity was effective in increasing peak effective force during the downstroke phase of the pedal cycle. This study sought to

investigate whether the changes in force application and crank angular velocity, elicited by the different chainrings and positioning of the crank, were associated with altered soleus, medial gastrocnemius and vastus lateralis MTU kinematics over the range of cadences and loads studied. The main findings show that the MTU kinematics studied here were significantly influenced by the elliptical chainrings, with the most striking result being the altered velocities of the SOL and MG MTU (Table 4.2) as well as shifts in where during the pedal cycle peak lengthening and shortening velocity occurred (Table 4.3).

Table 4.1 Post hoc comparisons indicating direction of MTU length changes in each muscle for different chainrings relative to circular chainring, and cadence conditions

CR	E_{1-}				E_{2-}				E_{1+}				E_{2+}			
Cad	90	110	130	150	90	110	130	150	90	110	130	150	90	110	130	150
SOL	–	–	–	–	–	–	–	–	–	–	–	–	–	–	–	–
MG	↓	–	↑	–	–	–	↑	↑	↓	–	↑	↓	↓	–	↑	↓
VL	↓	↓	–	↓	↓	↓	↓	↓	↓	↓	↓	↓	↑	↓	↓	↓

Note: Arrows indicate elliptical chainrings directional difference in peak MTU length in comparison to circular chainring. ↑denotes an increase in operating length; ↓ denotes a decrease in operating length; and — denotes no significant difference.

Table 4.2 Post hoc comparisons indicating direction of MTU velocity changes in each muscle for different chainrings relative to circular chainring, and cadence conditions .

CR	E_{1-}				E_{2-}				E_{1+}				E_{2+}			
Cad	90	110	130	150	90	110	130	150	90	110	130	150	90	110	130	150
SOL	↓↑	↓↑	–	–	↓↑	↓↑	↓↑	↓↑	↓↑	↓↑	↑	↓↑	↓↑	↓↑	↓↑	↓↑
MG	↓	↓↑	↓↑	–	↓↑	↓↑	↓↑	↓↑	–	–	↓↑	–	↑↓	↑↓	↑↓	↑↓
VL	–	↓↑	↓↑	↓↑	–	↓↑	↓↑	↓↑	–	↓↑	↓↑	↓↑	–	↓↑	↓↑	↓↑

Note: Arrows indicate elliptical chainrings directional difference in MTU velocity in comparison to circular chainring. ↑ denotes an increase in lengthening velocity; ↓ denotes an increase in shortening velocity, and; — denotes no significant difference.

Table 4.3 Alteration in position of pedal cycle (in degrees) of peak lengthening and shortening velocity in the triceps the SOL (top two rows) and MG (bottom two rows)

CR	E_{1-}				E_{2-}				E_{1+}				E_{2+}			
Cad	90	110	130	150	90	110	130	150	90	110	130	150	90	110	130	150
Short	+6	+14	+14	+10	+19	+22	+25	+25	-6	-16	-6	-3	-17	-19	-16	-8
Len	+10	+15	+16	+9	+22	+22	+29	+29	-7	-12	-8	-9	-22	-25	-23	-18
Short	+7	+11	+13	+19	+17	+15	+17	+32	-13	-14	-13	-11	-25	-21	-28	-18
Len	+4	+5	+7	+11	+6	+14	+20	+27	-8	-8	-6	-10	-17	-21	-19	-15

Note: Positive values indicate a shift in peak lengthening/shortening velocity to later in the pedal cycle and negative values indicate a shift to earlier in the pedal cycle. Values represented in degrees. All values are significantly different from the circular chainring. Shaded rows represent alterations in the SOL and clear rows represent alterations in the MG.

4.6.1 Do changes in crank angular velocities explain changes in MTU velocities?

There is a well-established relationship between crank speed and the rate of change in fibre (Neptune and Herzog, 2000) and MTU (Brennan et al., 2018) lengths; and as crank speed increases, the series elastic tissue stretches at a greater velocity in order to contend with the increased force demands (Muraoka et al., 2001). This is typically associated with increments in cadence; however, here it was hypothesised that the alterations in the speed of the pedal over the course of a revolution (whilst maintaining a specific pedal frequency) caused by the elliptical chainrings would also impact the MTU velocity.

This study has shown for the first time, that the SOL, MG and VL MTU are significantly affected by a varied profile of crank angular velocity. The shifts in the occurrence of peak lengthening and shortening velocity associated with the different elliptical chainring conditions were in accordance with the variation in crank angular velocity associated with the respective chainring condition. The peak lengthening or shortening velocity was found to occur later in the pedal cycle when using the chainrings E_{1-} and E_{2-} than the circular chainring (Figures 4.3, 4.4 & 4.5). This coincides with the slowing of crank angular velocity during the down- and upstroke (Q2 & Q4) identified in Chapter Three (Figure 3.3B). Conversely, conditions E_{1+} and E_{2+} were associated with an advance in peak lengthening and shortening velocity, occurring during the slowing of crank angular velocity over the top and bottom dead centres (Q1 & Q3) induced by these conditions. There was a significant interaction between cadence and chainring in both the SOL and MG MTU velocities, and the degree of shift varied across cadences in both MTUs (Figure 4.3). In these results, different behaviours are apparent between the SOL and MG values, despite them being considered synergists and both spanning the ankle joint. This reveals some striking non-uniformity within the same synergistic group, that will be discussed later in this chapter.

In addition to the shifts in the location of peaks in shortening and lengthening velocities, the magnitudes of the peaks varied significantly between the chainring conditions in the SOL and MG (Figures 4.4, 4.5 & 4.6). An increase in eccentricity of the chainring was associated with an increase in shortening and lengthening velocities in both MTUs, for both crank orientations. The combination of altered timing and magnitude in the MTU velocities has important ramifications, as despite increments in the shortening velocity occurring

whilst using chainrings E_{1+} and E_{2+}, the altered timing could limit the contribution to effective mechanical output at the crank. The triceps surae are responsible for transferring force from the limb to the crank (Raasch et al., 1997), and if the timing of shortening-lengthening velocity is not conducive for force production (Neptune and Kautz, 2001) then power may be lost when the crank is slowing down during the downstroke when the elliptical chainrings are in use.

The effects of altered crank angular velocity on the VL MTU were far more subtle than seen in MG and SOL, nonetheless, they were significant (Figure 4.6). This was unsurprising considering the significant, yet small effects of the elliptical chainrings on the knee joint kinematics presented in Figure 3.7B. From these findings, it could be suggested that the elliptical chainring conditions have a larger effect on the distal muscles; rather than the muscles in the proximal segments of the legs. Given the larger changes in SOL and MG MTU behaviours compared to VL MTU, and that both VL and SOL are monoarticular, it would appear that location in the limb is of greater importance than the number of joints spanned in determining the effects of using different elliptical chainrings. Although it is not possible to confirm whether this is the case here, based upon the small number of muscles studied, it would be an interesting avenue to explore in greater detail through performing additional simulations on the musculoskeletal models to provide data from other MTUs in the leg. It is also important to acknowledge individual muscles possess their own force-velocity properties owing to their size and fibre type, and the performance characteristics they exude in response to the same task will likely reflect this (Zajac, 1989). Therefore, the differences between muscles found here could also result more from their individual properties than their location in the limb per se.

4.6.2 Do changes in joint kinematics explain changes in MTU lengths?

Muscle-tendon unit behaviour has been identified as being closely related to the behaviour of the joints to which they insert (Too, 1990). Alterations in joint kinematics were observed across the hip, knee and ankle (Figure 3.7), however, the responses in MTU length in conjunction with altered chainring geometry was more subtle than the MTU velocity behaviour. The SOL MTU length did not exhibit a significant response to the elliptical chainrings (Figure 4.3A). There were significant differences in MG MTU length between

the different chainring conditions. The largest distinction was 130 rpm (Figure 4.4E), where a significant difference between the elliptical chainrings and the circular was observable, and E_{2-} was associated with the MTU operating at a longer length than the circular, and E_{1-} conditions. This does follow the same pattern of effective crank force observed at this cadence in the previous chapter (Figure 3.5; column I), with peak MTU length and peak effective force occurring at the same position of the pedal cycle during Q2. However, despite operating over different lengths, the total length changes observed across all the chainrings over the course of the pedal cycle was similar.

The reduction in maximum length of the MG MTU (Figure 4.4; column I) with increments in cadence is consistent with earlier work (Gregor et al., 1987; Sanderson et al., 2006). Sanderson and colleagues (2006) attributed the effect to a concomitant reduction in ankle joint range of motion, given that, in their work, the knee kinematics were not affected by cadence manipulation to the same degree. However, data here show that ankle joint kinematics were seen to undergo the largest range of motion at 150 rpm (Figure 3.8D), coinciding with the narrowest range of MTU operating lengths (Figure 4.4G& Figure 4.5G) and no significant change in knee kinematics (Fig. 3.7). There are some key distinctions between the work presented in this chapter and that of Sanderson and colleagues (2006) that may explain this difference. Firstly, the cadences used in their study varied between 50 and 110 rpm, and the speeds of 90 to 150 rpm used in this study might have elicited different joint kinematics. Additionally, instead of an anatomically constrained model driven by experimental data like the one presented in this chapter, Sanderson et al (2006) used the equations developed by Grieve et al (1978) to calculate muscle length as a percent of segment length, which may not serve as an accurate method of predicting fascicle behaviour.

The behaviour of the shorter MG MTU lengths despite greater ankle joint range of motion suggests that there is an uncoupling between MTU behaviours and joint kinematics. In the previous chapter, a general increase in ankle joint range of motion with increased cadence across chainring conditions was found. We anticipated these effects would be evident in the MG MTU lengths. Additionally, in the SOL MTU there was no significant interaction between cadence and chainring, despite the ankle joint range of motion substantially increasing when the cadence reached 150 rpm (Table 3.3). This aspect was particularly

surprising, as SOL is a monoarticular muscle, yet the length changes observed here are uncoupled from the ankle kinematics. It is difficult to explain these results, particularly as the joint angle and MTU data are derived from the same model. How are larger ranges of ankle joint motion associated with a reduction in MG MTU length? This may indicate that the small changes in knee kinematics are important for determining the MTU behaviours. Equally, how can the SOL MTU length not be influenced by the changes in ankle joint angle that occur at faster cadence? This may suggest that movements out of the sagittal plane (not quantified in my kinematics analysis, but included in the MTU calculations) can be more influential on MTU lengths than first appreciated. These are aspects of the link between joint kinematics and MTU behaviours that warrant further investigation with the use of appropriate musculoskeletal model.

4.6.3 Do MTUs within a synergistic group respond similarly to altered chainring geometries?

In addition to the observations regarding the responses of the MTU to altered crank angular velocity and joint kinematics, there were additional interesting results to emerge from this data set. The MG MTU lengthened during the first 90^{o} of the pedal cycle, before shortening from 90 – 180^{o}. Conversely, the SOL MTU was shortening through this whole period (Figure 4.3; C-J). This period of the pedal cycle is considered to be the propulsive phase, which is the largest contributor to forward motion. As already eluded to, the ankle plantar flexor musculature is primarily responsible for the transmission of the forces generated at the hip to the pedal (Raasch et al., 1997). The significance of this is that when cycling under conventional conditions, with a circular chainring, the reaction forces at the pedal during the downstroke would typically cause ankle dorsiflexion and requires the triceps surae to maintain a stiff ankle or contribute to the pedal force through active plantarflexion. The differences in behaviours between the MG and SOL may suggest they contribute differently to force transmission and ankle stiffening. The SOL shortening velocity was low around top dead centre, enabling the MTU to work close to isometric to initiate plantar flexion. Initial lengthening of the MG may facilitate energy storage, release during the subsequent shortening and propulsive portion of the pedal cycle.

The positioning of the muscle in comparison with adjacent muscles and differences in

moment arm, along with muscle's position relative to fixed non-muscular structures such as bone and fascia will alter with any change of joint position. This positioning has been seen to affect resulting net joint moments in synergistic muscles (Maas and Sandercock, 2010). The individual components of triceps surae are seen to act independently within this study, with the MG lengthening whilst SOL is shortening (Figure 4.1B). It should be noted that the proximal tendon of the gastrocnemius crosses the knee joint, therefore flexion and extension of the knee joint invokes length changes of the MG without any (or at least very small on account of force transmission) changes of MTU length in the SOL. The increased extension at the knee when the elliptical chainrings were used were so small (~4°, Figure. 3.7) that it is unlikely to have affected the ability of the gastrocnemius to generate force. The distal gastrocnemii and SOL both form the long, compliant Achilles tendon, which is much longer than their respective muscle fibres (Trestik and Lieber, 1993). This large tendon length to muscle fibre ratio is proposed to allow enhanced energy recycling within the tendon during locomotion (Roberts and Azizi, 2011). Further, Hoy et al (1990) estimated that the MG moment arm is slightly larger than the SOL moment arm, and consequently the large differences in peak force between these muscles is reduced. The authors predicted that this difference allows the two moment arms to work together to provide a longer duration force as they generate similar torques around the ankle joint (Hoy et al., 1990). Additionally, the opposing behaviour of SOL and MG could contribute to shearing between separate portions of the Achilles tendon, similar to that previously suggested to occur for overland locomotion (Bojsen-Møller et al., 2004). This is interesting as our understanding of the SOL is quite often limited to extrapolated insight from our knowledge of the MG, however, despite functional synergy between these plantar flexor muscles, the mechanical behaviour of the SOL and MG MTU and fascicles have been previously been shown to differ during walking and running (Lai et al., 2015); and now they have also been observed to behave differently during cycling.

4.6.4 What are the implications of altered MTU velocities?

As previously mentioned, earlier research by Rankin and Neptune (2008) discounted the role of intrinsic contractile behaviour in the augmentation of average force when using a dynamically optimised non-circular chainring. There were dissimilarities between the dataset presented here and that of Rankin and Neptune's (2008), firstly this is an

examination of the MTU behaviour, and the outcomes are subject to the influence of tendinous structures previously discussed. Secondly, the chainrings eccentricities were developed to maximise crank power over three prescribed cadences in the study by Rankin and Neptune (2008), and further, were purported to support an increase in power by allowing a longer period of the pedal cycle to be available for power production equating to an increase in external work. In contrast with this, average power was controlled in this study, and this allowed for the observation that instead of a longer duration of force production during the downstroke, there was an increment in peak effective force which, depending on the crank orientation, occurred slightly before or after peak effective force in the circular chainring (Figure 3.5). The effect of altering the timing of peak shortening and lengthening velocities in the triceps surae are an important consideration, as previous studies have shown that peak muscle power occurs at approximately one-third of maximum contraction velocity (Sargeant, 1994), and influencing where during the pedal cycle this occurs could therefore have consequences for how forces are directed about the crank. Lastly, in Rankin and Neptune's (2008) observations lengths and shortening velocities of the muscle fibres were only considered during their active states, whilst the PC analysis performed here allowed the patterns of MTU behaviour to be statistically considered during all points of the pedal cycle.

It is important to note the contribution that MTU gearing might have played in the discrepancies between the work conducted by Rankin and Neptune (2008) and the work presented in this chapter. It is well documented that there can be an uncoupling between the tendon and fascicle velocities in the ankle plantar flexors during cycling (Dick and Wakeling, 2017; Griffiths, 1991; Lichtwark et al., 2007; Wakeling et al., 2011; Brennan et al., 2018), meaning it is not possible to generalise between behaviour of the contractile apparatus and MTU. Therefore, there is a limitation of using estimates of MTU length changes to infer contractile dynamics of the muscle, as this does not account for the effects of series elasticity in the tendinous connective tissues; and further, the decoupling has been observed to be heightened during augmented muscle activity, resulting in increased stiffness in the active muscle fibres (Lauber et al., 2014). Ultrasonography has been employed as a method of imaging the muscle fascicles, allowing the length changes and velocities to be robustly measured during many different locomotor tasks (Van Hooren et

al., 2020). Therefore, this chapter had originally aimed to compare the MTU data with fascicle data collected via B-mode ultrasonography. In total, 47080 frames of MG fascicle data were recorded and a computational approach was employed to automatically track and process the changes in fascicle geometry during cycling (Darby et al., 2013). However, due to the high pedalling cadences used in this study, the deformations of muscle tissue between frames was too large to allow reliable tracking of fascicle length using these computational techniques. An alternative computational approach is therefore required and, therefore, these images remain a component of my dataset that requires further analysis, with additional time required to identify the optimum analysis solution for robust measurements to be attained.

4.6.6 Conclusion

This study provides new evidence that manipulating the pattern of crank angular velocity via the use of elliptical chainrings is associated with alterations in operating lengths and velocities of lengthening and shortening of the SOL, MG and VL MTUs. Under *in vivo* conditions, a muscle performing repetitive contractions cannot instantaneously develop force as the shortening phase begins or instantaneously relax before the onset of the subsequent lengthening phase. Consequently, factors regulating the kinetics of activation and relaxation must also be determinants of the mechanical work under these conditions (Caiozzo and Baldwin, 1997). Therefore, these alterations in MTU kinematics must be considered within the context of neuromuscular control to fully understand their potential impact on cycling performance. The features of muscle recruitment during the cycle tasks studied here will therefore be explored in the next chapter.

Chapter 5. Muscle excitation patterns are altered in response to chainring geometry

5.1 Introduction

One of the basic problems in biomechanics, is understanding how motor patterns such as muscle activation timing and magnitude contribute to the performance of common motor tasks, like walking, running and cycling (Herzog, 2017). Little is known about the neural basis of movement control, in part due to the large number of degrees of freedom in the musculoskeletal system, and questions have arisen within scientific literature as to whether movement control strategies are the same across movements or unique and task dependent. As a step towards increasing our understanding of movement control, the goal of this work was to investigate the changes in muscle recruitment patterns in response to altered task mechanics. Pedalling was used as a movement paradigm since it consists of quasi-constrained cyclical movements that allow for accurate control of test conditions, such as pedalling cadence and load (Neptune and Herzog, 2000).

Changing the functional demands placed upon the muscles can influence the mechanical dynamics of the muscular contraction (Mileva and Turner, 2003; Sanderson and Amoroso, 2009). The response or adaptations of the neuromuscular system are reflected in the timing and amplitude of skeletal muscle excitation, which can influence the force and power production of the muscle (Askew and Marsh, 1998). These behaviours can be recorded using electromyography (EMG), with the myoelectric signal providing insight into the neuromuscular drive to the muscles.

During multi-muscle contractions, the spatiotemporal patterns of myoelectric signals describe the features of muscle coordination. Neuromuscular coordination pertains not only to the activation of different muscles in relation to one another, but also the activation of individual muscles in relation to the kinematics of that muscle (Hull and Hawkins, 1990). As multiple muscles can act upon the same joint, there are theoretically many different coordination strategies available to achieve the same motor goal (Crouzier et al., 2018). The responses of individual muscles to changes in mechanical demand can present as alterations in the onset and offset of excitation as well as the amplitude of excitation.

During cycling, these features are known to be affected by cadence, which is well documented within the literature (Marsh and Martin, 1995; Neptune et al., 1997; Wakeling and Horn, 2009). The excitation response of the individual muscles to increments in cadence is mixed, and whilst most muscles demonstrate a systematic shift in the timing of their activation during the pedal cycle, the degree of this shift appears different for each muscle, influencing the mechanical contribution they make toward the pedalling action (Wakeling and Horn, 2009; Blake and Wakeling, 2015). The influence of workload on muscle excitation is less well documented. However, Blake and Wakeling (2015) showed that power output was critically limited by the duration of muscle excitation when pedalling faster than 120 – 140 rpm. This led from previous work suggesting that power output and limb motion efficiency is limited by the coordination patterns between muscles, and not that of the maximum power achievable by the individual muscle groups (Wakeling and Horn, 2009).

During cycling, effective muscle coordination is required to provide an effective force profile, given that activation patterns can affect the direction (Herrmann and Flanders, 1998), magnitude and duration (Blake and Wakeling, 2015) of the external force developed. The force generation achieved to propel the bicycle forward had been attributed predominantly to the mono-articular muscles (i.e. vastus complex), during the propulsion phase. Biarticular muscles, activated at the top (rectus femoris) and bottom (gastrocnemii, semitendinosus, biceps femoris) of the pedal cycle, may assist in directing the pedal forces and redistributing net moments over the joints during these phases (Lima Da Silva et al., 2016). Therefore they contribute to the effectiveness of the pedalling technique through synchronising the smooth transfer of mechanical energy from the limbs to the crank (Raasch et al., 1997)

Studies examining muscular activity responses to non-circular chainrings using both maximal (Horvais et al., 2007) and submaximal (Horvais et al., 2007; Dagnese et al., 2011) trials have failed to find consistent changes in amplitude and timing of contraction in the muscles studied. Neptune and Herzog (2000) investigated whether chainring shape affected activation patterns, and found significant shifts in timing of muscle excitation with alterations in changes in pedal speed in the soleus, medial gastrocnemius, tibialis anterior, vastus medialis and gluteus maximus; but not in the biceps femoris or rectus femoris.

Additionally, the shifts were reported as being minor and seemingly accounted for the altered activation dynamics requiring muscle force to be produced in the same region of the crank cycle. Winters and Stark (1988) contended that average time constraints imposed by activation-deactivation dynamics range between 20 to 110 ms, therefore suggesting requirement for a 2-10° phase advance to account for the crank angular velocity changes associated with elliptical chainrings. However, Neptune and Herzog (2000) conducted their study at 200 watts with a cadence 90 rpm. It is unclear whether the alteration in timing of muscle excitation they found in conjunction with non-circular chainrings is consistent across other cadences, an important consideration given the cadence effects on force production and MTU kinematics found in previous chapters in this thesis.

The findings reported in the previous chapters of this thesis show that range of motion in the ankle and hip joint were increased when an elliptical chainring was used (Figure 3.7). Consequently, there was an adaptation in MTU behaviour whereby operating lengths and shortening velocities of the soleus, medial gastrocnemius and vastus lateralis were significantly affected (Figure 4.3 – 4.6). These alterations varied the crank forces, whereby increments in peak effective force were observed (Figure 3.5). Taken together, it is feasible to predict that alterations in muscle activation would occur in response to use of the elliptical chainrings. Therefore, the purpose of this study was to investigate the interaction between load, cadence and elliptical chainrings on excitation characteristics of the lower extremity muscles during cycling. The following hypotheses were examined: that the phase and the magnitude of EMG intensity would change in response to the different chainrings, but differences in response will occur between proximal and distal muscles. Specifically, it was hypothesised that the muscles of the triceps surae complex would show increased levels of EMG intensity with a significant change in phase, such that EMG intensity would occur within different portions of the pedal cycle (due to alterations in muscle-tendon unit velocity profiles, Figures 4.3-4.5) in response to chainring geometry and crank orientation. In contrast, no difference in magnitude nor phase of quadriceps EMG intensity will occur (due to the small changes in MTU velocity seen in VL, Figure 4.6).

5.2 Methods

In this chapter, data were used from eight well-trained cyclists (4 male, 4 female; age: 37.8 ± 15.3 years, mass: 70.1 ± 12.5 kg, height 176.1 ± 12.2 cm) performing 30 second bouts of pedalling effort of varying loads and cadence using chainrings of two levels of eccentricity and with two crank orientations relative to the major axis (Figure 3.1). Data acquisition for this study is described in Chapter Three. In addition to the previously described methodology for kinetics and kinematics data, bipolar surface electromyography (EMG) electrodes (Trigno Wireless EMG, Delsys Inc, USA) with a fixed inter-electrode distance of 10 mm were placed over the mid-bellies of the soleus (SOL), medial gastrocnemius (MG), lateral gastrocnemius (LG), vastus medialis (VM), rectus femoris (RF), vastus lateralis (VL), semitendinosus (ST), biceps femoris (BF) and gluteus maximus (GMAX) of the right leg. Before placement, the skin overlying each muscle was carefully prepared, with hair shaven off, the outer layer of epidermal cells abraded, and oil and dirt were removed from the skin with an alcohol swab. The EMG electrodes were paired with a host computer which was equipped with data acquisition software (Delsys). Data were sampled at 2000 Hz through a 16-bit data acquisition card (USB-6210, National Instruments Corp, Austin, TX) and synchronised with other data types through the Vicon optical capture system software (Vicon Nexus version 2.5, Vicon Motion Systems LTD, Oxford, UK) to ensure continuity between joint kinematics and crank forces.

5.2.1 Analysis of experimental data

5.2.1.1 EMG Intensities

EMG signals for each muscle were resolved into their intensities in both time and frequency space during each pedal revolution using EMG-specific wavelet analysis (Figure 5.1; Von Tscharner, 2000). A filter bank of ten non-linearly scaled wavelets were defined by their frequency bandwidth, centre frequency and time resolution using the methods described by Von Tscharner (2000). The wavelets had a frequency bandwidth spanning ~10 – 432 Hz, which was achieved by discounting intensities in the first wavelet to eliminate noise from movement artefact. The EMG intensities (the power of the signal) were interpolated to 100 points per cycle, starting at the top dead centre, and normalised to the mean for each muscle for each participant across all trials. EMG intensities were calculated as being the

sum of the intensities across all 10 wavelet domains for each time point, providing the energy envelope around the square of the signal, as is visible in Figure 5.1. Additionally, the total EMG intensity for each individual muscle per pedal cycle was calculated as the sum of the interpolated intensities across all wavelets, to provide indication of a total muscle response (Blake and Wakeling, 2015).

Principal component (PC) analysis was used to determine the primary EMG intensity pattern (waveform) for each muscle. Data were arranged into a $P \times N$ matrix **A**, where the interpolated EMG intensity data points per cycle (P = 100) were organised into N = 8 participants × 5 conditions × 11 trials × 26 pedal cycles rows. The mean was not subtracted beforehand, as has been described previously (Wakeling and Rozitis, 2004), allowing the total variability to be explained with PCI approximating the mean. In order to visualise the primary differences in EMG intensity for each condition and calculate the magnitude of excitation, the EMG intensity waveforms were reconstructed from the vector sum of the PC weightings and loading scores for the first ten PCs. PC analysis was completed using custom written code using Mathematica (Mathematica 11 software, Wolfram Research, Champaign, IL).

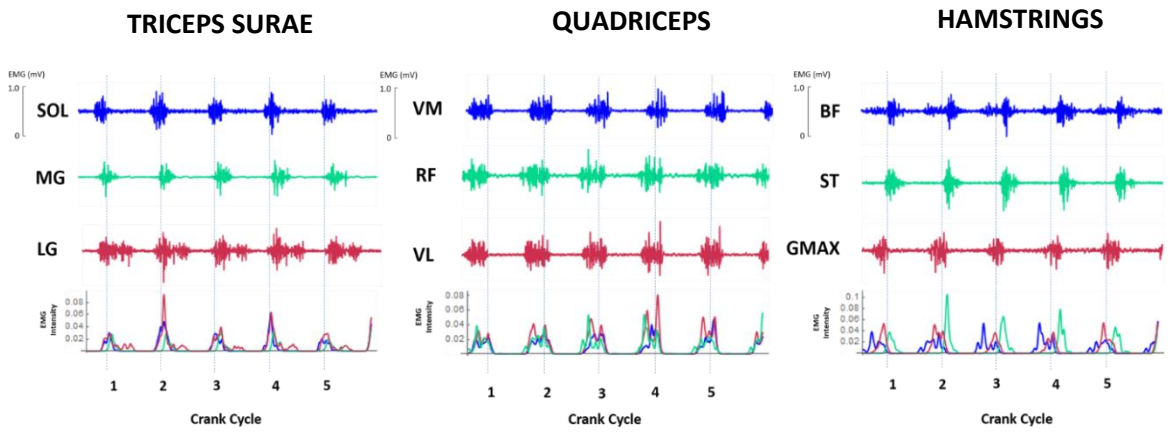

Figure 5.1 Experimental data from a representative participant cycling with a circular chainring. Plots show raw EMG recordings from the soleus, medial gastrocnemius, lateral gastrocnemius, vastus medialis, rectus femoris, vastus lateralis, biceps femoris, semitendinosus and gluteus maximus; with normalised EMG intensities for the respective muscle groups shown below with corresponding colours. Data is shown for five crank cycles pedalling at 90 rpm and 250 Watts using a circular chainring.

5.2.1.2 Calculation of Activation Burst Duration & Duty Cycle

In order to calculate the duration of muscle excitation per pedal cycle, an onset/offset threshold of 5% of the difference between minimum and maximum EMG intensity was

selected (Figure 5.2). The portion of the intensity waveform above this threshold was used to determine the duration of muscle excitation in each pedal cycle (Blake and Wakeling, 2015). The duty cycle was calculated as the duration of muscle excitation relative to the duration of the complete pedal cycle, determined from kinematics, and was also calculated from the EMG intensities for each muscle per pedal cycle.

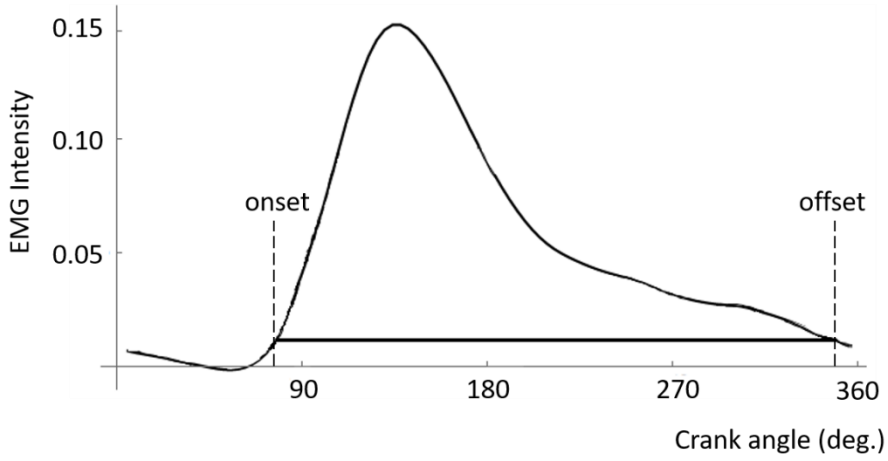

Figure 5.2 Schematic of EMG burst duration as a function of crank angle depicting the threshold of 5% of the difference between minimum and maximum value. The period between onset and offset (vertical dotted lines) represents the duration of the active muscle.

5.2.1.3 Phase Shift

Changes in the relative timing of the EMG excitation within the pedal cycle were also calculated for each muscle. A shift registration method (Ramsay and Silverman, 2005) was used to separately determine how features of the raw EMG intensity waveforms varied between chainrings over the four different cadences. This approach applies a cross-correlation between the EMG intensity for each cycle and the mean EMG intensity and identifies the phase shift that offers the greatest correlation with the reference mean EMG intensity. Here a positive phase shift indicates activation occurred later in the pedal cycle, while a negative phase shift indicates activation occurred earlier.

5. 3 Statistics

General linear model analysis of variance (ANOVA) was used to identify the effect of chainring eccentricity, crank orientation, cadence and load on the loading scores for the first five PCs (PCI-V_{LS}) for EMG intensity in each muscle. Additionally, two-way interaction between chainring condition, cadence and load on the muscles was determined, with subject defined as a random factor in all analyses. A *post hoc* Tukey test was performed to

determine where the significant differences between chainring condition for a given cadence or load occurred. Statistical analyses were processed using Minitab version 18 (Minitab Inc., State College, PA). All data are presented as means ± SD, and statistical tests were deemed significant at $\alpha = 0.05$.

5.4 Results

5.4.1 Multi-Muscle Excitation Patterns

The multi-muscle excitation patterns for each chainring-cadence combination can be seen in Figure 5.3. Alterations in the magnitude of EMG intensity is represented through changes in the colouring of the muscle excitation. In comparison to the circular chainring, increases in EMG intensity are evident in the distal muscles such as SOL and MG when the elliptical chainrings are used. In contrast, a decrease in EMG intensity is apparent in the quadriceps (e.g. VL, VM and RF) at the faster cadences (e.g. 150 rpm). Changes in the timing and duration of activation can be observed across muscles (e.g. a double burst in RF excitation is visible in the elliptical chainring conditions), although whether any systematic changes occur is harder to determine. The timing (phase), duration and magnitude of EMG signals have therefore been formally quantified and are presented in fuller detail for each muscle in the following sections.

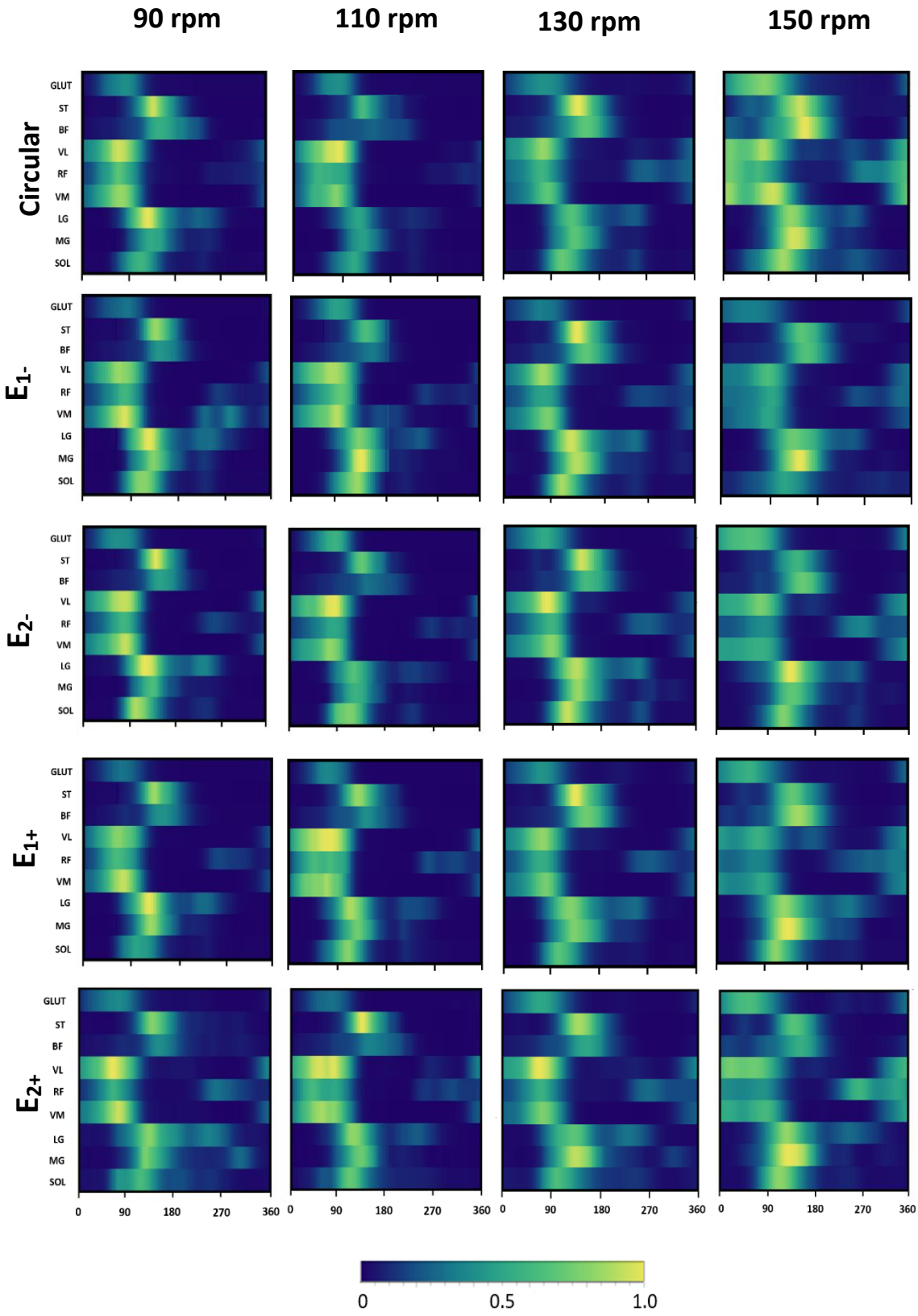

Figure 5.3 Muscle coordination patterns for each chainring-cadence combination. EMG intensity pattern for each chainring (rows) and cadence (columns) combination normalised to the maximum for each condition.

5.4.2 Triceps Surae

5.4.2.1 EMG Intensity Waveforms

Figure 5.4 shows the PC loading score based reconstructions of the EMG intensity waveforms, and depicts that the triceps surae became active during the downstroke, in Q2 of the pedal cycle. EMG intensity waveform loading scores were significantly different between chainrings (SOL: $P < 0.0001$; MG: $P < 0.0001$; LG: $P < 0.0001$), but not load (SOL: $P = 0.892$; MG: $P = 0.895$; LG: $P = 0.941$) or cadence (SOL: $P = 0.604$; MG: $P = 0.981$; LG: $P = 0.953$). Additionally, there was no interaction between chainring condition and cadence (SOL: $P = 0.951$; MG: $P = 1.000$; LG: $P = 0.994$). The elliptical chainrings were associated with an increase in magnitude of EMG intensity, which increased in conjunction with the level of eccentricity in the SOL; however, in the MG and LG, condition E_{1-} resulted in a greater increase in EMG intensity magnitude in comparison with E_{2-}. When the elliptical chainrings were orientated ahead of the major axis and in the non-optimal position (Figure 3.1; E_{1+} & E_{2+}) there was also an increase in magnitude of EMG intensity in comparison with the circular chainring, however, this was not as large as when presented at an optimal crank angle (E_{1-} and E_{2-}).

The total EMG intensities per pedal cycle for each muscle were also calculated and are displayed in Figure 5.5 (Column I). Statistical analysis showed that there was a significant difference associated with total EMG intensity and chainring condition (SOL: $P = 0.014$; MG: $P = 0.004$; LG: $P = 0.034$), cadence conditions (SOL: $P < 0.0001$; MG: $P < 0.0001$; LG: $P < 0.0001$), and a small significant effect of load in the SOL ($P = 0.049$), but not MG or LG (MG: $P = 0.263$; LG: $P = 0.76$).

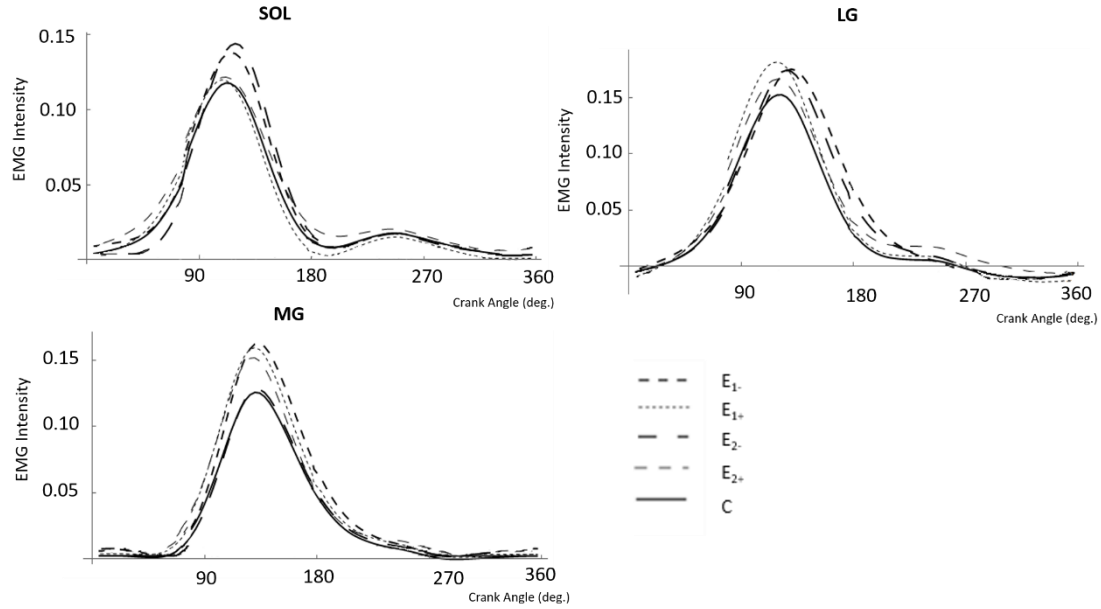

Figure 5.4 Principal component reconstructions of triceps surae EMG intensity. Visual representation of the first ten principal component loading scores for EMG intensity for the muscles of the triceps surae. Cadence and load are pooled, and waveforms are presented over the course of a pedal cycle.

5.4.2.2 Burst Durations and Duty Cycles

Box and whisker plots showing burst durations and duty cycles for each muscle in the triceps surae complex are shown in Figure 5.5 (Columns III & IV). Between the chainring conditions, SOL, MG, and LG displayed significant differences in burst durations ($P = 0.001$; $P < 0.0001$; $P < 0.0001$, respectively; Figure 5.5; Column IV) and duty cycles ($P < 0.0001$; $P < 0.0001$; $P = 0.001$, respectively; Figure 5.5; Column III). There was also a significant main effect of cadence on both burst duration ($P < 0.0001$; $P < 0.0001$; $P < 0.0001$) and duty cycle ($P < 0.0001$; $P < 0.0001$; $P < 0.0001$) and a significant chainring × cadence interaction on duty cycle (SOL: $P = 0.004$; MG: $P < 0.0001$; LG: $P = 0.006$) and burst duration (SOL: $P < 0.0001$; MG: $P = 0.001$; LG: $P = 0.048$). In the SOL, there was a trend for the E_{2+} condition to increase activation duration in comparison to the other chainrings, which was evident in the *post hoc* comparisons, where activation duration for E_{2+} was significantly longer than the other chainrings. This was apparent at cadences 90, 110 and 130 rpm. However, at 150 rpm, the differences between chainring conditions were less. The opposite was observed in the MG and LG, despite significant differences at all cadence intersections, the spread between the chainring conditions is much larger at 150 rpm than the slower cadences. In

Figure 5.5 (Columns III & IV), it is apparent that when pedalling at 150 rpm, there is longer burst duration and duty cycle in the circular chainring condition compared with the elliptical chainrings in the SOL.

5.4.2.3 Phase Shifts

Significant systematic phase shifts of EMG intensity to earlier in the pedal cycle were found with conditions E_{1-} and E_{2-} for all muscles in the triceps surae (SOL: $P < 0.0001$; MG: $P = 0.018$; LG: $P < 0.0001$; Figure 5.5; Column II) in comparison to the circular chainring. This pattern was found to occur across the four cadences. Conversely, conditions E_{1+} and E_{2+} were associated with a shift in EMG intensity to later in the pedal cycle. There was no significant effect of cadence on the EMG intensity phasing across the three muscles (SOL: $P = 0.877$; MG: $P = 0.316$; LG: $P = 0.155$), and no significant chainring × cadence interaction (SOL: $P = 0.214$; MG: $P = 0.338$; LG: $P = 0.856$).

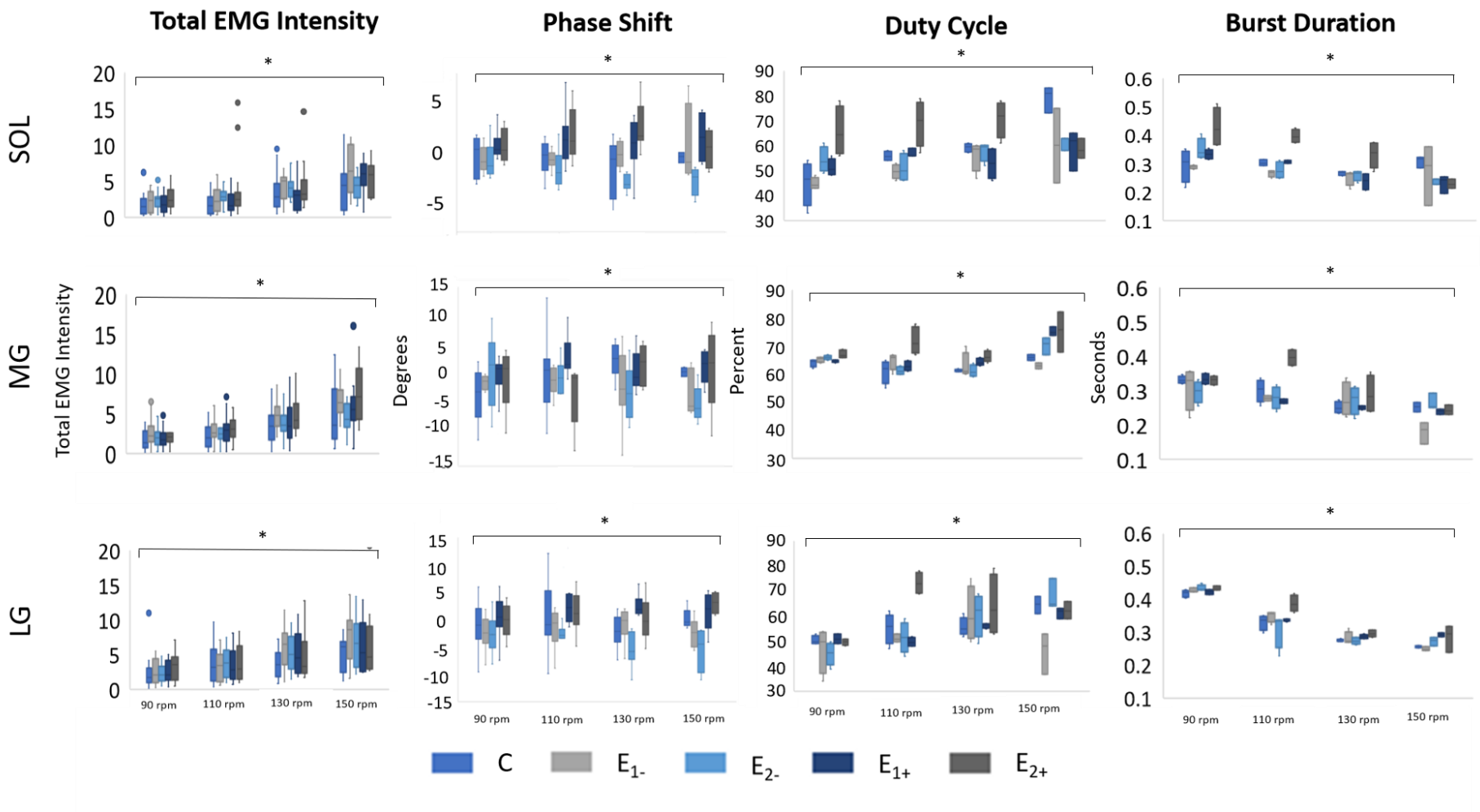

Figure 5.5 Total EMG Intensity, relative phase shifts, duty cycles and burst duration of EMG intensity in the triceps surae with pooled power outputs. Values are shown as box and whisker plots (median, interquartile range, SD and outliers) for eight participants and the five different chainring conditions represented as different colours across the range of four cadences. * denotes a significant main effect of chainring condition.

5.4.3 Quadriceps

4.4.3.1 EMG Intensity

The reconstructed EMG intensity waveforms for the quadriceps muscles are shown in Figure 5.7. Overall, assessment of the PCA loadings scores revealed a decrease in EMG intensity across the VM, RF and VL when using the elliptical chainrings in comparison to the circular chainring (VM: $P < 0.0001$; RF: $P < 0.0001$; VL: $P < 0.0001$; Figure 5.6). This was more prevalent in the biarticular muscle RF, than the monoarticular muscles VM and VL. *Post hoc* analysis showed that conditions E_{1-} and E_{2-} were significantly different to the circular chainring. The reconstructed EMG intensity waveforms show the largest difference in RF over the course of the pedal cycle was in Q1, whilst the crank passed through the top dead centre and moved toward 90° in the pedal cycle (Figure. 5.6). PC loading scores from conditions E_{1+} and E_{2+} were also significantly different from those from the other three chainring conditions, and whilst the waveforms for RF contained lower EMG intensity than the circular chainring, the EMG intensity remained higher than the E_{1-} and E_{2-} conditions.

Further *post hoc* examination of PC loading scores from VM and VL (Figure 5.6) showed similar results across the two muscles, however, the magnitude of excitation was larger in the VL than the VM. Significant differences in PC loading scores for circular and E_{1-} chainring conditions were present, which was coupled with an observable increment in EMG intensity in Q1 and the first half of Q2 in the circular chainring (Figure 5.8). There was no significant cadence effect on PC loading scores across the three quadriceps muscles (VM: $P = 0.471$; RF: $P = 0.407$; VL: $P = 0.631$), nor a significant chainring × cadence interaction (VM: $P = 0.984$; RF: $P = 0.973$; VL: $P = 0.946$).

Analysis of the total EMG intensities (Figure 5.7; Column I) showed different responses between chainring conditions across the three muscles (VM: $P = 0.375$; RF: $P = 0.003$; VL: $P < 0.0001$), whilst there was a consistent, significant effect of cadence (VM: $P < 0.0001$; RF: $P < 0.0001$; VL: $P < 0.0001$) and load (VM: $P = 0.004$; RF: $P = 0.03$; VL: $P < 0.0001$). From these data a relatively large degree of variation is apparent across participants, however, in the RF and VL, there is a trend toward lower total EMG intensity values in the E_{1-} and E_{2-} conditions, and an increase in the E_{1+} and E_{2+} conditions in comparison with the circular chainring.

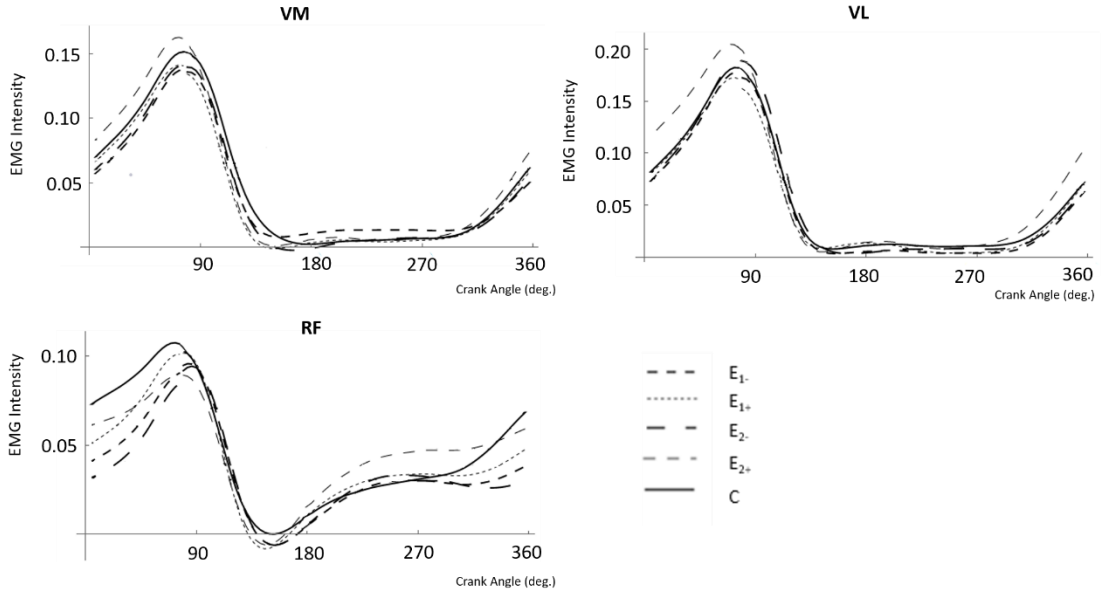

Figure 5.6 Principal component reconstructions of quadriceps EMG intensity. Visual representation of the first ten principal component loading scores for EMG intensity for the muscles of the quadriceps. Cadence and load are pooled, and waveforms are presented over the course of a pedal cycle.

5.4.3.2 Burst Durations and Duty Cycles

There was no significant effect of chainring condition on VM burst duration ($P = 0.076$) or duty cycle ($P = 0.068$), but there was an effect of cadence on both parameters ($P < 0.0001$ both cases). This presented itself as a decrease in burst duration as cadence increased (Figure 5.7; Column IV), and an increase in the proportion of the pedal cycle the muscle was active (Figure 5.7; Column III). There was a significant effect of chainring condition on the burst durations ($P < 0.0001$; $P = 0.004$) and duty cycles ($P < 0.0001$; $P = 0.002$) of the RF and VL, respectively. *Post hoc* analysis of the VL data showed significant difference between the circular and E_{1-} conditions, where the elliptical chainring was associated with a decrease in burst duration (Figure 5.7; Column IV) and duty cycle (Figure 5.7; Column III), having seemingly the opposite effect as the RF displayed. There were cadence effects on duty cycle ($P < 0.0001$) and burst duration ($P < 0.0001$) in both the RF and VL, with the same pattern of increments in cadence as seen in the VM. In the RF, *post hoc* analysis of the both duty cycle and burst duration showed a significant difference between the circular and E_{2-} conditions, and examination of the plots in Figure 5.7 (Columns III & IV) show an increase in duty cycle and excitation time associated with the E_{2-} in comparison with the circular and E_{1-} conditions. This was particularly prevalent at 150 rpm, where large alterations between

both elliptical chainrings and the circular chainring can be observed with the elliptical chainrings associated with longer excitation time in line with the level of eccentricity, however, there was no significant chainring × cadence interaction ($P = 0.559$).

5.4.3.3 Phase Shift

There was a significant effect of chainring on the EMG intensity phase across all three quadricep muscles (VM: $P < 0.0001$; RF: $P < 0.0001$; VL: $P < 0.0001$; Figure 5.7; Column II). There was once again a trend for the elliptical chainring conditions to be associated with a shift in EMG intensity to earlier in the pedal cycle compared to the circular chainring. Across the three quadriceps muscles, *post-hoc* comparisons revealed a significant difference in phase between the E_{2-} condition and the circular and E_{1-} conditions. Conditions E_{1+} and E_{2+} were again associated with a shift in EMG intensity to occur later in the pedal cycle in comparison to the circular and elliptical chainrings used with the crank optimally orientated. There was no significant effect of cadence on total EMG intensity (VM: $P = 0.588$; RF: $P = 0.366$; VL: $P < 0.780$). There was a small significant chainring × cadence interaction in the RF ($P = 0.046$), but none in the VM nor VL ($P = 0.071$ & $P = 0.857$, respectively).

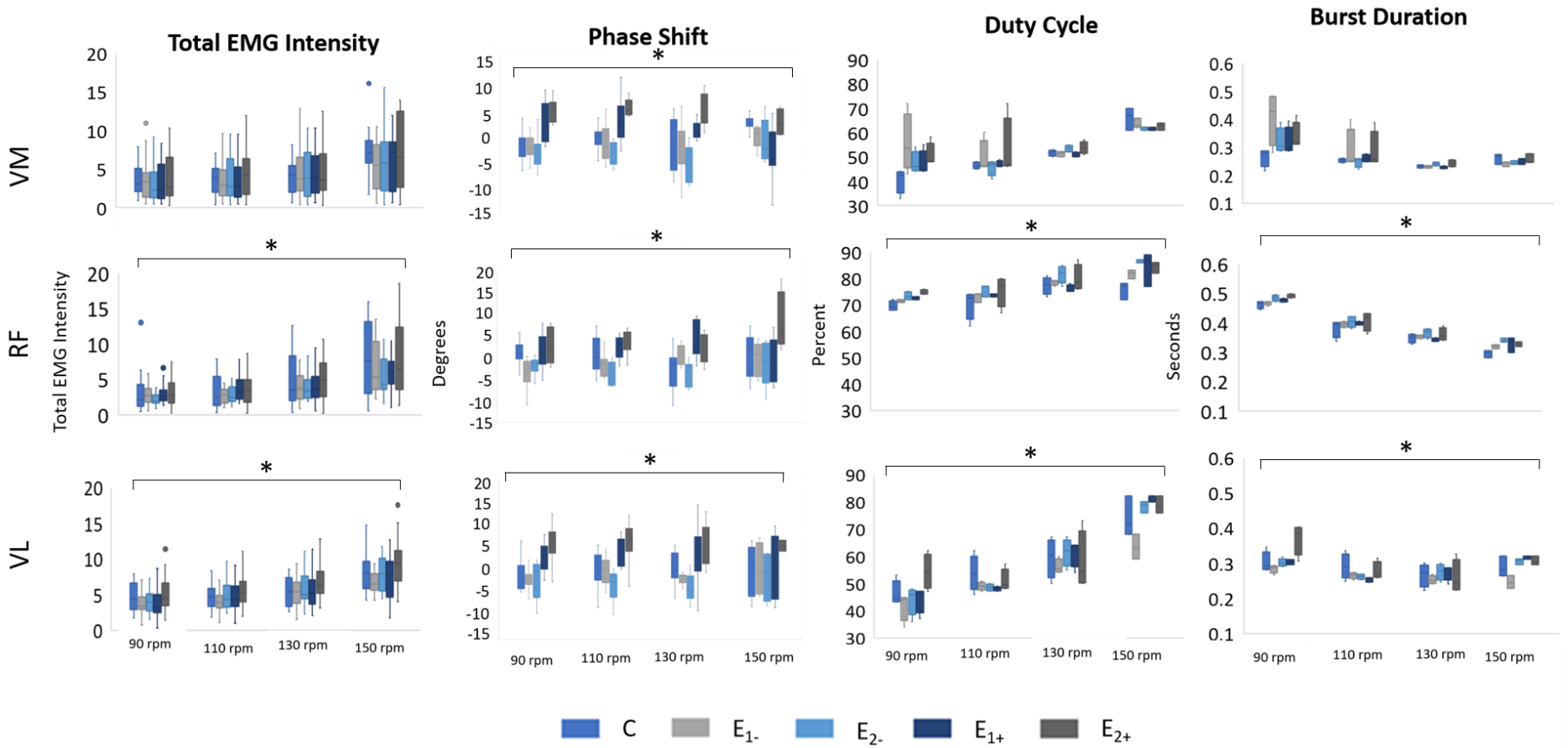

Figure 5.7 Total EMG Intensity, relative phase shifts, duty cycles and burst duration of EMG intensity in the quadriceps with pooled power outputs. Values are shown as box and whisker plots (median, interquartile range, SD and outliers) for eight participants and the five different chainring conditions represented as different colours across the range of four cadences. * denotes a significant main effect of chainring condition.

5.4.4 Hamstrings and GMAX

5.4.4.1 EMG Intensity

The reconstructed EMG intensity waveforms for the hamstring muscles and GMAX are shown in Figure 5.8. There was a significant difference in PC loading scores for the hamstrings (BF & ST) and the GMAX (BF: $P < 0.0001$; ST: $P < 0.0001$; GMAX: $P < 0.0001$). The reconstructions show a decrease in EMG intensity with increasing chainring eccentricity. In the BF, *post hoc* comparisons highlight a significant difference in PC loading scores between all three chainring eccentricities, but no effect of crank orientation, which is evident in the reconstruction (Figure 5.8). This is also the outcome of the *post hoc* comparisons in the ST, however, reconstructions reveal this difference to be more subtle than in the BF (Figure 5.8). *Post hoc* analysis on GMAX showed significant differences in PC loading scores between the circular and E_{1-} conditions, where the EMG intensity waveform was observed as being significantly lower in the elliptical chainring than the circular. The reconstruction of the GMAX shows an increase in intensity in the E_{2-} at 90° during peak excitation, above that of the circular, however, no significant differences in the PC loading scores were found in the *post-hoc* comparison. There was no significant cadence effect on EMG intensity PC loading scores in the hip extensor muscles (BF: $P = 0.995$; ST: $P = 0.693$; GMAX: $P = 0.830$), neither was any chainring x cadence interaction found (BF: $P = 0.967$; ST: $P = 0.996$; GMAX: $P = 0.992$).

Analysis of the sum of the EMG intensities (Figure 5.9; Column I) showed significant differences between chainring conditions in each of the hamstring muscles and GMAX (ST: $P = 0.007$; BF: $P < 0.0001$; GMAX: $P = 0.0017$). There were also significant differences in total EMG intensity of each muscle between cadences (ST: $P < 0.0001$; BF: $P < 0.0001$; GMAX: $P < 0.0001$), and loads (ST: $P = 0.026$; BF: $P = 0.02$; GMAX: $P = 0.007$). There was a general trend towards a lower total EMG present across all of these muscles when using an elliptical chainring in comparison to the circular, which was most noticeable in condition E_{1-}. At 150 rpm, there was a large decrease in total EMG intensity across all of the elliptical chainring conditions in comparison with the circular in the ST, BF and GMAX.

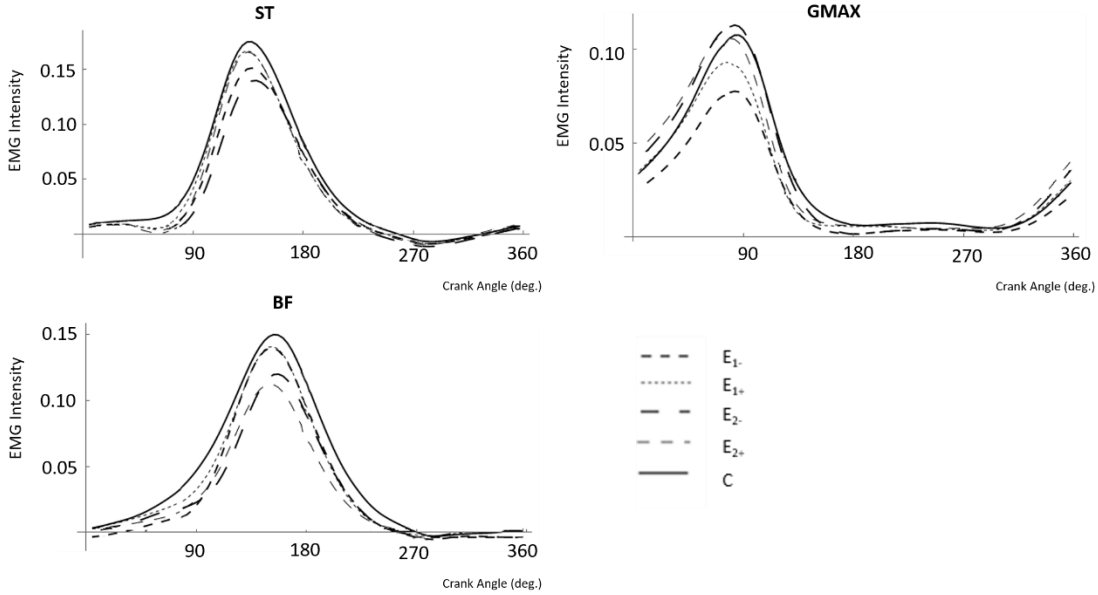

Figure 5.8 Principal component reconstructions of EMG intensity of the hamstring muscles (BF and ST) and GMAX. The waveforms have been reconstructed using the first ten principal component weights x loading scores representing >95% of the variability. Cadence and load conditions are pooled, and waveforms are presented over the course of a pedal cycle.

5.4.4.2 Burst Durations and Duty Cycles

There was a significant effect of chainring condition on duty cycle in each muscle (BF: P = 0.032; ST: P = 0.013; GMAX: P = 0.005) and on burst duration in the BF (P = 0.043) and GMAX (P = 0.006), but not the ST (P = 0.496). *Post hoc* comparison of the BF duty cycle and burst durations show that the E_{2-} condition significantly differs from the circular chainring, but despite there being no chainring × cadence interaction in burst duration (P = 0.815), nor duty cycle (P = 0.847), the differences between the two chainrings do not follow a systematic pattern across the cadences (Figure 5.9; Columns III & IV). At 90 rpm, there is an increase in duty cycle with the E_{2-} condition; however, at cadences 110 and 150 rpm, the two conditions are similar in terms of excitation duration and at 130 rpm there is a decrease in duty cycle. Conversely, there is a significant chainring × cadence effect in the ST duty cycle (P =0.008) and to a lesser extent in the GMAX duty cycle (P = 0.048). *Post hoc* analysis of both the ST and GMAX identified the duty cycles when using the elliptical chainrings as being significantly different from the circular, however, this response did not differ significantly between elliptical chainrings conditions. Scrutiny of the ST plots (Figure 5.9; Columns III & IV) shows various responses across cadences. However, there does appear to be a predominant trend for the elliptical chainring conditions to decrease muscle excitation, at both crank orientations, similarly to the differences identified in the ST EMG

intensity waveforms (Figure 5.8). Figure 5.9 (Column III) shows the chainring effects on duty cycle to be particularly evident at 130 and 150 rpm. Differences in the burst durations are also evident at these two cadences, where differences are also clear for the 90 rpm cadence. However, once again, the changes in patterns are not systematic across the cadences. At 90 rpm, the elliptical chainrings are associated with an increase in activation time in comparison to the circular chainring, however, at 130 and 150 rpm, there is a shorter activation time in the elliptical chainring conditions when presented at an optimal crank angle (E_{1-} and E_{2-}). There was a significant effect of cadence on the burst durations (BF: $P = 0.043$; ST: $P < 0.001$; GMAX: $P = 0.006$), and duty cycle (BF: $P < 0.0001$; ST: $P < 0.0001$; GMAX: $P < 0.0001$). Whereby a systematic increase in duty cycle and decrease in burst duration with increasing cadence was noted across the three muscles.

5.4.4.3 Phase Shift

There was a significant effect of chainring condition on the EMG intensity phase in the hamstring muscles and GMAX (Figure 5.9; Column II). This followed the same patterns as the previously discussed muscle groups, whereby conditions E_{1-} and E_{2-} were associated with a phase advance in EMG intensity, and with E_{1+} and E_{2+} EMG activation occurred later in the pedal cycle. There was no significant effect of cadence on the phase (BF: $P = 0.931$; ST: $P = 0.333$; GMAX: $P = 0.647$), and neither was a chainring x cadence interaction found (BF: $P = 0.567$; ST: $P = 0.754$; GMAX: $P = 0.453$).

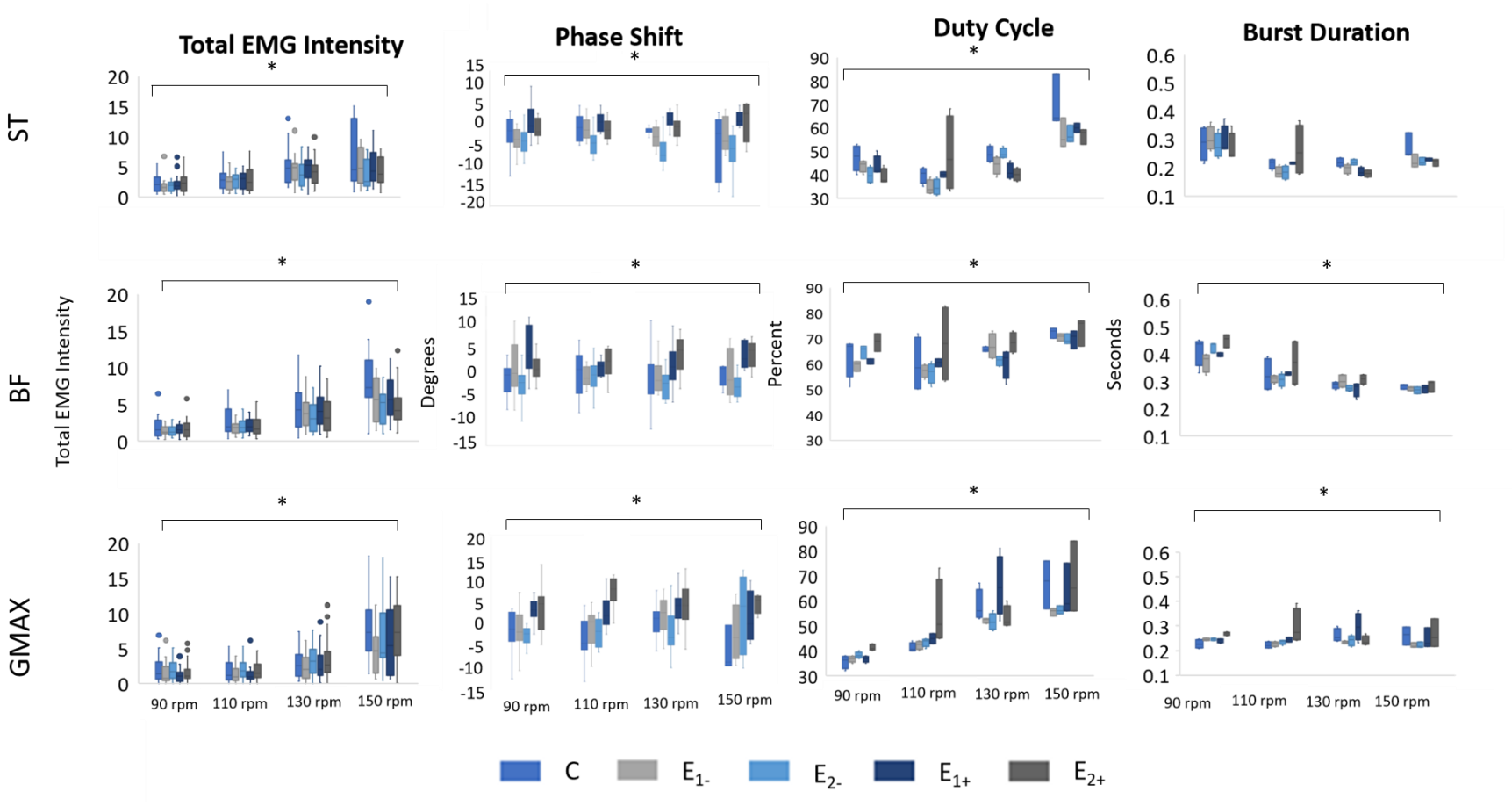

Figure 5.9 Total EMG Intensity, relative phase shifts, duty cycles and burst duration of EMG intensity in the hamstrings with pooled power outputs. Values are shown as box and whisker plots (median, interquartile range, SD and outliers) for eight participants and the five different chainring conditions represented as different colours across the range of four cadences. * denotes a significant main effect of chainring condition.

5.4.5 Total Muscle Response

Ten PC loading scores used to reconstruct the EMG intensity, with the cumulative percentage to the PC weightings explaining 98% of the total variability. An ANOVA was performed on the loading scores for the pooled nine muscles to detect an overall chainring response on EMG intensity. There was a significant effect of chainring ($P < 0.0001$) on PCI_{LS}. Further scrutiny determined that this was lowest in the circular condition, with no significant difference between the circular and E_{1-} condition. Chainrings E_{2-} and E_{2+} were significantly different and associated with larger loading scores, whilst E_{1+} was linked to the largest difference in loading score.

5.6 Discussion

This study investigated the influence of using different elliptical chainrings on muscle excitation across a range of cadence and load demands. One of the primary contributions of this research is that it amalgamates previously inconsistent findings concerning muscle excitation responses to changes in chainring geometry and crank orientation, by assessing the interaction between chainring condition and cadence and load on muscle recruitment. In agreement with the hypothesis that EMG phase and magnitude would be influenced by the elliptical chainrings, alterations in muscle coordination patterns were evident across chainring conditions and cadences in the muscles studied. This was seen as increased EMG intensity in the triceps surae when using elliptical chainrings, with differences in phase of the EMG intensity occurring, the direction of which was dependent on the crank orientation. Also as predicted, differences in excitation changes between proximal and distal muscle groups did occur, however the patterns were not in line with initial predictions. The response of the quadriceps, hamstrings and GMAX to the elliptical chainrings were opposing to that of the triceps surae, however a decrease in EMG intensity was observed rather than no significant difference in magnitude, and a phase shift did occur congruent with that of the triceps surae.

Taken together the results from the circular chainrings contain very similar features of muscle activation found in previous experiments. The muscle coordination patterns, revealed in the array plots (Figure 5.3) are also very similar to those reported by Blake and Wakeling (2015) and Wakeling and Horn (2009) as well as others (Dorel et al., 2009; Hug et al., 2013; Neptune

and Herzog, 2000). Equally, the increments and decrements of duty cycle and burst duration, respectively, as cadence advanced, were reported by Blake and colleagues (2015). These similarities therefore evidence that the dataset presented here are representative of muscle activations resulting from cycling with a circular chainring. The changes seen with the use of the elliptical chainrings can also therefore be considered representative of the effects of their use, which is further supported by the fact that similar changes in EMG phase related to use of elliptical chainrings have also been found previously (Neptune and Herzog, 2000).

5.6.1 Adaptations in the triceps surae

The triceps surae were active during the downstroke and between crank angles of 60° and 150° across all chainring conditions (Figures 5.3 & 5.4) which was consistent with previous cycling studies using a conventional circular chainring under similar mechanical demands (Blake and Wakeling, 2015). Although there were statistically significant shifts in muscle activation timings between the elliptical and circular chainrings (Figure 5.5; Column II), these phase shifts were minor in absolute terms. This is in keeping with previous reports suggesting a 2-10° phase advance in muscle activity was required when using elliptical chainrings in order to contend with the altered crank angular velocity profile (Winters and Stark, 1988). This could be attributed to the activation-deactivation dynamics associated with muscle force development interacting with the requirement for muscle forces to be produced in the same region of the pedal cycle, and therefore limiting the size of phase shift that can usefully occur.

Significant increases in EMG intensity amplitude in the SOL, MG and LG were noted when using the elliptical chainrings in the optimal crank orientation position (Figure 5.4), with the muscles becoming active in Q2, a region of slow crank angular velocity in conditions E_{1-} and E_{2-} (Figure 3.3B). Previous cycling studies have suggested that these muscles are important for the transfer of force to the crank (Martin and Nichols, 2018). The increase in EMG intensity in the triceps surae during the slower region of the crank velocity is not surprising when considering the increases in MTU velocity observed in the SOL (Figure 4.3) and MG (Figure 4.4) in Chapter Four. Specifically, if the MTU velocities reflect fibre kinematics, then it is possible that this reduction indicates the muscle may be working within force-velocity related changes in force production. The increased EMG intensity is, however, somewhat paradoxical

when considering that the triceps surae are typically associated with decreased activity during slower pedalling rates (Sanderson et al., 2006; Blake and Wakeling, 2015), however, during the slowest part of the pedal cycle (Q2 & Q4) there was an increase in both EMG intensity and MTU velocities here (Figures 4.3 & 4.4) in the E_{1-} and E_{2-} conditions.

During the SOL's most active phase (Q2; Figure 5.4) it was shortening (Figure 4.3A), and the velocity of lengthening and shortening increased when the elliptical chainrings were used. When the MG was most active, slightly later in Q2 (Figure 5.4), it transitioned from lengthening to shortening (Figure 4.4 & 4.5; Column I) and therefore seems to be undergoing a stretch-shortening cycle that could lead to force enhancement in this muscle (Herzog & Leonard, 2000). The differences in SOL and MG MTU lengths reported in Chapter 4 are striking, and further differences in the behaviours of these synergists are found here, with regard cadence related changes in burst duration and duty cycle. Specifically, the SOL duty cycle rose from 45% at 90 rpm in the circular chainring to 79% at 150 rpm, whilst the MG went from 50.5% to 64.6% between these cadences. This further highlights that the triceps surae seem to respond independently, with the longer duration recruitment of the SOL potentially a strategy to help maintain the ankle moment. Differences in duty cycles between cadences in the SOL was at its largest when the circular chainring was used with smaller differences occurring when the elliptical chainrings were employed (Figure 5.5), and as cadence increased, the duty cycle was lower in the elliptical chainrings compared to the circular. Larger duty cycles are considered a limitation of the activation-deactivation dynamics of a muscle (Blake and Wakeling, 2015) and result in an increase in negative muscular work and unnecessary co-contraction of antagonistic muscle pairs (Neptune and Herzog, 1999; Neptune and Kautz, 2001). The alterations in crank angular velocity caused by the elliptical chainrings may therefore lead to more favourable excitation-contraction coupling conditions in muscles such as soleus and support more economic locomotion.

5.6.2 Adaptations in the quadriceps

Changes in muscle excitation patterns were quite different in muscles in the proximal, compared to distal, segment of the leg. The vasti muscles are one of the leading power producing muscles in the pedal cycle, as they generate mechanical energy in Q1, which is then

transferred into the triceps surae and to the crank as the pedal cycle progresses (Raasch et al., 1997). As in MG, the VL EMG activity began to rise as the MTU was lengthening, persisting as the MTU transitioned to shortening. This muscle, therefore, may also enhance force production through the stretch-shortening cycle (Herzog and Leonard, 2000). Given the similar VM activity pattern (Figure 5.6) and anatomical location it is possible it may also utilise this force enhancement mechanism, although given the differences in SOL and MG this should not be assumed.

The elliptical chainrings were shown to lead to slower crank angular velocity in the region of the pedal cycle the vasti are active (Figure. 3.3), with significant but small effects on VL MTU velocity (Figure. 4.7). The vasti were however able to maintain power output in the different chainring conditions with lower activation (Figure. 5.6), indicating (in VL at least) a decoupling of the MTU kinematics and the activation pattern. The greater time spent in Q1 with the elliptical chainrings therefore seems to have reduced the activation required from these motor muscles to generate forces at the pedals. Further work is required to identify whether these changes are related to alterations in muscle fibre kinematics (as opposed to MTU kinematics), potentially highlighting the interplay between MTU gearing and neuromuscular drive to the muscles (Wakeling et al., 2011).

The RF displayed larger reductions in EMG intensity with the elliptical chainrings in comparison to the VM and VL (Figure 5.6). Previous studies have suggested that the biarticular RF is important in propelling the crank through flexion-extension transitions of the limb and transferring the mechanical energy across joints (Raasch et al., 1997). In comparison to this, the primary function of the VM and VL are to act as major power producers. Participants were instructed to maintain a specifically selected cadence (which was complied with, see Table 3.1), and consequently a constant power output was sustained throughout the trial. Conditions E_{1+} and E_{2+} were associated with increased crank angular velocity during Q2, with a concomitant reduction in effective force (Figure 3.5; Column I) and both VM and VL had greater EMG intensity in this quadrant in E_{2+}. The shifts in phase were significant across the quadriceps, but were however small, in-keeping with the previously identified 2-10° alteration in phase key in maintaining the required muscle force. Subtle differences in

activity of the vasti therefore occur with use of the elliptical chainrings studied here. One interesting avenue for future work would be to explore the potential influence of MTU and/or fibre length changes in light of altered activation phase within a work-loop based framework (Josephson, 1985) to better explore consequences for force and power production. The changes in activation and MTU kinematics however seem much smaller than the resulting effects on crank angular velocity and effective forces, highlighting the complexity of understanding the integration between neuromuscular mechanics and system level production of movement production.

5.6.3 Adaptations in the hamstrings and GMAX

The hamstrings (ST & BF) were active during the transition between Q2 and Q3 and into Q4, whilst GMAX was active at the end of Q4 into Q1 and the initial portion of Q2 (Figure 5.8), which is in accordance with previous studies (Neptune and Herzog, 2000; Blake and Wakeling, 2015). The changes in EMG intensity in the hip extensors was similar to the quadriceps, as EMG intensity was found to significantly decrease across the ST, BF and GMAX in conjunction with the elliptical chainring conditions. The GMAX is considered to be an important power producer during the pedal cycle, and changes in its activation patterns are similar to those seen in the power producers of VL and VM discussed above. In contrast, the hamstrings are classified as being critical muscles for the transition between extension and flexion and the orientation of force at the pedal across the bottom of the pedal cycle (Raasch et al., 1997). There was a decrease in ineffective crank force (Figure 3.3; Column II) and a rise in resultant crank force (Figure 3.3; Column III) in this region of the pedal cycle when using the elliptical chainrings, as the decrease in EMG intensity in the ST and BF (Figure 5.8). These changes in EMG intensity however contrast to those seen in LG and MG, the other biarticular muscles credited with transferring energy across joints and orientation of forces at the pedal. This highlights that whilst groups of muscles may be accredited with similar roles, specifics of their anatomical location and intrinsic properties likely play a larger role in determining their individual behaviours and contributions to pedalling.

5.6.4 What are the implications of alterations in muscle coordination?

Any alterations in muscle coordination have important implications for muscular efficiency, as the coordination of the lower extremity excitation during cycling affects the direction, amplitude and duration of the mechanical force expressed at the crank (Blake and Wakeling, 2015). Previous studies have shown a negative correlation between total EMG intensity and mechanical efficiency (Wakeling et al., 2010; Blake et al., 2012) as increased efficiency when pedalling at a constant load and cadence has been shown to result from a decrease in muscle excitation (Blake et al., 2012). Workload has been found to significantly influence muscle activity, in that, as workload increases, activation levels in the SOL, MG, VM, RF, BF, ST, GM and gluteus medius have been shown to increase (Ericson et al., 1985). However, as seen in the EMG changes reported here, this response is non-uniform and activity of muscles such as GM has been found to be much more susceptible to alterations in load than the VL, VM, MG and LG (Ericson et al., 1986). This again indicates the complexity of understanding how neuromuscular mechanics contribute to the completion of everyday tasks, highlighting the importance of probing different levels and elements of the neuromuscular system, rather than suggesting results from one or two muscles can be representative of all muscles in the system.

Blake and colleagues (2012) suggested a relationship between relative efficiency and mechanical output, as they saw muscle excitation was minimised with increasing cadences. Here, the decrease in EMG intensity across the proximal leg segment muscles occurred in conjunction with the increased mechanical output at the crank (Figure 3.3) when the elliptical chainrings were used and could therefore represent an increase in relative efficiency for these conditions. There was however, an increase in EMG intensity across the distal muscles (SOL, LG and MG) that could cancel any gains in efficiency seen from the behaviour of the proximal muscles. Indeed, Brennan and colleagues (2019) suggest that increases in activation, observed as high-frequency, short-duration contractions during augmented cadences are less economical. Nevertheless, Blake and Wakeling (2013) established a positive correlation between total EMG intensity and metabolic power. By conducting the total muscle response in this chapter, it was evident that the circular chainring was associated with a lower total muscle EMG, although this was not significantly different from E_{1-}. It was determined in Blake

and Wakeling (2013) that the prescribed muscle weighting coefficient had a significant effect on the estimation of metabolic power from the EMG and gas exchange sources, indicating that individual muscle importance is relative. In their study, proximal muscles received a higher weighting coefficient, and as much are more important in determining efficiency and metabolic power than the distal muscles. As such, it is important to note that all the muscles were equally weighted in the analysis performed in this chapter, and future work might consider the impact of adjusting this to assess whether elliptical chainrings lowered the total muscle response in light of the reduction in total EMG intensity present in these conditions.

5.7 Conclusion

This chapter investigated the influence of elliptical chainrings on muscle activation during cycling, and the subsequent relationship between the muscle activation adaptations with cadence and load. In dynamic movement tasks, the need for a specified combination of angular segmental motions further constrains the coordination solutions available to the neuromuscular system. However, alterations were found here in conjunction with changes in chainring geometry and crank orientation, consequently the variation in results presented highlights the complexity of adaptations in the neuromuscular system to alteration in motor task demand. Having quantified responses of the musculoskeletal system from crank kinetics and kinematics and joint kinematics (Chapter 3), through MTU kinematics (Chapter 4) and muscle activation patterns (Chapter 5) the final chapter of this thesis will collate these findings in the context of the wider literature and objectives stated at the end of Chapter 2.

Chapter 6. General Discussion

The overall goal of this thesis was to investigate the acute responses of the neuromusculoskeletal system to alterations in chainring eccentricity and the orientation of the crank against their major and minor axes, with the underlying aim of using the elliptical chainrings as a platform to understand more about how the human neuromuscular system behaves *in vivo*. Previous research on the effects of non-circular chainrings has primarily focused on either the direct performance implications (Horvais et al., 2007; Hintzy and Horvais, 2016; Leong et al., 2017), or utilised computational approaches to predict system adaptations that may occur (Kautz and Hull, 1995; Purdue et al., 2010; Rankin and Neptune, 2008). Consequently, there are pervasive gaps in our understanding of elliptical chainrings and the work I have completed provides a valuable bridge between the theoretical inferences and the empirical findings.

"In theory there is no difference between theory and practice, while in practice there is."

Benjamin Brewster, 1882

After a critical review of the literature (Chapter Two) it was clear that more work needed to be completed to establish better understanding of how the neuromusculoskeletal system reacts to a perturbation in task mechanics caused by alterations in chainring geometry, cadence and load; and subsequently how they integrate their response individually and between one another. It was contended that determining the adaptations in mechanical force output, joints and muscle-tendon unit kinematics and muscle coordination patterns would provide some of the insight required. To quantify the acute responses to these elliptical chainrings, it was necessary to complete an array of assessments within a cadence and load controlled experimental protocol. In addition to the successful manipulation of the crank angular velocity profile between each of the chainring conditions, there are a few major findings from this research that will be discussed below.

6.1 Internal and external effects of elliptical chainrings

In Chapter Three, the crank angular velocity profile associated with the two elliptical chainrings was identified, including the effects of altering the crank orientation. Within this chapter, joint kinematics were found to be affected; however, the ankle produced the largest alteration in range of motion in response to the altered chainring geometry, whilst knee and hip motions were largely preserved. It was suggested that this could represent a strategy to maintain the mechanical environment within which the power-producing muscles in the quadriceps and gluteus maximus operated. In contrast, the muscles of the triceps surae complex were subject to greater perturbations at the ankle joint, particularly through bottom dead centre (Q3) of the pedal cycle where increased ankle plantar flexion was observed (Figure 3.7).

Alterations in crank force resulting from the use of the elliptical chainrings were also established in Chapter 3, and a cadence-dependant influence of the elliptical chainrings on effective and ineffective forces over the course of the pedal cycle was determined. As such, the effect of elliptical chainrings on effective force was larger as cadence increased up to 130 rpm. Between the cadences of 130 and 150 rpm, a critical limit was seemingly met, and there was a decrease in range of crank forces between the chainring conditions observed at 150 rpm. Another interesting finding of this chapter were the asymmetries in crank force production between the left and right leg that became evident as cadence increased. As such, at cadences 130 and 150 rpm, there was a visible shift in the crank angle at which peak effective force in the left crank was achieved (Figure 3.5; Column I), and consequentially, an alteration in the pattern of resultant force (Figure 3.5; Column III). This is in contention with previous observations in cycling research, whereby increases in intensity are typically met with increases in symmetry (Carpes et al., 2007a; Carpes et al., 2007b). Cyclists mostly work at moderate intensities during training and prolonged competition (Golich and Broker, 1996), however, when tasked with cycling at high cadence, asymmetries could emerge due from greater consistency in the kinematics of the dominant leg and consequently, its ability to orient pedal forces (Edeline et al., 2004).

Such findings highlight the value of using principal component analysis as a means of

quantifying variability and revealing temporal patterns of change in recorded data. As no *a priori* assumptions of the potential location of differences in data were required, and the waveform across the pedal cycle was assessed, the approach can be considered to allow an unbiased assessment of these data. The PCA approach therefore not only effectively distinguished differences in the waveform shape between chainring conditions, but also highlighted other variability in the waveform data that was not intentionally being investigated. Each PC weighting reveals a feature of the variability within the data set and the individual contributions from each PC weighting were used to express an estimated waveform explaining more than 90% of the variability. Identifying these individual components and their contributions to the net pattern of effective force enabled the shift in the pattern of effective crank force production that may have been missed if just the mean of the data were used.

Prior to commencing the analysis of these data, a one-legged musculoskeletal model was deemed appropriate to provide an accurate representation of neuromusculoskeletal system response. This was based on the kinematics data collected, which included a static calibration trial taken on the bike, but none of the participant standing on the ground. When establishing the model, it became clear that, although requested to, participants had not sat symmetrically on the bike during the static trial and as such creating a two-legged model with appropriate error was not feasible. As the literature largely suggests forces are applied symmetrically between the right and left pedals due to the constrained path of the cranks and pedals (Kautz et al., 1991) it was decided a one-legged model would be appropriate to meet the objectives set. However, on reflection of the mechanical output at the crank, it is clear that left and right lower body segments have not behaved in the same way. It is a common assumption within the cycling literature that performance is symmetric between the legs, due in part to the methodology employed to analyse the mechanical outputs. In contrast, the results presented here suggest that there is a degree of asymmetry present and that this is cadence dependant. Due to the implications for performance and possible injury risk, this area warrants further investigation.

Chapter Four extended the participant specific musculoskeletal simulations developed in Chapter Three, providing predictions of MTU behaviour of the SOL, MG and VL. This was a

novel approach as predictions of MTU lengths and velocities have not previously been quantified using an anatomically constrained model. While the elliptical chainrings had little effect on the MTU lengths, velocity changes were much greater. The triceps surae were affected to a larger extent than VL, with changes in the timing of lengthening and shortening velocities and an increase in magnitude in association with increasing chainring eccentricities. Alterations in MTU velocity were also observed in the vastus lateralis, however, these effects were more subtle, and likely reflected the smaller changes in knee compared to ankle kinematics seen. The consistencies evident between the joint and MTU kinematics in the model were unsurprising, however, there were some outcomes of the simulation which were unexpected and highlight the strengths of using an anatomically constrained model. The discrepancies observed between larger ankle joint ranges of motion and decreases in medial gastrocnemius MTU lengths when pedalling at high cadences (150 rpm) contradict previous reports (Gregor et al., 1987; Sanderson et al., 2006). These reports predicted MTU lengths from joint kinematics based on marker trajectories, with no constraints on physically plausible skeletal movements imposed. This means skin motion artefacts could influence joint kinematics, a factor that does not influence the predictions from the musculoskeletal simulations used here. Therefore, there is a need to consider this type modelling and simulation approach when examining the behaviour of the musculoskeletal system during dynamic tasks, particularly where large ranges of joint motion occur. However, this type of analysis is a time-consuming process and as such, the sample size of this dataset was just eight, despite nineteen participants taking part in the original study. Future could be improved by increasing the number of participants to ensure findings are widely generalizable, although it should be noted that the PCA approach ensured that the variability within this specific data set were quantified.

The use of a musculoskeletal model has provided a novel perspective on the response of the muscle-tendon unit mechanics, however, the behaviour of the muscle fibres cannot be inferred from this, and additional work is needed if we are to understand the relationship between contractile tissue and the series elastic element. I had aimed to be able to address this element, and had collected ultrasound data from the MG. However, at the high cadences large inter-frame muscle deformations occurred that were too big for current computational

image analysis approaches to robustly quantify. Therefore, the planned muscle fascicle data were not considered reliable enough and have not been included here. Work will be commenced to resolve this issue, and therefore the data set I have accrued will in the future be used to investigate the behaviour of both the MTU and fascicle elements.

The final experimental chapter (Chapter Five) examined the effects of the elliptical chainrings on the activation patterns of nine leg muscles. Wavelet analysis was performed as a means of extracting a deeper understanding of the excitation pattern by considering the EMG intensity spectral properties and recovering additional information encoded in the EMG signal (von Tscharner, 2000; Wakeling, 2009; Wakeling and Rozitis, 2004). The advantage of using this approach and measuring EMG intensity in this study, is that the wavelets have been specifically designed for analysis of EMG data, as their time resolutions are mapped against excitation-contraction coupling and hence force production. This means time constants are consistent within this data analysis, and between others using this method, making the results directly comparable to others who have used the technique unlike other methods such as calculating the root mean square (von Tscharner, 2000). Using this method also presents an opportunity for further downstream analyses such as consideration of the relative efficiency associated with the chainring conditions (Blake and Wakeling, 2015) and also the relationship between EMG intensity and metabolic power (Blake et al., 2013) which could present as an interesting avenue for future work to determine the wider (e.g. system level) effects of using elliptical chainrings.

From the EMG analysis, striking differences in the responses of the proximal and distal muscles to the elliptical chainrings emerged. Whilst it was originally hypothesised that the pattern of activation in the power-producing muscles of the quadriceps would be preserved, due to the small changes in knee kinematics and VL MTU behaviours, there was a reduction in EMG intensity pervasive across the proximal muscles in conjunction with the elliptical chainrings. In contrast, there was an increase in EMG intensity seen across the distal limb muscles. In addition, biarticular muscles responsible for transferring force across the joints to the crank (RF, MG & LG) showed a larger response to the elliptical chainrings than the monoarticular muscles (VM, VL & GMAX), which are considered to be responsible for

generating the force. Furthermore, systematic changes in the phase of muscle excitation were observed between the chainring conditions, and whilst chainrings E_{1-} and E_{2-} were associated with excitation occurring earlier in the pedal cycle than the circular chainring, conditions E_{1+} and E_{2+} were associated with a later activation. This was in opposition of the changes in MTU velocity timing observed with the different chainrings in Chapter Four, whereby E_{1+} and E_{2+} were associated with a phase advance in lengthening and shortening velocity and E_{1-} and E_{2-} were associated with a delay. The MTU velocities could be decoupled from the fascicle velocities (Dick and Wakeling, 2017; Wakeling et al., 2011), and therefore the data presented cannot be fully interpreted or understood until fascicle behaviours are quantified. However, results like this highlight the challenges of assessing responses of the neuromusculoskeletal system to alterations in external mechanics, given that much is still not understood about the complexity of neuromuscular drive being translated from motor unit excitation through to net joint torque production and completion of dynamic tasks such as cycling.

As previously mentioned, it is important to consider that the sample size data are presented from is eight throughout this thesis. Data from the same participants were used for the crank reaction force analysis, were scaled in the musculoskeletal model and included in the EMG signal analysis. EMG data are however considered much noisier than kinematics or kinetic data (Chowdhury et al., 2013). Therefore, within the context of EMG analysis, variability in the individual responses in excitation patterns could affect the results and are highlighted by the data spread evident in presented results (Figures 5.5, 5.7 & 5.9; Columns III & IV). This has influenced the patterns of change in burst durations and duty cycles seen across the individual muscles in response to different chainrings. A clearer trend for changes could be provided by increasing the number of participants analysed in this chapter and/or also increasing the number of pedal cycles analysed. However, it also highlights the individuality of muscle recruitment (Hug et a., 2008) and responses of the neuromuscular system to task demands and mechanics, noted as a current challenge for the biomechanics community to address (Herzog, 2017).

6.2 Where do we go from here?

In this thesis, a more comprehensive understanding has been established regarding how the neuromusculoskeletal system is affected when external mechanics at the crank are manipulated. This initial piece of research has emphasised that although changes are present, they vary across different levels of the system (e.g. joint *versus* MTU *versus* muscle activation) and highlight why it is not possible to predict consistent effects on cycling performance. While the key objectives of the thesis have been met, more questions that warrant investigation in the future are now apparent. Recommendations for future work are therefore:

a. To create a rigid ankle structure to assess whether the greater perturbations experienced at the ankle in association with the elliptical chainrings have an impact on the crank reactive force;
b. calculate the crank inertial load of the different chainrings to better understand how they impact the muscular and non-muscular components of force production, and how this relates to the cadence interactions observed in this thesis;
c. to assess the freely chosen cadence when using the elliptical chainrings and measure the impact this has on gross efficiency;
d. quantify fascicle length and velocity from recorded ultrasound data, and compare them to reported MTU behaviours (i.e. MTU gearing) and activation patterns;
e. assess the implications of the alterations in MTU, fascicle behaviour and activation patterns on mechanical power output within a work-loop based framework;
f. further analyse EMG intensity data to determine the implications of chainring geometry on relative muscle efficiency and metabolic power.

One further avenue which would be interesting to explore, although not directly related to the study of elliptical chainrings, would be to develop a two-legged musculoskeletal muscle and investigate the association between the asymmetrical pedal force profiles and joint, MTU and fascicle kinematics and muscle activation. This should include consideration of power production at faster cadences, and whether differences in asymmetries exist between cyclists with different levels of experience and performance.

6.3 Summary

The overarching aim in completing a pedalling task, is to successfully accelerate the crank against frictional and inertial loads. The extent to which elliptical chainrings help or hinder specific aspects of performance is still unknown. However, the experimental data I have presented confirm certain theoretical predictions regarding the effects of elliptical chainrings. An increased amount of time spent during the downstroke (Q2) in conditions E_{1-} and E_{2-} were observed, with an increment in effective crank force production and decrease in ineffective force evident during the downstroke. Concurrent with this, a clear response of the neuromusculoskeletal system was detected in association with alterations in chainring geometry and crank orientation, presenting as adaptations in joint kinematics, muscle-tendon unit velocity and muscle coordination patterns. From a practical standpoint, the use of non-circular chainrings in professional sport and link to victory suggests that their effects are not deleterious, and the ultimate goal of research in this area would be ascertain how the changes presented here link to cycling performance. From a fundamental science standpoint, altering the drivetrain kinematics has convincingly shown that elliptical chainrings can be used as a method of manipulating muscle-tendon unit behaviour and muscle excitation patterns that in future could be used as a means of generating greater understanding of the mechanical behaviour of these complex systems *in vivo*.

Chapter 7. References

Adam, A., Luca, C. J. De and Erim, Z. (1998) 'Hand Dominance and Motor Unit Firing Behavior.' *Journal of Neurophysiology*, 80(3) pp. 1373–1382.

Ahlquist, L. E., Bassett, D. R., Sufit, R., Nagle, F. J. and Thomas, D. P. (1992) 'The effect of pedaling frequency on glycogen depletion rates in type I and type II quadriceps muscle fibers during submaximal cycling exercise.' *European Journal of Applied Physiology and Occupational Physiology*, 65(4) pp. 360–364.

Ahn, A. N. (2012) 'How muscles function - The work loop technique.' *Journal of Experimental Biology*. The Company of Biologists Ltd pp. 1051–1052.

Anderson, F.C. and Pandy, M.G. (2001) 'Dynamic optimization of human walking.' *Journal of Biomechanical Engineering*, 123(5) pp.381–90.

Anguera, J. A., Russell, C. A., Noll, D. C. and Seidler, R. D. (2007) 'Neural correlates associated with intermanual transfer of sensorimotor adaptation.' *Brain Research*, 1185 pp. 136-151.

Arnold, E., Hamner, S., Seth, A., Millard, M. and Delp, S. (2013) 'How muscle fibre lengths and velocities affect muscle force generation as humans walk and run at different speeds.' *Journal of Experimental Biology*, 216 pp. 2150–2160.

Askew, G. N. and Marsh, R. L. (1998) 'Optimal shortening velocity (V/V(max)) of skeletal muscle during cyclical contractions: Length-force effects and velocity-dependent activation and deactivation.' *Journal of Experimental Biology*. 201(10) pp. 1527–1540.

Azizi, E. and Roberts, T. J. (2010) 'Muscle performance during frog jumping: influence of elasticity on muscle operating lengths.' *Proceedings of the Royal Society B: Biological Sciences*, 277(1687) pp. 1523–1530.

Barratt, P. R., Martin, J. C., Elmer, S. J. and Korff, T. (2016) 'Effects of pedal speed and crank length on pedaling mechanics during submaximal cycling.' *Medicine and Science in Sports and Exercise*, 48(4) pp. 705–713.

Barry, N., Burton, D., Sheridan, J., Thompson, M. and Brown, N. A. T. (2015) 'Aerodynamic performance and riding posture in road cycling and triathlon.' *Proceedings of the Institution of Mechanical Engineers, Part P: Journal of Sports Engineering and Technology*, 229(1) pp. 28–38.

Baum, B. S. and Li, L. (2003) 'Lower extremity muscle activities during cycling are influenced by load and frequency.' *Journal of Electromyography and Kinesiology*. 13 (2) pp 181-190.

Beelen, A. and Sargeant, A. J. (1991) 'Effect of fatigue on maximal power output at different contraction velocities in humans.' *Journal of Applied Physiology*, 71(6) pp. 2332–2337.

Berg-Robertson, A. M. and Biewener, A. A. (2012) 'Muscle function during takeoff and landing flight in the pigeon (Columba livia).' *Journal of Experimental Biology*. 215(23) pp. 4104–4114.

Biewener, A. A. (2016) 'Locomotion as an emergent property of muscle contractile dynamics.' *Journal of Experimental Biology*, 219 pp. 285–294.

Biewener, A. A., Konieczynski, D. D. and Baudinette, R. V (1998) ‘In vivo muscle force–length behavior during steady-speed hopping in tammar wallabies.’ *The Journal of Experimental Biology*, 201 pp. 1681–1694.

Biewner, A. A. and Roberts, T. J. (2000) ‘Muscle and tendon contributions to force, work and elastic energy savings: a comparative perspective.’ *Exercise and Sport Science Reviews*, 28(3) pp. 99–107.

Bini, R. R. and Dagnese, F. (2012) ‘Noncircular chainrings and pedal to crank interface in cycling: a literature review.’ *Brazilian Journal of Kinantropometry and human performance*, 14(4) pp. 470–482.

Bini, R.R., Hume, P., Croft, J. and Kilding, A. (2013) 'Pedal force effectiveness in cycling: A review of constraints and training effects.' *Journal of Science in Cycling,* 2 (1) pp. 11-24.

Bini, R.R. and Hume, P. (2015) 'Relationship between pedal force asymmetry and performance in cycling time trial.' *The Journal of Sports Medicine and Physical Fitness,* 55 (9) pp. 892-898.

Bikecad (2018) *Bicycle frame dimensions,* viewed 20.08.2019, <https://www.bikecad.ca/taxonomy/term/25>

Blake, O. M., Champoux, Y. and Wakeling, J. M. (2012) ‘Muscle Coordination Patterns for Efficient Cycling.’ *Medicine & Science in Sports & Exercise*, (14) pp. 926–938.

Blake, O.M. and Wakeling, J.M (2013) 'Estimating changes in metabolic power from EMG.' *SpringerPlus,* 2 pp. 229.

Blake, O. M. and Wakeling, J. M. (2015) ‘Muscle coordination limits efficiency and power output of human limb movement under a wide range of mechanical demands.’ *Journal of Neurophysiology*. American Physiological Society, 114(6) pp. 3283–3295.

Blocken, B., Defraeye, T., Koninckx, E., Carmeliet, J. and Hespel, P. (2013) ‘CFD simulations of the aerodynamic drag of two drafting cyclists.’ *Computers and Fluids*, 71, pp. 435–445.

Boonstra, T. W., Daffertshofer, A., van Ditshuizen, J. C., van den Heuvel, M. R., Hofman, C., Willigenburg, N. W. and Beek, P.J. (2008). 'Fatigue-related changes in motor- unit synchronization of quadriceps muscles within and across legs.' *Journal of Electromyography and Kinesiology*, 18(5) pp. 717-731.

Bojsen-Møller J, Hansen P, Aagaard P, Svantesson U, Kjaer M, Magnusson SP. (2004) 'Differential displacement of the human soleus and medial gastrocnemius aponeuroses during isometric plantar flexor contractions in vivo.' *Journal of Applied Physiology* 97(5) pp, 1908-1914.

Boyd, T. F., Neptune, R. R. and Hull, M. L. (1997) ‘Pedal and knee loads using a multi-degree-of-freedom pedal platform in cycling.’ *Journal of Biomechanics*. 30 (5) pp. 505-511.

Brennan, S. F., Cresswell, A. G., Farris, D. J. and Lichtwark, G. A. (2018) ‘The effect of muscle-tendon unit vs. fascicle analyses on vastus lateralis force-generating capacity during constant power output cycling with variable cadence.’ *Journal of Applied Physiology*, 124 pp. 993–1002.

Brennan, S. F., Cresswell, A. G., Farris, D. J. and Litchtwark, G. A. (2019) 'The effecct of cadence on the mechanics and energetics of constant power cycling. *Medicine and Science in Sports and Exercise,* 51 (5) pp. 941-950.

Brewster, B (1882) The Yale Literary Magazine, Conducted by the Students of Yale College, Volume 47, Number 5.

Brown, D. A, Kautz, S. A. and Dairaghi, C. A. (1996) 'Muscle activity patterns altered during pedaling

at different body orientations.' *Journal of Biomechonics*. 30 (5) 505-511.

Brown, David A., Kautz, S. A. and Dairaghi, C. A. (1996) 'Muscle activity patterns altered during pedaling at different body orientations.' *Journal of Biomechanics*, 29(10) pp. 1349–1356.

Caiozzo, V. J. and Baldwin, K. M. (1997) 'Determinants of work produced by skeletal muscle: potential limitations of activation and relaxation.' *The American Journal of Physiology*, 273(3 Pt 1) pp. 1049–1056.

Cano-Corres, R., Sánchez-Álvarez, J. and Fuentes-Arderiu, X. (2012) 'The Effect Size: Beyond Statistical Significance.' *EJIFCC*, 23(1) pp. 19–23.

Carpes, F. P., Diefenthaeler, F., Bini, R. R., Stefanyshyn, D., Faria, I. E. and Mota, C. B. (2010) 'Does leg preference affect muscle activation and efficiency?' *Journal of Electromyography and Kinesiology*, 20(6) pp. 1230–1236.

Carpes, F. P., Mota, C. B. and Faria, I. E. (2010) 'On the bilateral asymmetry during running and cycling - A review considering leg preference.' *Physical Therapy in Sport*. 11 (4) pp. 136-142.

Carpes, Felipe Pivetta, Rossato, M. F., Faria, I. E. and Mota, C. B. (2007b) 'Influence of exercise intensity on bilateral pedaling symmetry.' *In* Duarte, M. and Almeida, & G. L. (eds) *Progress in motor control IV*. 11th ed., São Paulo, Brazil: Human Kinetics, pp. S54–S55.

Carpes, F. P., Rossato, M., Faria, I. E. and Mota, C. B. (2007a) 'Bilateral pedaling asymmetry during a simulated 40-km cycling time-trial.' *Journal of Sports Medicine and Physical Fitness*, 47(1) pp. 51–57.

Cavagna, G. A. (2006) 'The landing-take-off asymmetry in human running.' *Journal of Experimental Biology*. J Exp Biol, 209(20) pp. 4051–4060.

Charteris, J. and Goslin, B. R. (1986) 'In Vivo Approximations of the Classic In Vitro Length-Tension Relationship: An Isokinetic Evaluation.' *The Journal of Orthapaedic and Sports Therapy,* 7 (5) pp 222-231.

Chau, T. (2001) 'A review of analytical techniques for gait data. Part 1: Fuzzy, statistical and fractal methods.' *Gait and Posture*. 13 (1) pp.49-66.

Chowdhury, R.H., Reaz, M.B., Ali, M.A., Bakar, A.A., Chellappan, K. and Chang, T. G. (2013) 'Surface electromyography signal processing and classification techniques.' *Sensors (Basel)*. 13(9) pp. 12431-12466

Cohen, J. (1988) '*Statistical Power Analysis for the Behavioural Sciences.*' New York, NY: Routledge Academic.

Cordova, A., Latasa, I., Seco, J., Villa, G. and Rodriguez-Falces, J. (2014) 'Physiological Responses during Cycling With Oval Chainrings (Q-Ring) and Circular Chainrings.' *Journal of Sports Science and Medicine*, 13 pp. 410–416.

Coyle, E. F., Feltner, M. E., Kautz, S. A., Hamilton, M. T., Montain, S. J., Baylor, A. M., Abraham, L. D. and Petrek, G. W. (1991) 'Physiological and biomechanical factors associated with elite endurance cycling performance.' *Medicine and Science in Sports and Exercise*, 23(1) pp. 93–107.

Crenshaw, S. J. and Richards, J. G. (2006) 'A method for analyzing joint symmetry and normalcy, with an application to analyzing gait.' *Gait and Posture*, 24(4) pp. 515–521.

Crouzier, M., Lacourpaille, L., Nordez, A., Tucker, K. and Hug, F. (2018) 'Neuromechanical coupling within the human triceps surae and its consequence on individual force-sharing strategies.' *Journal*

of Experimental Biology, 221 doi:10.1242/jeb.187260

Dagnese, F., Carpes, F. P., De, E., Martins, A., Stefanyshyn, D. and Bolli Mota, C. (2011) 'Effects of a noncircular chainring system on muscle activation during cycling.' 21 (1) pp 13-17.

Darby, J., Li, B., Costen, N., Loram, I. and Hodson-Tole, E. (2013) 'Estimating Skeletal Muscle Fascicle Curvature from B-Mode Ultrasound Image Sequences.' *IEEE Trans Biomed Eng*, 60(7) pp. 193–1945.

Davies, C. T. M. (1980) 'Effect of air resistance on the metabolic cost and performance of cycling.' *European Journal of Applied Physiology and Occupational Physiology*. Springer-Verlag, 45(2–3) pp. 245–254.

Defraeye, T., Blocken, B., Koninckx, E., Hespel, P. and Carmeliet, J. (2010) 'Computational fluid dynamics analysis of cyclist aerodynamics: Performance of different turbulence-modelling and boundary-layer modelling approaches.' *Journal of Biomechanics*, 43(12) pp. 2281–2287.

Delp, S. L., Anderson, F. C., Arnold, A. S., Loan, P., Habib, A., John, C. T., Guendelman, E. and Thelen, D. G. (2007) 'OpenSim: Open-source software to create and analyze dynamic simulations of movement.' *IEEE Transactions on Biomedical Engineering*, 54(11) pp. 1940–1950.

Deluzio, K. J., Wyss, U. P., Zee, B., Costigan, P. A. and Sorbie, C. (1997) 'Principal component models of knee kinematics and kinetics: Normal vs. pathological gait patterns.' *Human Movement Science*. 16 (2-3) pp. 201-217.

Dick, T. J. M. and Wakeling, J. M. (2017) 'Shifting gears: dynamic muscle shape changes and force-velocity behavior in the medial gastrocnemius.' *Journal of Applied Physiology*, 123(6) pp. 1433–1442.

Dick, T. J. M., Biewener, A. A. and Wakeling, J. M. (2017) 'Comparison of human gastrocnemius forces predicted by Hill-type muscle models and estimated from ultrasound images.' *Journal of Experiemental Biology,* 1 (220) pp. 1643-1653.

Dorel, S., Drouet, J-M., Couturier, A., Champoux, Y. and Hug. F. (2009) 'Changes in Pedaling Technique and Muscle Coordination during an Exhaustive Exercise.' *Medicine and Science in Sports and Exercise,* 41(6) pp. 1277-1286.

Edman, K. A. P., Elzingat, G., Noblet, M. I. M., Elzinga, G. and Noble, M. I. M. (1978) 'Enhancement of Mechanical Performance by Stretch during Tetanic Contractions of Vertebrate Skeletal Muscle Fibres.' *Journal of Physiology*, 281 pp. 139–155.

Edwards, L. M., Jobson, S. A., George, R., Day, S. H. and Nevill, A. M. (2007) 'The effect of crank inertial load on the physiological and biomechanical responses of trained cyclists.' *Journal of Sports Sciences*, 25(11) pp. 1195–1201.

Edeline O, Polin D, Tourny-Chollet C, Weber J. (2004) 'Effect of workload on bilateral pedaling kinematics in non-trained cyclists.' *Journal of Human Movement Studies,* 46 pp. 493-517.

Elmer, S. J., Barratt, P. R., Korff, T. and Martin, J. C. (2011) 'Joint-specific power production during submaximal and maximal cycling.' *Medicine and Science in Sports and Exercise*, 43(10) pp. 1940–1947.

Ericson, M. O., Bratt, A., Nisell, R., Arborelius, U. P. and Ekholm, J. (1986) 'Power output and work in different muscle groups during ergometer cycling.' *European Journal of Applied Physiology and Occupational Physiology*, 55(3) pp. 229–35.

Ericson, M. O., Nisell, R., Arborelius, U. P. and Ekholm, J. (1985) 'Muscular activity during ergometer

cycling.' *Scandinavian Journal of Rehabilitation Medicine*, 17(2) pp. 53–61.

Faulkner, S. H., Ferguson, R. A., Gerrett, N., Hupperets, M., Hodder, S. G. and Havenith, G. (2013) 'Reducing muscle temperature drop after warm-up improves sprint cycling performance.' *Medicine and Science in Sports and Exercise*, 45(2) pp. 359–365.

Fintelman, D. M., Sterling, M., Hemida, H. and Li, F. X. (2015) 'The effect of time trial cycling position on physiological and aerodynamic variables.' *Journal of Sports Sciences*, 33(16) pp. 1730–1737.

Fregly, B. J. and Zajac, F. E. (1996) 'A state-space analysis of mechanical energy generation, absorption, and transfer during pedaling.' *Journal of Biomechanics*. 29 pp 81-90.

Fregly, B. J., Zajac, F. E. and Dairaghi, C. A. (2000) 'Bicycle drive dynamics: Theory and experimental validation.' *Journal of Biomechanical Engineering*, 122(4) pp. 446–452.

Gaesser, G. A. and Brooks, G. A. (1975) 'Muscular efficiency during steady rate exercise: effects of speed and work rate.' *Journal of Applied Physiology*, 38(6) pp. 1132–1139.

Galantis, A. and Woledge, R. C. (2003) 'The theoretical limits to the power output of a muscle-tendon complex with inertial and gravitational loads.' *Proceedings of the Royal Society London B*, 270(1523) pp. 1493–8.

Gonzalez, H. and Hull, M. L. (1989) 'Multivariable optimization of cycling biomechanics.' *Journal of Biomechanics*, 22(11–12) pp. 1151–1161.

Golich, D., and Broker, J. (1996). 'SRM bicycle instrumentation and the power output of elite male cyclists during the 1994 Tour Dupont.' *Performance and Conditioning for Cycling,* 2(9), 6.

Gregor, R. J., Komi, P. V. and Jarvinen, M. (1987) 'Achilles tendon forces during cycling.' *International Journal of Sports Medicine*, 8(1) pp. 9–14.

Griffiths, R. I. (1991) 'Shortening of muscle fibres during stretch of the active cat medial gastrocnemius muscle: the role of tendon compliance.' *The Journal of Physiology*, 436(1) pp. 219–236.

Hansen, E. A., Jorgensen, L. V., Jensen, K., Fregly, B. J. and Sjogaard, G. (2002) 'Crank inertial load affects freely chosen pedal rate during cycling.' *Journal of Biomechanics*, 35 pp. 277-285.

Hansen, E. A., Jensen, K., Hallén, J., Rasmussen, J. and Pedersen, P. K. (2009) 'Effect of Chain Wheel Shape on Crank Torque, Freely Chosen Pedal Rate, and Physiological Responses during Submaximal Cycling.' *Journal of Physiological Anthropology*, 28(6) pp. 261–267.

Hasson, C. J., Caldwell, G. E. and Van Emmerik, R. E. A. (2008) 'Changes in Muscle and Joint Coordination in Learning to Direct Forces.' *Human Movement Science*, 27 pp. 590–609.

Haut, T. L. and Haut, R. C. (1997) 'The state of tissue hydration determines the strain-rate-sensitive stiffness of human patellar tendon.' *Journal of Biomechanics*, 30(1) pp. 79–81.

Hedges, L.V. and Olkin, I. (1985) *'Statistical Methods in Meta-Analysis.*' San Diego, CA: Academic Press.

Henneman, E., Somjen, G. and Carpenter, D. O. (1965) 'Excitability and inhibitability of motoneurons of different sizes.' *Journal of Neurophysiology*, 28(3) pp. 599–620.

Herrmann, U. and Flanders, M. (1998) 'Directional tuning of single motor units.' *Journal of Neuroscience*. 18(20) pp. 8402–8416.

Herzog, W. (2017) ‘Skeletal muscle mechanics: Questions, problems and possible solutions.’ *Journal of NeuroEngineering and Rehabilitation*, 14 (98) doi: 10.1186/s12984-017-0310-6.

Herzog, W., and Leonard, T.R. (2000) 'The history dependence of force production in mammalian skeletal muscle following stretch-shortening and shortening-stretch cycles' *Journal of Biomechanics,* 33 (5) pp. 531-542.

Herzog, W., Leonard, T. and Wu, J. (2000) ‘The relationship between force depression following shortening and mechanical work in skeletal muscle.’ *Journal of Biomechanics*, 33(6) pp. 659–668.

Herzog, W., Nigg, B. M., Read, L. J. and Olsson, E. (1989) ‘Asymmetries in ground reaction force patterns in normal human gait.’ *Medicine and Science in Sports and Exercise*, 21(1) pp. 110–114.

Hill, A. V (1938) ‘The heat of shortening and the dynamic constants of muscle.’ *Proceedings of the Royal Society of London. Series B - Biological Sciences*, 126(843) pp. 136–195.

Hintzy, F. and Horvais, N. (2016) ‘Non-circular chainring improves aerobic cycling performance in non-cyclists.’ *European Journal of Sport Science*, 16(4) pp. 427–432.

Hodson-Tole, E. F. and Wakeling, J. M. (2007) ‘Variations in motor unit recruitment patterns occur within and between muscles in the running rat (Rattus norvegicus).’ *Journal of Experimental Biology*, 210(13) pp. 2333–2345.

Hoffer, J. A., Loeb, G. E., Sugano, N., Marks, W. B., O’Donovan, M. J. and Pratt, C. A. (1987) ‘Cat hindlimb motoneurons during locomotion. III. Functional segregation in sartorius.’ *Journal of Neurophysiology*, 57(2) pp. 554–562.

Horvais, N., Samozino, P., Zameziati, K., Hintzy, F. and Hautier, C. (2007) ‘Effects of a non circular chainring on muscular, mechanical and physiological parameters during cycle ergometer tests.’ *Isokinetics and Exercise Science*, 15(4) pp. 271–279.

Hoy, M. G., Zajac, F. E. and Gordon, M. E. (1990) ‘A musculoskeletal model of the human lower extremity: The effect of muscle, tendon, and moment arm on the moment-angle relationship of musculotendon actuators at the hip, knee, and ankle.’ *Journal of Biomechanics*, 23(2) pp. 157–169.

Hue, O., Chamari, K., Damiani, M., Blonc, S. and Hertogh, C. (2007) ‘The use of an eccentric chainring during an outdoor 1 km all-out cycling test.’ *Journal of Science and Medicine in Sport*. 10 (3) pp. 180-186.

Hue, O., Galy, O., Hertogh, C., Casties, J. F. and Prefaut, C. (2001) ‘Enhancing cycling performance using an eccentric chainring.’ *Medicine and Science in Sports and Exercise*, 33(6) pp. 1006–1010.

Hue, O., Racinais, S., Chamari, K., Damiani, M., Hertogh, C. and Blonc, S. (2008) ‘Does an eccentric chainring improve conventional parameters of neuromuscular power?’ *Journal of Science and Medicine in Sport*, 11(3) pp. 264–270.

Hug, F., Drouet, J.M., Champoux, Y., Couturier, A. and Dorel S. (2008) Interindividual variability of electromyographic patterns and pedal force profiles in trained cyclists. *European Journal of Applied Physiology,* 104: 667-678.

Hug, F., Boumier, F. & Dorel, S. (2013) 'Altered muscle coordination when pedaling with independent cranks.' *Frontiers in Physiology,* 4; pp. 1-7.

Huijing, P. A. (1998) ‘Muscle, the motor of movement: properties in function, experiment and modelling.’ *Journal of Electromyography and Kinesiology*, 8 pp. 61–77.

Hull, M. L., Kautz, S. and Beard, A. (1991) ‘An angular velocity profile in cycling derived from mechanical energy analysis.’ *Journal of Biomechanics*. Elsevier, 24(7) pp. 577–586.

Huxley, A. F. and Simmons, R. M. (1971) ‘Proposed Mechanism of Force Generation in Striated Muscle.’ *Nature*, 233(5321) pp. 533–538.

Jay, G. D. and Waller, K. A. (2014) ‘The biology of Lubricin: Near frictionless joint motion.’ *Matrix Biology*. 39 pp. 17-24.

Jeukendrup, A. E., Craig, N. P. and Hawley, J. A. (2000) ‘The bioenergetics of world class cycling.’ *Journal of Science and Medicine in Sport*, 3(4) pp. 414–433.

Josephson, R. K. (1985) ‘Mechanical Power output from Striated Muscle during Cyclic Contraction.’ *Journal of Experimental Biology*, 114(1) pp. 493-512.

Kautz, S.A., Feltner, M.E., Coyle, E.F. and Bailey, M.P. (1991) 'The pedaling technique of elite endurance cyclists: changes with increasing workload at constant cadence.' *International Journal of Sports Biomechanics,* 7 pp. 29-53.

Kautz, S. A. and Hull, M. L. (1993) ‘A theoretical basis for interpreting the force applied to the pedal in cycling.’ *Journal of Biomechanics*, 26(2) pp. 155–165.

Kautz, S. A. and Hull, M. L. (1995) ‘Dynamic optimization analysis for equipment setup problems in endurance cycling.’ *Journal of Biomechanics*, 28(11) pp. 1391–1401.

Kautz, S. A., Hull, M. L. and Neptune, R. R. (1994) ‘A comparison of muscular mechanical energy expenditure and internal work in cycling.’ *Journal of Biomechanics*, 27(12) pp. 1459–1467.

Kautz, S. A. and Neptune, R. R. (2002) Biomechanical Determinants of Pedaling Energetics: Internal and External Work Are Not Independen*t*. *Exercise and Sport Science Reviews,* 30 (4) 159-165.

Komi, P. V. (1996) ‘Optic fibre as a transducer of tendomuscular forces.’ *European Journal of Applied Physiology and Occupational Physiology*, 72(3) pp. 278–280.

Korff, T., Romer, L. M., Mayhew, I. and Martin, J. C. (2007) ‘Effect of Pedaling Technique on Mechanical Effectiveness and Efficiency in Cyclists.’ *Medicine and Science in Sports and Exercise*, 39(6) pp. 991–995.

Lai, A. K. M., Arnold, A. S. and Wakeling, J. M. (2017) ‘Why are antagonist muscles co-activated in my simulation? A musculoskeletal model for analysing human locomotor tasks.’ *Annual Review of Biomedical Engineering*, 45(12) pp. 2762–2774.

Lai, A. K. M., Biewener, A. A. and Wakeling, J. M. (2018) ‘Metabolic cost underlies task-dependent variations in motor unit recruitment.’ *Journal of the Royal Society Interface*, 15(148) doi: 20180541.

Lai, A., Lichtwark, G. A., Schache, A. G., Lin, Y., Brown, N. A. T. and Pandy, M. G. (2015) 'In vivo behaviour of the human soleus muscle with increasing walking and running speeds.' *Journal of Applied Physiology,* 118 pp. 1266 - 1275.

Lai, A., Schache, A. G., Brown, N. A. T. and Pandy, M. G. (2016) ‘Human ankle plantar flexor muscle-tendon mechanics and energetics during maximum acceleration sprinting.’ *Journal of the Royal Society Interface*, 13 (121) doi: 20160391

Lallement, P. (1866) *Improvement in velocipedes*, 59915.

Lauber, B., Lichtwark, G.A. and Cresswell, A.G. (2014) 'Reciprocal activation of gastrocnemius and

soleus motor units is associated with fascicle length change during knee flexion. *Physiological Reports,* 2 (6) doi: 10.14814/phy2.12044

Leong, C.-H., Elmer, S. J. and Martin, J. C. (2017) 'Noncircular Chainrings Do Not Influence Maximum Cycling Power.' *Journal of Applied Biomechanics*, 33 pp. 410–418.

Lichtwark, G. A., Bougoulias, K. and Wilson, A. M. (2007) 'Muscle fascicle and series elastic element length changes along the length of the human gastrocnemius during walking and running.' *Journal of Biomechanics*. 40(1) pp. 157–164.

Lieber, R. L. and Friden, J. (2000) 'Functional and clinical significance of skeletal muscle architecture.' *Muscle & Nerve*. 23(11) pp. 1647–1666.

Lima Da Silva, J. C., Tarassova, O, Ekblom, M, M., Andersson, E., Rönquist, G and Arndt, A. (2016) 'Quadriceps and hamstring muscle activity during cycling as measured with intramuscular electromyography.' *European Journal of Applied Physiology*, 116 pp. 1807–1817.

Lu, T. W. and O'Connor, J. J. (1999) 'Bone position estimation from skin marker co-ordinates using global optimisation with joint constraints.' *Journal of Biomechanics*, 32 pp. 129–134.

Maas, H. and Sandercock, T. G. (2010) 'Force Transmission between Synergistic Skeletal Muscles through Connective Tissue Linkages.' *Journal of Biomedicine and Biotechnology*. 2010 pp. 1–9.

Maganaris, C. N., Narici, M. V and Reeves, N. D. (2004) 'Functional implications of tendon viscoelasticity.' *J Musculoskel Neuron Interact*, 4(2) pp. 205–208.

Malfait, L., Storme, G. and Derdeyn, M. (2010) 'Comparative biomechanical study of circular and non-circular chainrings for endurance cycling at constant speed,' Unpublished.

Marsh, A. P. and Martin, P. E. (1995) 'The relationship between cadence and lower extremity EMG in cyclists and noncyclists.' *Medicine and Science in Sports and Exercise*, 27(2) pp. 217–225.

Marsh, A. P. and Martin, P. E. (1997) 'Effect of cycling experience, aerobic power, and power output on preferred and most economical cycling cadences.' *Medicine and science in sports and exercise*, 29(9) pp. 1225–32.

Marsh, A. P., Martin, P. E. and Sanderson, D. J. (2000) 'Is a joint moment-based cost function associated with preferred cycling cadence?' *Journal of Biomechanics*, 33(2) pp. 173–180.

Martin, J. C. (2007) 'Muscle power: the interaction of cycle frequency and shortening velocity.' *Exercise and Sport Science Reviews*, 35(2) pp. 74–81.

Martin, J, C. and Brown, N. A. T. (2009) 'Joint-specific power production and fatigue during maximal cycling.' *Journal of Biomechanics*, 42(4) pp. 474–479.

Martin, J, C and Brown, N. A. T. (2009) 'Joint-specific power production and fatigue during maximal cycling.' *Journal of Biomechanics*, 42 pp. 474–479.

Martin, J. C., Lamb, S. M. and Brown, N. A. T. (2002) 'Pedal trajectory alters maximal single-leg cycling power.' *Medicine and science in sports and exercise*, 34(8) pp. 1332–1336.

Martin, J. C. and Nichols, J. A. (2018) 'Simulated work loops predict maximal human cycling power.' *Journal of Experimental Biology*, 221 pp. 1–12.

Martin, J. C. and Spirduso, W. W. (2001) 'Determinants of maximal cycling power: crank length, pedaling rate and pedal speed.' *European Journal of Applied Physiology*, 84 pp. 413–418.

McCartney, N., Heigenhauser, G. J. F., Sargeant, A. J. and Jones, N. L. (1983) 'A constant-velocity cycle ergometer for the study of dynamic muscle function.' *Journal of Applied Physiology Respiratory Environmental and Exercise Physiology*, 55(1) pp. 212–217.

McDaniel, D. P., Shaw, G. A., Elliott, J. T., Bhadriraju, K., Meuse, C., Chung, K.-H. and Plant, A. L. (2007) 'The Stiffness of Collagen Fibrils Influences Vascular Smooth Muscle Cell Phenotype.' *Biophysical Journal*, 92(5) pp. 1759–1769.

McDaniel, J., Behjani, N. S., Elmer, S. J., Brown, N. A. T. and Martin, J. C. (2014) 'Joint-Specific Power-Pedaling Rate Relationships During Maximal Cycling.' *Journal of Applied Biomechanics*, 30 pp. 423–430.

Mileva, K. and Turner, D. (2003) 'Neuromuscular and biomechanical coupling in human cycling Adaptations to changes in crank length.' *Experimental Brain Research*, 152 pp. 393–403.

Miller, N. R. and Ross, D. (1980) 'The Design of Variable-Ratio Chain Drives for Bicycles and Ergometers—Application to a Maximum Power Bicycle Drive.' *Journal of Mechanical Design*, 102(4) pp. 711–717.

Mornieux, G., Golhofer, A. and Stapelfeldt, B. (2010) 'Muscle Coordination while Pulling up During Cycling.' *International Journal of Sports Medicine*, 31 pp. 843–846.

Muraoka, T., Kawakami, Y., Tachi, M. and Fukunaga, T. (2001) Muscle fiber and tendon length changes in the human vastus lateralis during slow pedaling. *Journal of Applied Physiology,* 91 (5) 2035-2040.

Murian, A., Deschamps, T., Bourbousson, J., Temprado, J.J., (2008) 'Influence of an exhausting muscle exercise on bimanual coordination stability and attentional demands.' *Neuroscience Letters*. 432 (1), 64–68.

Neptune, R. R. and Herzog, W. (1999) 'The association between negative muscle work and pedaling rate.' *Journal of Biomechanics*, 32(10) pp. 1021–1026.

Neptune, R. R. and Herzog, W. (2000) 'Adaptation of muscle coordination to altered task mechanics during steady-state cycling.' *Journal of Biomechanics*, 33(2) pp. 165–172.

Neptune, R. R. and Hull, M. L. (1995) 'Accuracy Assessment of Methods for Determining Hip Movement in Seated Cycling.' *Journal of Biomechanics*, 28(4) pp. 423–437.

Neptune, R. R. and Kautz, S. A. (2001) 'Muscle Activation and Deactivation Dynamics: The Governing Properties in Fast Cyclical Human Movement Performance?' *Exercise and Sport Sciences Reviews*, 29(2) pp. 76–81.

Neptune, R. R., Kautz, S. A. and Hull, M. L. (1997) 'The effect of pedaling rate on coordination in cycling.' *Journal of Biomechanics*, 30(10) pp. 1051–1058.

Newmiller, J., Hull, M. L. and Zajac, F. E. (1988) 'A mechanically decoupled two force component bicycle pedal dynamometer.' *Journal of Biomechanics*, 21(5) pp. 375–386.

O'Hara, C. R., Clark, R. D., Hagobian, T. and Mcgaughey, K. (2012) 'Effects of Chainring Type (Circular vs . Rotor Q-Ring) on 1km Time Trial Performance Over Six Weeks in Competitive Cyclists and Triathletes.' *International Journal of Sport Science and Engineering*, 6(1) pp. 25–40.

Okajima S (1983) 'Designing chainwheels to optimize the human engine.' *Bike Technology* 2: pp. 1–7.

O'Symetric (2020) O'Symetric Victories. Viewed 01/07/2020. <https://www.osymetric.com/en/>

Patterson, R. P. and Moreno, M. I. (1990) ‘Bicycle pedalling forces as a function of pedalling rate and power output.’ *Medicine and Science in Sports and Exercise*, 22(4) pp. 512–516.

Powell, P. L., Roy, R. R., Kanim, P., Bello, M, A, Edgerton, V. R. (1984) 'Predictability of skeletal muscle tension from architectural determinations in guinea pig hindlimbs.' *Journal of Applied Physiology: Respiratory and Environmental Exercise Physiology*, 57 (6) pp. 1715-1721.

Rotor Q-Ring (2020) The Science of Q Rings. Accessed 01/07/2020. <https://rotoruk.co.uk/p1.asp?cat=1064>

Raasch, C. C., Zajac, F. E., Ma, B. and Levine, W. S. (1997) ‘Muscle coordination of maximum-speed pedaling.’ *Journal of Biomechanics*. 30 (6) pp. 595-602.

Ramsay, J. and Silverman, B. W. (2005) *Functional Data Analysis*. *Functional Data Analysis*. Springer-Verlag.

Rankin, J. W. and Neptune, R. R. (2008) ‘A theoretical analysis of an optimal chainring shape to maximize crank power during isokinetic pedaling.’ *Journal of Biomechanics*, 41(7) pp. 1494–1502.

Roberts, T. J. and Azizi, E. (2011) ‘Flexible mechanisms: The diverse roles of biological springs in vertebrate movement.’ *Journal of Experimental Biology*, pp. 353–361.

Roberts, T. J., Marsh, R. L., Weyand, P. G. and Taylor, C. R. (1997) ‘Muscular force in running turkeys: The economy of minimizing work.’ *Science*, 275(5303) pp. 1113–1115.

Robinson, R. O., Herzog, W. and Nigg, B. M. (1987) ‘Use of force platform variables to quantify the effects of chiropractic manipulation on gait symmetry.’ *Journal of Manipulative and Physiological Therapeutics*, 10(4) pp. 172–176.

Robertson, B. D. and Sawicki, G. S. (2015) ‘Unconstrained muscle-tendon workloops indicate resonance tuning as a mechanism for elastic limb behavior during terrestrial locomotion.’ *Proceedings of the National Academy of Sciences of the United States of America*, 112(43) pp. 5891–5898.

Ross, S. A. and Wakeling, J. M. (2016) ‘Muscle shortening velocity depends on tissue inertia and level of activation during submaximal contractions.’ *Biology Letters*, 12(6) pp. 1-4.

Samozino, P., Horvais, N. and Hintzy, F. (2006) ‘Interactions between cadence and power output effects on mechanical efficiency during sub maximal cycling exercises.’ *European Journal of Applied Physiology*, 97(1) pp. 133–139.

Sanderson, D. J. and Amoroso, A. T. (2009) ‘The influence of seat height on the mechanical function of the triceps surae muscles during steady-rate cycling.’ *Journal of Electromyography and Kinesiology*. 19(6) pp. 465–471.

Sanderson, D. J. and Black, A. H. (2003) ‘The effect of prolonged cycling on pedal forces.’ *Journal of Sport Sciences*, 21(3) pp. 191–199.

Sanderson, D. J., Martin, P. E., Honeyman, G. and Keefer, J. (2006) ‘Gastrocnemius and soleus muscle length, velocity, and EMG responses to changes in pedalling cadence.’ *Journal of Electromyography and Kinesiology,* 16 (6) 642-649.

Sargeant, A. J. and Davies, C. T. M. (1977) ‘Forces applied to cranks of a bicycle ergometer during one-and two-leg cycling.’ *Journal of Applied Physiology*, 42(4) pp. 513–518.

Schiaffino, S. and Reggiani, C. (2011) ‘Fiber Types In Mammalian Skeletal Muscles.’ *Physiological*

Reviews, 91 pp. 1447–1531.

Shadwick, R. E., Katz, S. L., Korsmeyer, K. E., Knower, T. and Covell, J. W. (1999) 'Muscle dynamics in skipjack tuna: timing of red muscle shortening in relation to activation and body curvature during steady swimming.' *Journal of Experimental Biology*, 202 pp. 2139–2150.

Strutzenberger, G., Wunsch, T., Kroell, J., Dastl, J. and Schwameder, H. (2014) Effect of chainring ovality on joint power during cycling at different workloads and cadences. *Sports Biomechanics,* 13 (2) pp. 97-108.

da Silva, J.C.L., Tarassova, O., Ekblom, M.M., Andersson, E., Rönquist, G. and Arndt, A. (2016) 'Quadriceps and hamstring muscle activity during cycling as measured with intramuscular electromyography.' *European Journal of Applied Physiology*, 116 pp. 1807-1817.

Van Sickle Jr, J. and Hull, M. L. (2007) 'Is economy of competitive cyclists affected by the anterior-posterior foot position on the pedal?' *Journal of Biomechanics*, 40 pp. 1262–1267.

Škof, B. and Strojnik, V. (2007) 'The Effect of Two Warm-Up Protocols on Some Biomechanical Parameters of the Neuromuscular System of Middle Distance Runners.' *The Journal of Strength and Conditioning Research*, 21(2) pp. 394–399.

Smak, W., Neptune, R. R. and Hull, M. L. (1999) 'The influence of pedaling rate on bilateral asymmetry in cycling.' *Journal of Biomechanics*. 32 (9) pp. 899-906.

van Soest, A. J. (2014) 'From bicycle chain ring shape to gear ratio: Algorithm and examples.' *Journal of Biomechanics*, 47(1) pp. 281–283.

van Soest, A. J. K. and Casius, L. J. R. (2000) 'Which factors determine the optimal pedaling rate in sprint cycling.' *Medincine and Science in Sports and Exercise*, 32(11) pp. 1927–1934.

Teixeira, L. A., and Caminha, L. Q. (2003). 'Intermanual transfer of force control is modulated by asymmetry of muscular strength.' *Experimental Brain Research,* 149(3), pp. 312-319.

Too, D. (1990) Biomechanics of Cycling and Factors Affecting Performance. *Review Article Sports Medicine*. 10 (5) pp 286-302.

Von Tscharner, V. (2000) 'Intensity analysis in time-frequency space of surface myoelectric signals by wavelets of specified resolution.' *Journal of Electromyography and Kinesiology*. 10 (6) pp. 433-445.

Von Tscharner, V. and Goepfert, B. (2006) 'Estimation of the interplay between groups of fast and slow muscle fibers of the tibialis anterior and gastrocnemius muscle while running.' *Journal of Electromyography and Kinesiology*. 16(2) pp. 188–197.

Umberger, B. R., Gerritsen, K. G. M. and Martin, P. E. (2006) 'Muscle fiber type effects on energetically optimal cadences in cycling.' *Journal of Biomechanics*, 39 pp. 1472–1479.

Wakeling, J. M. (2009) 'Patterns of motor recruitment can be determined using surface EMG.' *Journal of Electromyography and Kinesiology*. 19(2) pp. 199–207.

Wakeling, J, M., Blake, O, M. and Chan, H, K. (2010) 'Muscle coordination is key to the power output and mechanical efficiency of limb movements.' *The Journal of Experimental Biology*, 213 pp. 487–492.

Wakeling, J. M., Blake, O. M. and Chan, H. K. (2010) 'Muscle coordination is key to the power output and mechanical efficiency of limb movements.' *Journal of Experimental Biology*, 213(3) pp. 487–492.

Wakeling, J. M., Blake, O. M., Wong, I., Rana, M. and Lee, S. S. M. (2011) ‘Movement mechanics as a determinate of muscle structure, recruitment and coordination.’ *Philosophical Transactions of the Royal Society B: Biological Sciences*, 366(1570) pp. 1554–1564.

Wakeling, J. M. and Horn, T. (2009) ‘Neuromechanics of Muscle Synergies During Cycling.’ *Journal of Neurophysiology*, 101(2) pp. 843–854.

Wakeling, J. M. and Rozitis, A. I. (2004) ‘Spectral properties of myoelectric signals from different motor units in the leg extensor muscles.’ *Journal of Experimental Biology*, 207 pp. 2519–2528.

Wakeling, J. M., Uehli, K. and Rozitis, A. I. (2006) ‘Muscle fibre recruitment can respond to the mechanics of the muscle contraction.’ *Journal of the Royal Society Interface*, 3 pp. 533–544.

Welbergen, E. and Clijsen, L. P. V. M. (1990) ‘The influence of body position on maximal performance in cycling.’ *European Journal of Applied Physiology and Occupational Physiology*. 61(1–2) pp. 138–142.

Williams, C. D., Salcedo, M. K., Irving, T. C., Regnier, M. and Daniel, T. L. (2013) ‘The length-tension curve in muscle depends on lattice spacing.’ *Proceedings of the Royal Society B: Biological Sciences*, 280 (1766) doi. 20130697.

Wilson, S. . (1973) ‘Bicycle Technology’ pp. 81–91.

Wilson, A. and Lichtwark, G. (2011) ‘The anatomical arrangement of muscle and tendon enhances limb versatility and locomotor performance.’ *Philosophical Transactions of the Royal Society B: Biological Sciences*, 366(1570) pp. 1540–1553.

Winters, J. M. (1990) ‘Hill-Based Muscle Models: A Systems Engineering Perspective.’ *Multiple Muscle Systems*, pp. 69–93.

Woledge, R.C., Curtin, N.A. and Homsher, E. (1985) 'Energetic aspects of muscle contraction.' *Monographs of the Physiological Society,* 41 pp. 1-357.

Zajac, F. E. (1989) ‘Muscle and tendon: properties, models, scaling, and application to biomechanics and motor control.’ *Critical Reviews in Biomedical Engineering,* 17(4) pp. 359–411.

Zajac, F. E. and Faden, J. S. (1985) ‘Relationship among recruitment order, axonal conduction velocity, and muscle-unit properties of type-identified motor units in cat plantaris muscle.’ *Journal of Neurophysiology*, 53(5) pp. 1303–1322.

Zameziati, K., Mornieux, G., Rouffet, D. and Belli, A. (2006) ‘Relationship between the increase of effectiveness indexes and the increase of muscular efficiency with cycling power.’ *European Journal of Applied Physiology*, 96(3) pp. 274–281.

Zamparo, P., Minetti, A. E. and Di Prampero, P. E. (2002) ‘Mechanical efficiency of cycling with a new developed pedal-crank.’ *Journal of Biomechanics*, 35(10) pp. 1387–1398.